

Chesapeake Bay Impact Structure—Development of “Brim” Sedimentation in a Multilayered Marine Target

Henning Dypvik

Department of Geosciences, University of Oslo, P.O. Box 1047, Blindern, NO-0316 Oslo, Norway

Gregory S. Gohn[†]

Lucy E. Edwards[†]

J. Wright Horton Jr.[†]

David S. Powars[†]

Ronald J. Litwin

U.S. Geological Survey, 926A National Center, Reston, Virginia 20192, USA

ABSTRACT

The late Eocene Chesapeake Bay impact structure was formed in a multilayered target of seawater underlain sequentially by a sediment layer and a rock layer in a continental-shelf environment. Impact effects in the “brim” (annular trough) surrounding and adjacent to the transient crater, between the transient crater rim and the outer margin, primarily were limited to the target-sediment layer. Analysis of published and new lithostratigraphic, biostratigraphic, sedimentologic, petrologic, and mineralogic studies of three core holes, and published studies of a fourth core hole, provided information for the interpretation of the impact processes, their interactions and relative timing, their resulting products, and sedimentation in the brim.

Most studies of marine impact-crater materials have focused on those found in the central crater. There are relatively few large, complex marine craters, of which most display a wide brim around the central crater. However, most have been studied using minimal data sets. The large number of core holes and seismic profiles available for study of the Chesapeake Bay impact structure presents a special opportunity for research.

The physical and chronologic records supplied by study of the sediment and rock cores of the Chesapeake Bay impact indicate that the effects of the initial, short-lived contact and compression and excavation stages of the impact event primarily were limited to the transient crater. Only secondary effects of these processes are evident in the brim. The preserved record of the brim was created primarily in the subsequent modification stage.

*E-mails: henning.dypvik@geo.uio.no; ggohn@usgs.gov; leedward@usgs.gov; whorton@usgs.gov; dspowars@usgs.gov; rlitwin@usgs.gov.

[†]These authors are listed alphabetically.

Dypvik, H., Gohn, G.S., Edwards, L.E., Horton, J.W., Jr., Powars, D.S., and Litwin, R.J., 2018, Chesapeake Bay Impact Structure—Development of “Brim” Sedimentation in a Multilayered Marine Target: Geological Society of America Special Paper 537, p. 1–68, <https://doi.org/10.1130/2018.2537>.

© 2018 The Authors. Gold Open Access: This paper is published under the terms of the CC-BY license and is available open access on www.gsapubs.org.

In the brim, the records of early impact processes (e.g., outgoing tsunamis, overturned flap collapse) were modified or removed by later processes. Transported and rotated, large and small clasts of target sediments, and intervals of fluidized sands indicate that seismic shaking fractured and partially fluidized the Cretaceous and Paleogene target sediments, which led to their inward transport by collapse and lateral spreading toward the transient crater. The succeeding inward seawater-resurge flow quickly overtook and interacted with the lateral spreading, further facilitating sediment transport across the brim and into the transient crater. Variations in the cohesion and relative depth of the target sediments controlled their degree of disaggregation and redistribution during these events. Melt clasts and shocked and unshocked rock clasts in the resurge sediments indicate fallout from the ejecta curtain and plume.

Basal parautochthonous remnant sections of target Cretaceous sediments in the brim thin toward the collapsed transient crater. Overlying seawater-resurge deposits consist primarily of diamictons that vary laterally in thickness, and vertically and laterally in maximum grain size. After cessation of resurge flow and re-establishment of pre-impact sea level, sandy sediment gravity flows moved from the margin to the center of the partially filled impact structure (shelf basin). The uppermost unit consists of stratified sediments deposited from suspension. Postimpact clayey silts cap the crater fill and record the return to shelf sedimentation at atypically large paleodepths within the shelf basin.

An unresolved question involves a section of gravel and sand that overlies Neoproterozoic granite in the inner part of the brim in one core hole. This section may represent previously unrecognized, now parautochthonous Cretaceous sediments lying nonconformably above basement granite, or it may represent target sediments that were moved significant distances by lateral spreading above basement rocks or above a granite megaclast from the overturned flap.

The Chesapeake Bay impact structure is perhaps the best documented example of the small group of multilayer, marine-target impacts formed in continental shelves or beneath epeiric seas. The restriction of most impact effects to the target-sediment layer in the area outside the transient cavity, herein called the brim, and the presence of seawater-resurge sediments are characteristic features of this group. Other examples include the Montagnais (offshore Nova Scotia, Canada) and Mjølnir (offshore Norway) impact structures.

INTRODUCTION

Impacts of cosmic projectiles into targets with multiple layers of differing material strength, rheological response, and thickness produce a class of impact structures that differ in their size, and various aspects of their configuration, from impacts into homogeneous targets for a given set of impactor parameters (e.g., Oberbeck and Quaide, 1968; Schenk, 2002; Dypvik et al., 2004; Collins et al., 2008a, 2008b; Senft and Stewart, 2007, 2008). Earth's seawater targets produce a distinct subclass of layered-target impact structures due to the presence of the seawater layer in epeiric seas, continental shelves, and the deep ocean.

An inherent aspect of marine-target impacts is the prompt return of the seawater toward and into the transient cavity, if it is not blocked by an uplifted cavity rim and (or) overturned flap (Ormö and Lindström, 2000). This resurge significantly modifies

earlier-formed impact features, and some of the material ejected from the transient cavity is transported toward and into the cavity. If readily eroded sediments constitute the layer beneath the seawater layer, a large volume of this material also is transported inward and redeposited.

Early overviews of impact structures in the marine-target subclass, and their formative mechanisms, were provided by Jansa et al. (1989), Jansa (1993), Ormö and Lindström (2000), Ormö et al. (2002), Shuvalov and Trubestkaya (2002), and Dypvik and Jansa (2003), among others. Today, a large and growing list of field and modeling studies of Earth's marine-target impact structures is available. References cited herein provide an introduction to the recent literature.

The late Eocene (ca. 35.4 Ma) Chesapeake Bay impact structure formed when an impactor (~3.2 km in diameter) struck a layered continental-shelf target (seawater-sediments-basement rocks) in the area that is now the Atlantic Coast and offshore areas

of Virginia, United States (Fig. 1; Powars et al., 1993; Poag et al., 1994; Koeberl et al., 1996; Collins et al., 2008b; Horton and Izett, 2005). The complex final configuration of this structure was significantly controlled by the variable responses of the three target layers, with greatly differing strengths, during the impact event.

This report is focused on the types and timing of the impact processes that formed the outer part of the Chesapeake Bay impact structure, where the preserved record of impact deformation is primarily limited to the target's sediment layer. This part of the Chesapeake Bay impact structure often has been called the "annular trough," but it also has been called the "brim" (Figs. 2 and 3). The latter term derives from the shape of the entire Chesapeake Bay impact structure, which is commonly described as an "inverted sombrero" (e.g., Powars, 2000; Turtle et al., 2005; Kenkmann et al., 2013). The deep, collapsed, and filled transient crater (central crater) represents the crown of the upside-down hat, and the thinner layer of deformed target sediments outside the central crater is the brim. As the study of impact structures continues, it may prove useful to restrict use of the term "brim" to characterizing a subclass of marine-target impact structures with a thin outer zone where deformation primarily occurred in a weak sediment layer below a water layer and above crystalline rocks or strongly indurated sediments.

CHESAPEAKE BAY IMPACT STRUCTURE— HISTORY OF INVESTIGATIONS

Early Investigations

D.J. Cederstrom (1945, 1957) conducted regional hydrogeologic studies of deep water wells in the 1940s that later provided the first indication of a large subsurface structure of uncertain origin in the southern Chesapeake Bay area. Cederstrom (1957) recognized a transition from a thinner section of Eocene sediments (including sediments now assigned to the Paleocene) south of the James River (Fig. 1) to a thicker Eocene section north of the river. He also noted the presence of Upper Cretaceous sediments south of the James River and their absence in the area immediately north of the river. In addition, he noted that gravity data indicated that the top of basement was shallower south of the James River and deeper north of the river. These patterns led Cederstrom (1945) to infer a zone of northwest-trending basement faulting located at depth along the trend of the James River, which Powars (2000) called the James River structural zone. The part of this fault near the southeastern end of the York-James Peninsula and Norfolk, Virginia (Fig. 1), approximates the southern boundary of the Chesapeake Bay impact structure in that area. Cederstrom's

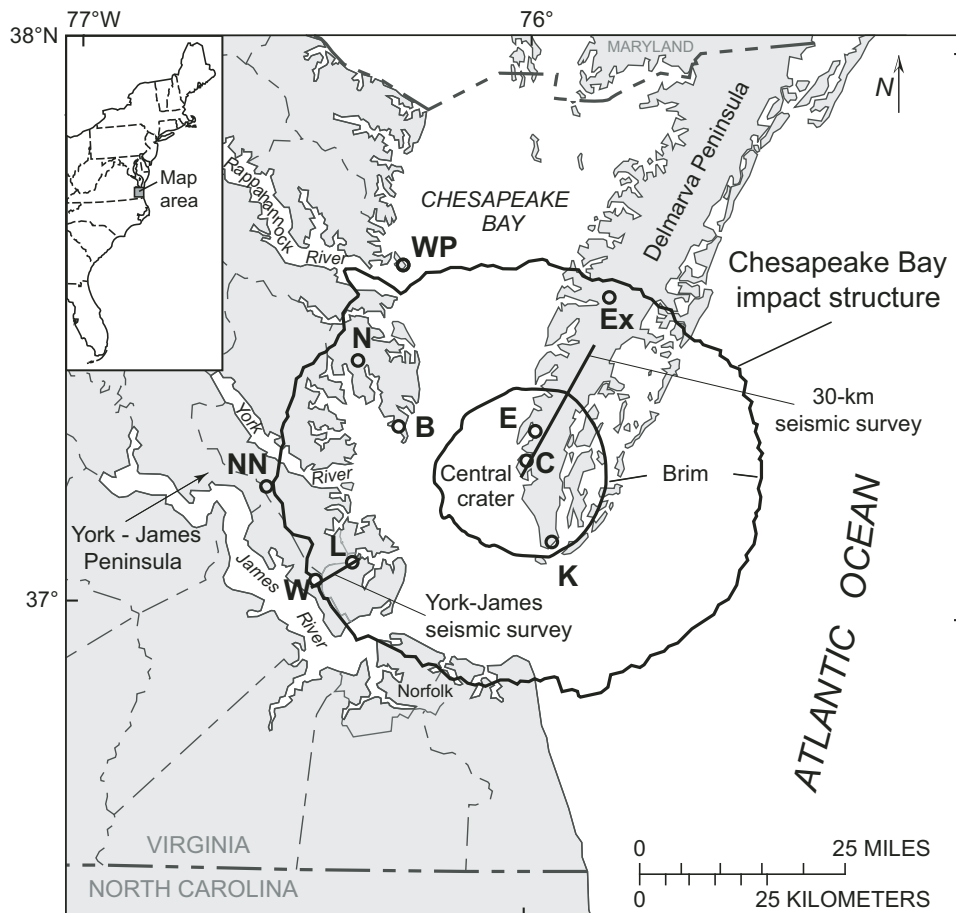


Figure 1. Location of the Chesapeake Bay impact structure in the subsurface of the Virginia Coastal Plain, USA, modified from Horton et al. (2009b). The Watkins School (W), Langley (L), and Bayside (B) cores are the main focus of this report. Data from the Cape Charles (C), Eyreville (E), and Exmore (Ex) cores also were used. Other previously studied core holes include Newport News Park (NN), North (N), Windmill Point (WP), and Kiptopeke (K).

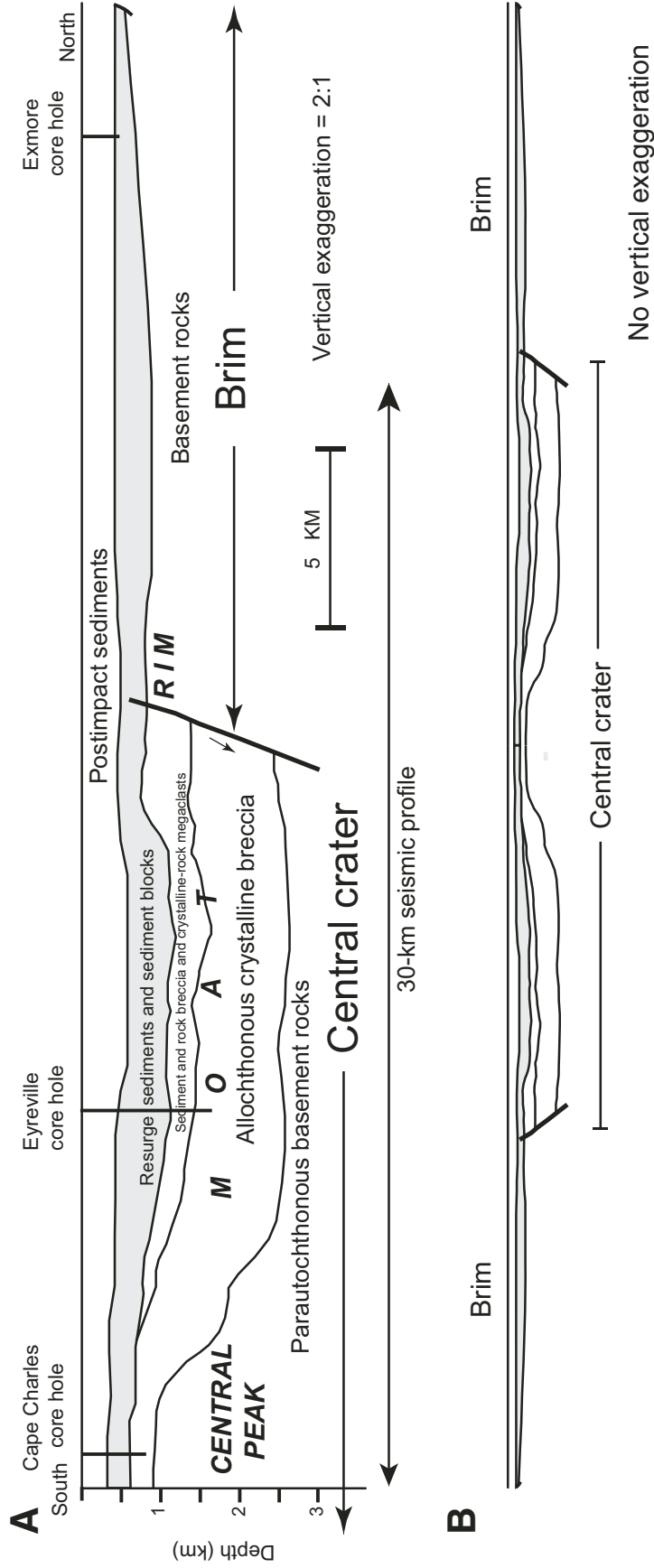


Figure 2. Cross sections of the Chesapeake Bay impact structure (CBIS) on the Delmarva Peninsula simplified from the 30 km seismic survey of Catchings et al. (2008). (A) Generalized radial cross section from the central peak to the outer margin of the brim showing the principal elements of the CBIS. (B) Simulated cross section of the entire CBIS, constructed using data from part A and a horizontally “flipped” version of part A, to illustrate the inverted sombrero shape of the CBIS.

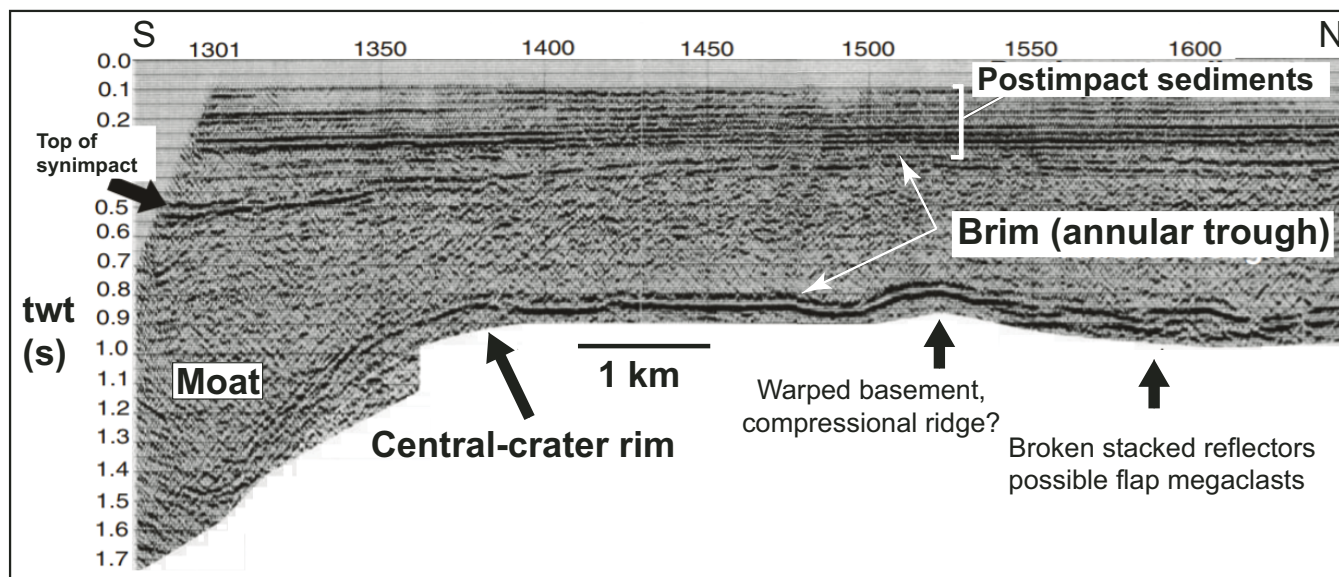


Figure 3. Interpreted seismic profile showing the transition from the brim to the moat of the central crater in the Chesapeake Bay impact structure, modified from Powars et al. (2009, their figure 2A); twt—two-way traveltime.

Eocene basin north of the James River is now known to be the southwestern part of the Chesapeake Bay impact structure.

Cederstrom (1957) also named a new stratigraphic unit, the Mattaponi Formation, which he mapped in the subsurface west of Chesapeake Bay using water-well cuttings. This enigmatic unit was characterized by a wide variety of sediment types and a mixture of Cretaceous, Paleocene, and Eocene foraminifera (J.A. Cushman cited in Cederstrom, 1957) that notably exceeded the degree of mixing typically seen in drill cuttings. The Mattaponi Formation was largely ignored or misused in subsequent stratigraphic and groundwater investigations (see discussions in Powars, 2000; Poag et al., 2004) and eventually was abandoned by Ward (1984). However, the rediscovery of this unit in core holes in the late 1980s led to the recognition of the Chesapeake Bay impact structure.

Discovery Phase

The discovery phase of investigations began slowly in 1981, when dinoflagellate assemblages in core samples from a drill hole at the City of Hampton, Virginia, were examined for age determinations (Edwards, 1996). One core sample contained a mixed assemblage of early Eocene, middle Eocene, and late Eocene taxa. This unusual result was attributed to drilling contamination. Subsequently, two other core samples indicated similar mixed ages. This conundrum was not resolved until 1985, when the U.S. Geological Survey (USGS) and the Virginia Water Control Board began a cooperative program to drill continuously sampled core holes in the outer Virginia Coastal Plain (Powars et al., 1992). Nine core holes were drilled between 1986 and 1995. The Exmore, Kiptopeke, Newport News Park, and Windmill

Point core holes were drilled into or near the Chesapeake Bay impact structure (Fig. 1). The other five core holes were drilled at greater distances outside the Chesapeake Bay impact structure in the Virginia Coastal Plain (Powars et al., 1992; Powars and Bruce, 1999; Powars, 2000).

Of these, the core hole drilled in 1986 near Exmore, Virginia, east of Chesapeake Bay on the Delmarva Peninsula (Fig. 1), encountered sections of well-known Upper Eocene, Oligocene, Miocene, and Pleistocene marine and paralic sediments in normal stratigraphic order, but it also encountered a basal unsorted and unstratified unit that consisted primarily of sediment clasts in a sediment matrix. Most clasts could be recognized as pieces of the known Cretaceous, Paleocene, and lower to middle Eocene formations in the region, some of which yielded fossil assemblages with complementary ages. The matrix consisted of calcareous, clayey quartz-glaucouite-feldspar sand that contained a mixture of Cretaceous, Paleocene, and Eocene fossils. A similar section was subsequently found in the Kiptopeke, Newport News Park, and Windmill Point cores (Fig. 1). The resemblance of this unit to Cederstrom's Mattaponi Formation suggested that this unit was widespread in the southern Chesapeake Bay area.

Powars et al. (1992) informally named this unit the Exmore beds and suggested that it originated as a subaqueous channel fill or as a debris flow at the base of a paleoshelf or a fault scarp. Poag et al. (1992) referred to the unit as the Exmore boulder bed and suggested that it was produced by a huge impact-generated oceanic wave train that scoured the Virginia inner shelf and coastal plain. They illustrated a lightly shocked quartz grain from the Exmore unit in a new drill hole at Newport News Park (Fig. 1) near the structure's outer margin, as presently known, which supported the connection with an impact event. They further

suggested that a possible impact structure located on the outer continental shelf offshore of New Jersey could have been the source of the wave train. Poag and Poppe (1998) subsequently named that feature the Toms Canyon impact structure. The Toms Canyon feature is not presently recognized as a confirmed impact structure in the Earth Impact Database (2018).

Subsequently, Powars et al. (1993) proposed that the buried Chesapeake Bay structure was, in fact, an *in situ* impact structure and not the result of processes generated by a distant impact event. A following article by these authors used petroleum-industry seismic-reflection surveys acquired in Chesapeake Bay and its tributary rivers (see following section), the results of the core-drilling program, and comparison with the Miocene Ries impact structure of Germany to interpret the presence of a buried, 85-km-wide, peak-ring impact structure in the southern Chesapeake Bay area (Poag et al., 1994). The name of the Exmore unit was changed in that paper to the “Exmore breccia,” using the then-current interpretation that the unit consisted primarily of ejecta.

In a concurrent study, Poag and Aubry (1995) assigned a late Eocene age to the “Exmore breccia” on the basis of the youngest planktic foraminifera, calcareous nannofossils, and bolboformids found in cores of the unit. Noting this age, Poag et al. (1994) suggested that the Chesapeake Bay structure was the likely source of the Eocene North American tektite strewn field (Glass, 1989).

Koeberl et al. (1996) provided additional data and analysis that further substantiated the interpretation of the Chesapeake Bay impact structure as a large impact structure. A newly compiled gravity map showed a prominent circular negative anomaly that spatially corresponded with the previously defined “inner basin” (central crater on Fig. 1). This feature is now known to be the collapsed and filled transient cavity of the impact structure (e.g., several chapters in Gohn et al., 2009a, 2009b). Koeberl et al. (1996) also examined a total of 65 samples of the Exmore sediments from four core holes. Of these, 14 contained deformed mineral grains with features typical of the high-pressure alteration seen in minerals from impact structures. Shocked quartz and feldspar were present as separate grains and as grains in rock clasts, and some granitoid rock clasts were partially to almost totally melted.

Investigations in 1996–2004

The confirmation of the Chesapeake Bay feature as a large, buried impact structure was followed by a series of articles that provided more detailed analyses of its structure, age, stratigraphy, and formative processes. The principal new data sets for these studies were seismic-reflection surveys that were acquired by the USGS or provided to the USGS by several organizations between 1975 and 2000 (Powars and Bruce, 1999, Appendix 3; Poag et al., 2004, p. 77–85). Chief among these were 310 km of 48-fold, multichannel seismic-reflection profiles collected in Chesapeake Bay by Teledyne Exploration Company for Texaco, Inc. (now Chevron, Inc.), and Exxon Exploration Company.

Poag (1996, 1997) used the seismic-reflection profiles and existing drill-hole data to illustrate the principal structural elements of the Chesapeake Bay impact structure. He characterized the structural outer rim of the annular trough as “a 90 km diameter ring of terraced normal-fault blocks, which forms a ~320 m–1,200 m high rim escarpment” (Poag, 1996, p. 223). Essentially undisturbed pre-impact sediments and basement rocks were interpreted to be present outside this outer-rim escarpment.

Inward from the rim, the structure was interpreted to consist of a flat-floored annular trough (brim of this report; Figs. 1, 2, and 3) filled with ~250 m of “Exmore breccia” above a 200–800-m-thick interval of slumped megablocks of pre-impact sediments that overlie basement rocks. The transition interval from the annular trough inward to a central structural low called the inner basin was interpreted as a peak ring. This term implies the outflowing collapse of a central uplift to produce the peak ring and genetically associated inner basin (Melosh, 1989; Kenkmann et al., 2013). Poag et al. (1999) used the same terminology for these features, but they also tentatively recognized a central peak at the center of the inner basin, thereby suggesting the presence of a crater that was morphologically intermediate between a central peak and a peak ring structure (Melosh, 1989, chap. 8).

In addition to the structural morphology, Poag (1996, 1997) also described the lithologic composition and distribution of the “Exmore breccia” and its paleontologically determined late Eocene age using material from the available core holes. In addition, Poag and Aubry (1995) and Poag and Commeau (1995) analyzed new and existing biostratigraphic data to update and summarize the regional stratigraphic setting of the Chesapeake Bay impact structure.

Poag (2002) discussed the transition from late synimpact to early postimpact sediments in the Chesapeake Bay impact structure using cores from the then newly drilled National Aeronautics and Space Administration (NASA)–Langley core hole (see next section) and the Exmore and Windmill Point core holes. He placed the boundary in the uppermost part of the “Exmore breccia” between a thin layer of possible fallout microspherules, represented as molds in pyritic, fine-grained sediments, and an overlying thin layer that contained reworked microfossils but no indigenous fauna (“dead zone”). This “dead zone” is overlain by burrowed, fine-grained shelf sediments with an indigenous microfauna in the postimpact Chickahominy Formation. Poag (2002, his figure 5) and Poag et al. (2004, their figure 6.32) also illustrated glass microspheres in thin sections of sediments that were stratigraphically deeper than the pyrite-lattice layer at Langley in the Exmore core and the Newport News or Windmill Point cores (compare cited figures).

In 1997, the USGS and the Hampton Roads Planning District Commission (HRPDC) began a research program to investigate the subsurface geologic and hydrogeologic settings of the Chesapeake Bay impact structure and surrounding areas in southeastern Virginia. In the first phase, Powars and Bruce (1999) published lengthy descriptions of the stratigraphic units underlying the York-James Peninsula (Fig. 1), including those within

the impact structure, using new and old data from the recently drilled core holes and over 100 water wells. Locations of these drill holes and the stratigraphic tops of units were included as tables, and descriptions of cuttings from several of Cederstrom's (1945, 1957) water-well logs were reprinted. The geographic distributions of the stratigraphic units in the subsurface were shown in figures, and seismic profiles and drill-hole cross sections were shown on plates.

Powars and Bruce (1999) divided the crater-fill section on the York-James Peninsula into two units, in a manner similar to Poag (1996, 1997). The upper unit was informally called the "Exmore tsunami-breccia" and was interpreted to be the result of "gigantic tsunami backwash into the crater." The lower unit was informally called the megablock beds. Despite limited drill-hole data, this unit was interpreted to consist of Lower Cretaceous fluvial-deltaic sediments.

In the second phase of the USGS-HRPDC study, Powars (2000) completed a regional stratigraphic and hydrogeologic analysis of the Virginia Coastal Plain south of the James River using new core holes and existing water wells (Fig. 1). Drill-hole cross sections in this report only extended a short distance across the outer rim of the Chesapeake Bay impact structure and into the annular trough (brim), where they primarily intersected only the "Exmore tsunami breccia."

Poag et al. (2004) published a wide-ranging summary of the Chesapeake Bay impact structure investigations conducted and published to that time. Major topics included the geologic and geophysical frameworks of the Chesapeake Bay impact structure and the surrounding area, the developmental history and age of the structure, impact models and comparisons to other impact structures, biospheric effects of the impact, and some early analyses of recently drilled core holes (see next section). Numerous seismic profiles and core photos were included, and tables and maps listed and illustrated borehole locations and seismic track lines.

Second Core-Drilling Program and York-James Seismic Survey

A second round of core drilling by the USGS, the Virginia Department of Environmental Quality (VDEQ), and the HRPDC took place in 2000–2002. This program was focused on learning more about the stratigraphy, structure, and boundary of the Chesapeake Bay impact structure, and its relationship to the saline groundwater known to be present within the structure, in the area west of Chesapeake Bay (Fig. 1). Core holes were drilled at the NASA–Langley Research Center to a depth of 635.10 m (Horton et al., 2005a, 2005b, 2005c, 2005d, 2005e), at North to 435.1 m (Horton et al., 2008), at Watkins School to 300.4 m (Edwards et al., 2010), and at Bayside to 728.47 m (this report; Fig. 1). The Langley and Bayside holes reached unshocked Neoproterozoic granite below sections of impact-disrupted and postimpact sediments. The North core hole stopped within a section of impact-disrupted crater sediments below postimpact sediments, and the Watkins School core hole stopped within undisrupted Cretaceous

sediments below a thin section of seawater-resurge deposits beneath overlying postimpact sediments at the margin of the Chesapeake Bay impact structure.

In conjunction with the new drilling, the USGS completed a high-resolution seismic-reflection survey from the NASA–Langley site to near the Watkins School site on the York-James Peninsula in 2000 (Fig. 1). Results of part of this study were published in Catchings et al. (2005) and Horton et al. (2008).

International Continental Scientific Drilling Program and USGS Drilling and Geophysical Studies in the Central Crater

The International Continental Scientific Drilling Program (ICDP) and the USGS conducted a series of investigations within the Chesapeake Bay impact structure central crater (collapsed transient crater) in 2004–2006. The USGS drilled a partially cored test hole into the central peak near Cape Charles (Fig. 1) to a depth of 823 m in 2004 (Sanford et al., 2004; Gohn et al., 2007; Horton et al., 2004, 2005c, 2008). Postimpact (0–355 m) and synimpact (355–655 m) sediments were recovered as cuttings above a mostly cored section of crystalline-clast suevite, blocks of shocked Neoproterozoic quartzofeldspathic gneiss, and blocks of slaty metamorphic rocks (655–823 m). The Cape Charles core hole demonstrated the feasibility of drilling in the central crater and provided a P-wave velocity log to 823 m depth in advance of drilling a planned ICDP-USGS deep core hole.

The USGS also acquired a series of seismic profiles across the central crater in the Cape Charles area in 2004. Several short, high-resolution seismic-reflection profiles were acquired, two of which crossed the proposed ICDP-USGS drill site and subsequently were published by Powars et al. (2009). Catchings et al. (2008) acquired a 30-km-long refraction and low-resolution seismic line that extended from the central peak near Cape Charles beyond the margin of the central crater to a point in the brim south of Exmore (Figs. 1 and 2). These surveys confirmed some of the primary structural elements of the Chesapeake Bay impact structure and the viability of the site previously selected for the planned ICDP-USGS core hole. However, the interpreted distribution of rock and sediment types led to the conclusion that the Chesapeake Bay impact structure is a central-peak structure with an uplifted rim as the boundary of the collapsed transient crater (Fig. 2), rather than a peak-ring structure or peak-ring and central-peak structure as previously interpreted (e.g., Poag et al., 2004).

Following these studies, the ICDP and USGS drilled three vertically overlapping core holes at Eyreville Farm, located north of Cape Charles, to a total depth of 1766 m in the outer part (moat) of the central crater in 2005–2006 (Fig. 1). The results of the initial investigations of these cores and related data were published in 42 chapters in Gohn et al. (2009a). The cored section consisted of postimpact sediments (0–444 m), Exmore resurge sediments (444–867 m), sediment boulders and sand (867–1096 m), a granite megaclast (1096–1371 m), sand and crystalline blocks (1371–1397), suevite and clast-rich melt rocks (1397–1474 m),

polymict impact breccia and blocks of cataclastic gneiss (1474–1551 m), and a basal section of schist, gneiss, coarse to pegmatite granite, and impact-breccia dikes and veins (1551–1766 m).

Beneath the resurge sediments, the allochthonous rocks and sediments between depths of 867 m and 1397 m at Eyreville were interpreted to be derived from the rim of the transient cavity as one or more sediment and (or) rock avalanches (Edwards et al., 2009; Gohn et al., 2009b; Horton et al., 2009b; Kenkmann et al., 2009). The melt-bearing section, from 1397 m to 1551 m, was interpreted to represent a complex interaction of the excavation flow in the transient cavity with material slumped from the cavity wall, ejecta returning from the ejecta plume, and slumped material from the central peak (Horton et al., 2009b; Wittmann et al., 2009). The basal section of the core consisted of allochthonous basement-derived rocks that were moved but not ejected by the excavation flow (Horton et al., 2009b). A zone of graphitic cataclasite at the top of the basement-derived rock section likely represents a low- to moderate-dipping fault contact with the overlying melt-bearing section (Horton et al., 2009b).

History of Groundwater Studies

The decades-long geologic study of the genesis of the Chesapeake Bay impact structure was accompanied throughout by associated groundwater studies of hydrologic anomalies in the southern Chesapeake Bay area. Early groundwater studies discovered a broad high-salinity anomaly within the impact structure (Sanford, 1913; Cederstrom, 1943, 1957). This “salt-water wedge” extends up to 50 km inland from the modern coast. Groundwater salinities higher than seawater occur in thick zones below a depth of ~300 m and are ubiquitous below ~600 m (McFarland and Bruce, 2005). The location of the “wedge” corresponds to the location of the Chesapeake Bay impact structure, thereby suggesting a causal relationship with the impact event.

Sanford (2002) proposed that the groundwater within the central crater consists of seawater emplaced at the time of impact and that subsequent upward flow rates and molecular diffusion rates were insufficient to remove the saline water. Subsequently, Sanford (2003) used a simulation of heat conduction, which assumed a 1000 °C initial postimpact crustal temperature at depth, with temperatures peaking in the overlying sediment after ~10,000 yr, to suggest that the pressure and temperature conditions within the sediment during that time would have allowed for phase separation and generation of residual brine at depth.

Poag et al. (2004) considered a variety of previously proposed models for the generation of the saline water in the Chesapeake Bay impact structure. They preferred a model in which flash vaporization of seawater at the point of impact and seawater boil-off at greater radial distances, followed by thousands of years of heating by shock-heated basement, produced the saline water, in general agreement with Sanford (2003). The deposition of postimpact fine-grained Eocene sediments would have sealed the structure before a significant amount of the saline water could be lost due to upward flow and molecular diffusion.

Sanford et al. (2009) suggested a pre-impact origin for the brine in the deep Eyreville core holes on the basis of its major-ion chemistry. They also indicated that upward transport of the brine was produced primarily by molecular diffusion and slow compaction-driven upward flow. Most recently, Sanford et al. (2013) noted the presence of remnant Early Cretaceous brines in several deep drill holes along the outer U.S. Atlantic coastal margin. In this context, they suggested, on the bases of chemical, isotopic, and physical data from the deep brine in the Chesapeake Bay impact structure, that it also is in situ, connate, high-salinity seawater from the incipient, small Early Cretaceous North Atlantic Ocean.

BRIM OF THE CHESAPEAKE BAY IMPACT STRUCTURE

Structural Morphology of the Chesapeake Bay Impact Structure

Early studies of the Chesapeake Bay impact structure, discussed above, classified this structure as a complex peak-ring (or peak ring–central peak) impact crater that was significantly modified by ocean resurge (Poag, 1996, 1997; Poag et al., 2004; Powars and Bruce, 1999; Powars, 2000). More recently, Poag (2012) substituted the term “crystalline inner ring” for the term “peak ring.”

The core-drilling programs and seismic-reflection surveys conducted since 2000 eventually led to a revised interpretation of the Chesapeake Bay impact structure as a complex central-peak crater modified by ocean resurge (Figs. 1, 2, and 3; Horton et al., 2005a, 2008; Catchings et al., 2008; Edwards et al., 2010). In this interpretation, the structure includes a central, ~35-km-diameter, collapsed and filled transient crater. This central crater consists of a collapsed central peak surrounded by an annular moat (ring “syncline” or doughnut-shaped depression) bounded by a raised rim that previously had been interpreted as a collapsed peak ring. The central-crater rim is the inner margin of an ~25-km-wide outer annular trough, herein called the brim, which is the focus of this report. The outer margin of the brim is generally cited as the outer rim of the impact structure. However, Powars et al. (2002, 2016) defined an outer fracture zone on the basis of localized occurrences of faulted target sediments and seawater-resurge sediments found outside the traditional outer margin of the brim. The presence of these distal features indicates that effects of the impact extend beyond the generally cited ~85 km diameter of the combined central crater and brim, but the details of these features and their distribution are not adequately known at present.

Data Sets

Core Holes

This report primarily uses core-hole data to interpret the impact processes (and their mutual interactions and relative

timing) that produced the disruption, erosion, transport, and redeposition of the target-sediment layer outside the transient crater. We studied or restudied cores from three sites (Watkins School, Langley, Bayside; Fig. 1) that provide a radial transect of the postimpact target-sediment layer in the brim on the western side of the structure. The basal sections of rock recovered in the Langley and Bayside cores also were examined because of their possible involvement with the deformation and movement of the target-sediment layer. In addition, we compared the analyses of the three brim cores to published analyses of the displaced target sediments recovered in the Eyreville cores from the collapsed transient cavity (Edwards et al., 2009; Gohn et al., 2009b; Kenkmann et al., 2009).

New X-ray diffraction (XRD) mineralogic data were acquired from the three cores, and new optical mineralogic, petrologic, stratigraphic, sedimentologic, and paleontologic data were acquired from the impact-generated and modified sediments, and the basal granite, in the Bayside core.

Seismic Surveys

Seismic-reflection surveys have played an important role in the study of the Chesapeake Bay impact structure. Low-resolution marine surveys (e.g., Powars and Bruce, 1999; Poag et al., 1999, 2004) and high-resolution land surveys, particularly high-resolution surveys across the Langley and Eyreville core sites (Catchings et al., 2005; Powars et al., 2009), provided constraints on the interpretations used in the following discussion. The seismic-refraction and low-resolution reflection survey along a radial 30 km transect of the central crater and part of the brim (Catchings et al., 2008) was used in interpreting the central (collapsed transient) crater (Fig. 2).

Hydrocode Models

Studies using hydrocode models have produced significant advances in understanding the Chesapeake Bay impact event. We used the two-layer numerical model of Collins and Wünnemann (2005), and the three-layer models of Crawford and Barnouin-Jha (2004), Collins et al. (2008b), Kenkmann et al. (2009), and Wünnemann et al. (2010), in combination with core-hole data and seismic surveys, to provide constraints and possibilities for interpreting the evolution of the Chesapeake Bay impact structure brim, as summarized below in a conceptual model.

Pre-Impact Target Materials

Layer Thicknesses

The Chesapeake Bay impact target consisted of an eastward-deepening layer of seawater estimated to range from ~0 to ~200 or possibly ~300 m across the Eocene shelf and ~70 to ~130 m in the midshelf impact zone (Poag, 2012; Poag et al., 2004; Horton et al., 2005d). Below the water layer, an eastward-thickening layer of Cretaceous and Paleogene sediments (~350 to ~1700 m) rested on continental basement rocks (Powars and Bruce, 1999; Powars et al., 2008, 2016; Poag et al., 2004).

Basement Rocks

Cored sections of basement rocks from the brim consist of Neoproterozoic granitic rocks at Langley and Bayside (Horton et al., 2002a, 2002b, 2005b, 2005c). Blocks of slaty metamorphic rocks and shocked Neoproterozoic granitic gneiss are present with suevite in the central peak at Cape Charles (Horton et al., 2004, 2005d, 2008). Clasts representing a variety of metaigneous and metasedimentary target rocks are present in suevite and shocked and unshocked rock breccias beneath sediment-clast breccias in the moat of the central crater at Eyreville (Bartosova et al., 2009; Horton et al., 2009a, 2009b; Wittmann et al., 2009). Regional studies of rocks beneath the sediments of the Virginia Coastal Plain suggest that the impact structure straddles the boundary between greenschist-facies rocks of the Chesapeake terrane to the west and amphibolite-facies rocks of the Hatteras terrane to the east (Horton et al., 2011, 2014, 2016).

Potomac Formation

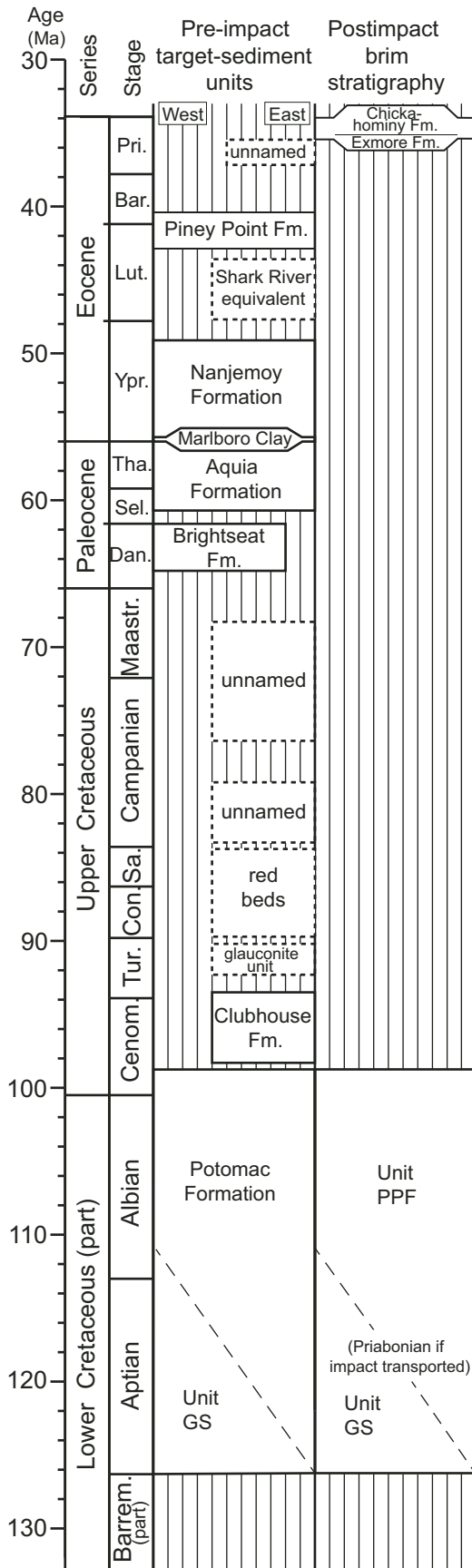
The basement rocks were covered by widespread sediments of the Lower to lower Upper Cretaceous Potomac Formation at the time of impact (Fig. 4; Powars and Bruce, 1999; Powars, 2000; Poag et al., 2004; Gohn et al., 2005; Hochuli et al., 2006; Powars et al., 2016). This unit also is referred to as the Potomac Group in Maryland and by some authors in Virginia. The Potomac Formation primarily consists of: cross-bedded, feldspathic, sandy gravels, gravelly sands, and sands; and oxidized or dark-gray muds with roots casts, lignite, and sparse caliche. These sediments are commonly arranged in cyclic fining-upward successions that are up to 30 m thick and suggest fluvial deposition in mixed-load channels, levees, and floodplains (Miall, 2010). The Potomac Formation is as thin as ~200 m west of the impact structure and as thick as ~650 m in the onshore areas northeast and southeast of the structure. For the immediate impact area, we estimate a pre-impact thickness of ~400 to ~500 m.

Upper Cretaceous Marine and Nonmarine Sediments

Upper Cretaceous sediments were present above the Potomac Formation only in the northeastern and southern parts of the target area (Fig. 4; Powars and Bruce, 1999; Poag et al., 2004; Gohn et al., 2005). They include Cenomanian, Campanian, and Maastrichtian marine beds and Coniacian–Santonian marine and nonmarine beds. The Cenomanian beds are assigned to the Clubhouse Formation (Weems et al., 2007), but the sediments of other ages are unnamed. The marine beds primarily consist of fossiliferous, glauconitic, muddy, fine-grained sands. Coniacian–Santonian oxidized sandy gravels, sands, and clays resemble the Potomac Formation. The maximum combined pre-impact thickness of these units increases from ~40 m northeast of the impact structure to ~125 m southeast of the structure.

Paleogene Marine Sediments

Two categories of Paleogene target units are represented in the studied cores: (1) those that are present in cores near the impact structure and in cores and outcrops of the updip Virginia Coastal



Plain, and (2) those that are not presently known from the Virginia Coastal Plain but must have been present during the late Eocene.

Known Paleogene units in Virginia include: the Brightseat (Lower Paleocene) and Aquia (Upper Paleocene) Formations, the Marlboro Clay (Lower Eocene), and the Nanjemoy (Lower Eocene) and Piney Point (Middle Eocene) Formations (Fig. 4; Powars and Bruce, 1999; Powars, 2000; Poag et al., 2004; Powars et al., 2016). These marine units are locally absent due to pre-impact erosion and typically consist of glauconitic, quartz sand that is variably fossiliferous, calcareous, and muddy. They are mostly unconsolidated but are locally indurated, typically by carbonate cement. The Marlboro Clay is a relatively thin (0–15 m), kaolin-rich unit that lacks sand and thus is more cohesive than the other Paleogene units. The known combined thickness of the Paleogene units is 8–80 m in the target area.

A previously unknown target unit of middle Eocene age is represented in the studied cores by microfossils that are younger than those in the Nanjemoy Formation and older than those in the Piney Point Formation. These fossils are reworked into matrix and clasts of the synimpact Exmore Formation (Frederiksen et al., 2005). Sediments of similar age from a core in Maryland were termed “Shark River equivalent,” in reference to a formation recognized in New Jersey (Alemán-González et al., 2012; see also Fig. 2 herein). Its reported thickness is 16 m in Maryland.

Frederiksen et al. (2005) reported that microfossils younger than the middle Eocene Piney Point Formation and older than the postimpact, Upper Eocene Chickahominy Formation are abundant in the matrix, and in a single silty-clay clast, of the Exmore Formation. Sediments of this age represent the youngest target sediments, some of which were still accumulating on the continental shelf at the time of the late Eocene impact (“unnamed” unit in Priabonian of Fig. 4).

Sediments Modified and (or) Redeposited by the Impact

Postimpact Sediment Groups

The target sediments can be combined into two lithologically contrasting groups for the purpose of identifying patterns of postimpact sediment distribution. Various mixtures of these groups constitute most of the materials found in the present impact-modified sediment layer of the brim.

Impact-generated clasts and disaggregated sediments from the moderately consolidated Lower and Upper Cretaceous

←

Figure 4. Stratigraphy of the pre-impact target sediments and the post-impact brim sediments. The gravel and sand unit (unit GS) is shown provisionally as a pre-impact Cretaceous target-sediment unit that was transported during the Eocene impact event and as an Eocene impact-generated and transported unit. The parautochthonous Potomac Formation (unit PPF) is shown provisionally as part of the pre-impact Cretaceous Potomac Formation that was transported during the Eocene impact event. These interpretations are considered in the Discussion section of the text. Time-scale abbreviations follow International Chronostratigraphic Chart (2018) (Cohen et al., 2013).

Potomac Formation are characterized by the presence of: quartz-feldspar-rich silt, sand, and fine gravel; dense, mottled, red, brown, and light-greenish-gray clays; and dark-gray, carbonaceous clays. Potomac-derived sediments do not contain glauconite or calcareous macrofossils and microfossils. Only sediments from the thinner and less widespread Coniacian–Santonian oxidized unit and perhaps the Eocene Marlboro Clay somewhat resemble the sediments of the Potomac Formation.

In contrast, clasts and disaggregated sediments from the poorly consolidated Upper Cretaceous and Paleogene marine units typically contain glauconite, calcareous macrofossils and microfossils, and carbonate cements. The generally medium- to dark-gray and medium- to dark-greenish-gray colors of the marine sediments also contrast with the oxidation colors of most Potomac sediments.

Deep Impact-Modified Target Sediments

Variably impact-modified, partial sections of the basal Potomac Formation are present in the studied cores from the brim (Fig. 4). The Potomac Formation in the Watkins School core is minimally disrupted (Edwards et al., 2010), whereas partial sections of Potomac sediments, represented by a parautochthonous Potomac Formation (PPF) unit at Langley and Bayside, and perhaps a gravel and sand (GS) unit at Bayside (Gohn et al., 2005), are more significantly disrupted and more deeply eroded. Redeposited boulders, blocks, and smaller clasts of Potomac Formation sediments are recognizable throughout the overlying synimpact Exmore Formation, except in its uppermost stratified member.

Exmore Formation

The Exmore Formation contains the record of catastrophic sediment erosion, transportation, and deposition by seawater-resurge mass flows and the transition back to normal shelf deposition within the impact structure. Powars et al. (1992) informally defined the Exmore beds on the basis of a cored section from the brim at Exmore, Virginia (Fig. 1). Through the years, the name, boundaries, and inferred formative processes of this unit have been repeatedly revised. Eventually, Edwards et al. (2009) formally defined the Exmore Formation on the basis of a thick cored section in the Eyreville core, which is located in the central crater (Fig. 1). Edwards et al. (2009) also recognized informal members of the Exmore Formation in the Eyreville core. From base to top, they are the lower diamicton member, block-dominated member, upper diamicton member, and stratified member. Stratigraphic subdivisions of these members are referred to here as subunits.

Early Postimpact Sediments

Chickahominy Formation

Fine-grained marine sediments of the upper Eocene Chickahominy Formation overlie the Exmore Formation across the entire impact structure and represent the return to normal shelf sedimentation (Fig. 4; Powars, 2000; Powars and Bruce, 1999;

Powars et al., 2005, 2009; Poag, 2012; Poag et al., 2004; Brown et al., 2009; Edwards et al., 2009, 2010). Thicknesses of the Chickahominy Formation in the cored sections vary from 3 to 94 m. Today, it occurs only in the subsurface near and above the impact structure.

METHODS AND TERMINOLOGY

Methods

We used site descriptions and photographs of the cores and published, unpublished, and newly collected lithologic, petrologic, mineralogic, paleontologic, and sedimentologic data from the Watkins School, Langley, and Bayside cores to document the spatial distribution of features indicative of in-place target disruption and the processes of sediment erosion, transportation, and redeposition during the impact event. Catalogued features included: undisrupted and minimally disrupted sediments; the composition, size distribution, internal disruption, and rotation of target-sediment clasts; variations in the proportions, types, and ages of the clasts, disaggregated target sediments, and faunas and floras, in mixed sections; the proportions and types of ejecta clasts; the presence or absence of shock features in mineral grains within rock clasts and individual mineral grains; the compositions, types of stratification (if any), and grain-size distributions of resedimented units; and the presence of liquefaction and fluidization features.

The Langley and Bayside cores were examined, measured, and sedimentologically logged in detail at a scale of 1:50 at the USGS core storage facilities in Reston, Virginia, during 2007 and 2011 by H. Dypvik. Samples (20–40 g) were collected during this work from various sediment and rock units and split into two parts. One part was impregnated with blue-stained epoxy, cut, and polished for thin section analysis. The other part was crushed to powder in a micronizer and analyzed on a Bruker 8 X-ray diffractometer located at the Department of Geosciences, University of Oslo, Oslo, Norway. Generally, XRD bulk analyses were run, but some selected clay-fraction analyses also were conducted on untreated, ethylene-glycolated, and heat-treated (350 °C, 550 °C) powders, respectively. Semiquantitative mineral calculations were done using the positions and heights of selected characteristic mineral peaks. See Ferrell and Dypvik (2009) for details of the whole-rock XRD quantification method.

Forty-four thin sections of samples from the Bayside core were examined at the USGS facilities in Reston, Virginia, by optical petrographic microscope for mineralogy, texture, and features diagnostic of shock metamorphism. These thin sections included six of fresh granite, five of altered granite, seven of rock clasts from the gravel and sand unit (unit GS), and 26 rock clasts from the Exmore Formation at depths ranging from 653.89 m to 299.62 m. In addition, quartz and feldspar grains from acid-etched residues of seven sediment samples below the Exmore Formation in the gravel and sand (GS) and parautochthonous Potomac Formation (PPF) units, at depths ranging from 708.39 to 682.87 m, also were

examined by optical petrographic microscope for possible evidence of shock-induced planar deformation features.

Palynological processing of cleaned and scraped core material was performed in USGS laboratories using digestion in hydrochloric and hydrofluoric acids. Most samples were subjected to oxidation in nitric acid and to either heavy liquid (zinc chloride at 2.0 specific gravity) or repeated soap floats and centrifugation. Residues were sieved at 10 μm or 20 μm and 200 μm , stained with Bismark brown, and mounted in glycerin jelly. Three hundred specimens were counted for estimates of fragmental versus whole/nearly whole cysts. Laboratory notations on the reaction of samples to HCl (none, mild, moderate, or vigorous) were used to note relative calcium carbonate contents.

Terminology

Sediment grain-size classes and nomenclature used in this report follow the extended Udden-Wentworth scale of Blair and McPherson (1999) as modified by Blair and McPherson (2009), including the terms “granule” (2–4 mm), “pebble” (4–64 mm), “cobble” (64–256 mm), “boulder” (0.256–4.1 m), “block” (4.1–65.5 m), and “megablock” (65.5–1048.6 m). The term “granule” is retained from the 1999 size scale. This grain-size nomenclature does not carry any shape connotations.

The “megablock” clasts of this report previously were referred to as “slabs” in the earlier nomenclature of Blair and McPherson (1999), and the term “slabs” was used throughout the published multichapter report on the Eyreville core (Gohn et al., 2009a). “Megaclast” is used here as a general term for clasts that are larger than boulders. The term “megablock” has been used in a similarly general sense in earlier reports about the Chesapeake Bay impact structure. Apparent diameters recorded for clasts that are larger than the core diameter are one-dimensional values determined from their vertical extent in the cores. The term “diamicton” was defined by Flint et al. (1960a, 1960b) as a descriptive name for unconsolidated, unsorted, or poorly sorted sediments that contain a wide range of particle sizes. The term does not carry any genetic connotations. The terms “autochthonous” (formed or produced in the place where now found), “allochthonous” (formed or produced elsewhere than in its present place; of foreign origin, or introduced), and “parautochthonous” (a rock unit that is intermediate in tectonic character between autochthonous and allochthonous) are used here as defined in the online American Geosciences Institute *Glossary of Geology* (2015).

CORE DATA

Watkins School Core

Location and Stratigraphy

The USGS Watkins School core hole was drilled to a depth of 300.4 m in Newport News, Virginia, in 2002 (Fig. 1). It is located close to the outer margin of the brim, ~45 km from the center of the impact structure. This core hole penetrated Eocene to Pleisto-

cene postimpact sediments, Eocene synimpact sediments of the Exmore Formation, and bottomed in sediments of the Cretaceous Potomac Formation. Edwards et al. (2010) described the complex drilling history and the lithologic, petrologic, stratigraphic, and paleontologic aspects of the core. Shelton et al. (2006) and Self-Trail et al. (2009) described the effects of the impact on calcareous nannofossil assemblages of the target sediments. Poag (2012) discussed the biostratigraphy, biofacies, and postimpact recovery of the bolboformid and benthic and planktic foraminiferal assemblages of the Chickahominy Formation.

Potomac Formation, Lower and Upper Cretaceous (300.35–196.63 m)

A 103.7 m section of the Potomac Formation was cored at Watkins School (Figs. 5 and 6). Its upper contact with the Exmore Formation is irregular and erosive (Fig. 6), but the lower contact was not reached during drilling. A high-resolution seismic-reflection profile acquired adjacent to the Watkins School drill site shows the top of pre-Cretaceous rocks at a depth of ~540 m (Catchings et al., 2005; Edwards et al., 2010), indicating a local thickness of ~343 m for the Potomac Formation.

The recovered Potomac section consists of 10 fining-upward units of terrigenous, fluvial sediments, including sandy gravels, pebbly sands, silty to moderately well-sorted sands, clayey silts, and silty clays (Edwards et al., 2010). Sediment colors range from brown and red to light, medium, and dark gray. Horizontal and low-angle laminations are the most common sedimentary structures. Cross-laminations in sets and cosets of variable height, and root structures, are less common. Sparse centimeter-scale fluidization features are present near the tops of some fining-upward successions. The fluidization features probably resulted from rapid sediment loading at the overlying unit boundary and are not considered to be impact-generated features. The Cretaceous bedding is not rotated, and exotic Cretaceous and Paleogene marine sediments and fossils, as well as impact ejecta, are absent.

The Potomac section is uniformly noncalcareous and nonglaucconitic. The quartz sands in the section typically are feldspathic and fine to very coarse grained. XRD analysis of one silty clay sample indicated a clay mineral suite consisting of mixed-layer illite/smectite, illite, kaolinite, and chlorite/smectite in decreasing order of abundance (Table 1; Fig. 7). The detrital silt fraction of that sample consists of quartz with ~15% total feldspar.

Pollen and spore assemblages in four samples from the Potomac section have Cretaceous ages in normal stratigraphic order from middle to late Albian to early Cenomanian (Edwards et al., 2010). This age range is typical of the upper part of the Potomac Formation throughout the Mid-Atlantic region (Doyle and Robbins, 1977; Benson, 2006; Hochuli et al., 2006). The highest sample (211.2 m) was assigned to pollen zone III, which is the youngest zone found regionally in the Potomac Formation (Edwards et al., 2010). Sections of pre-impact Upper Cretaceous, Paleocene, and Eocene sediments are absent in the Watkins School core, presumably due to resurge erosion.

Watkins School Core

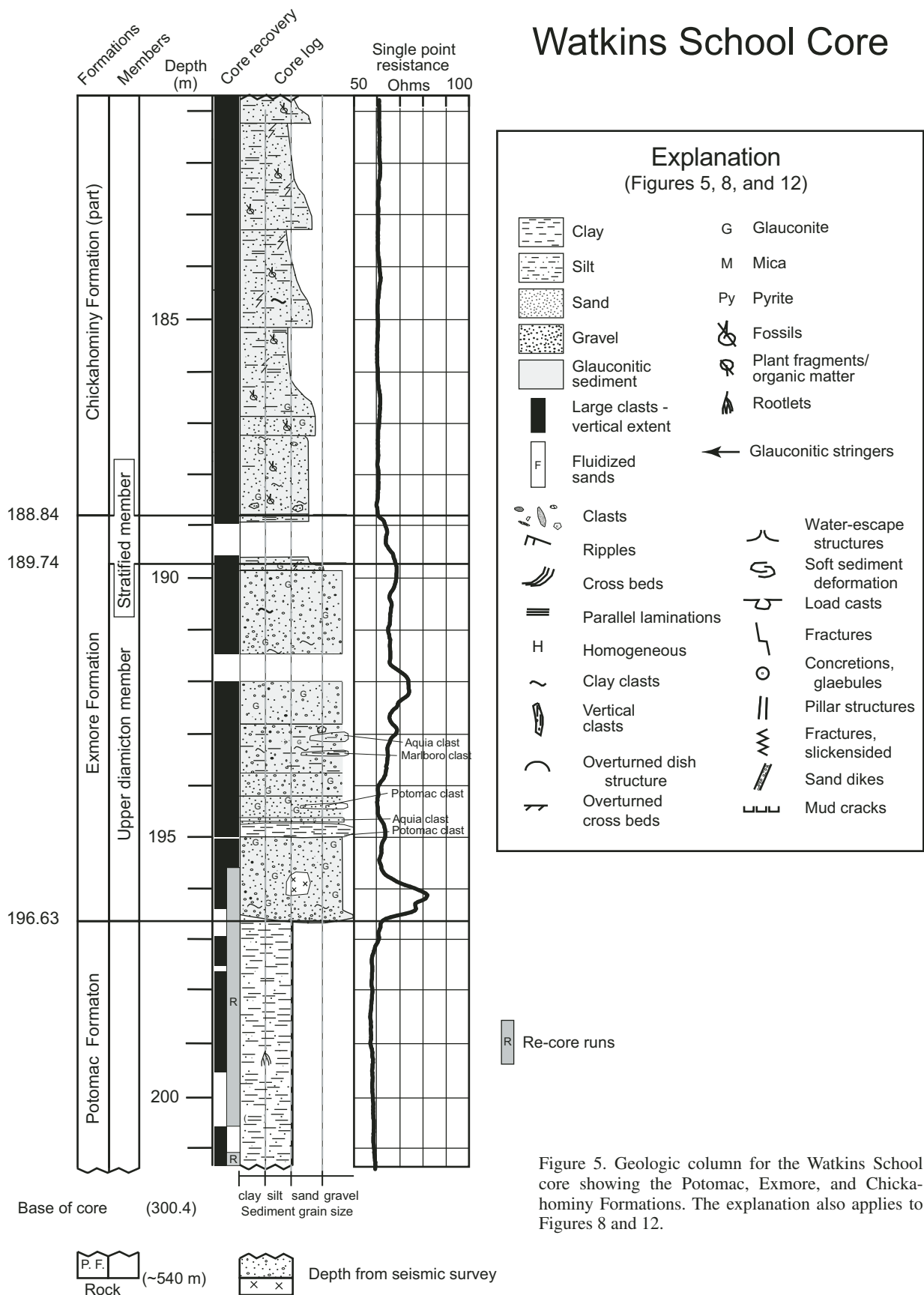
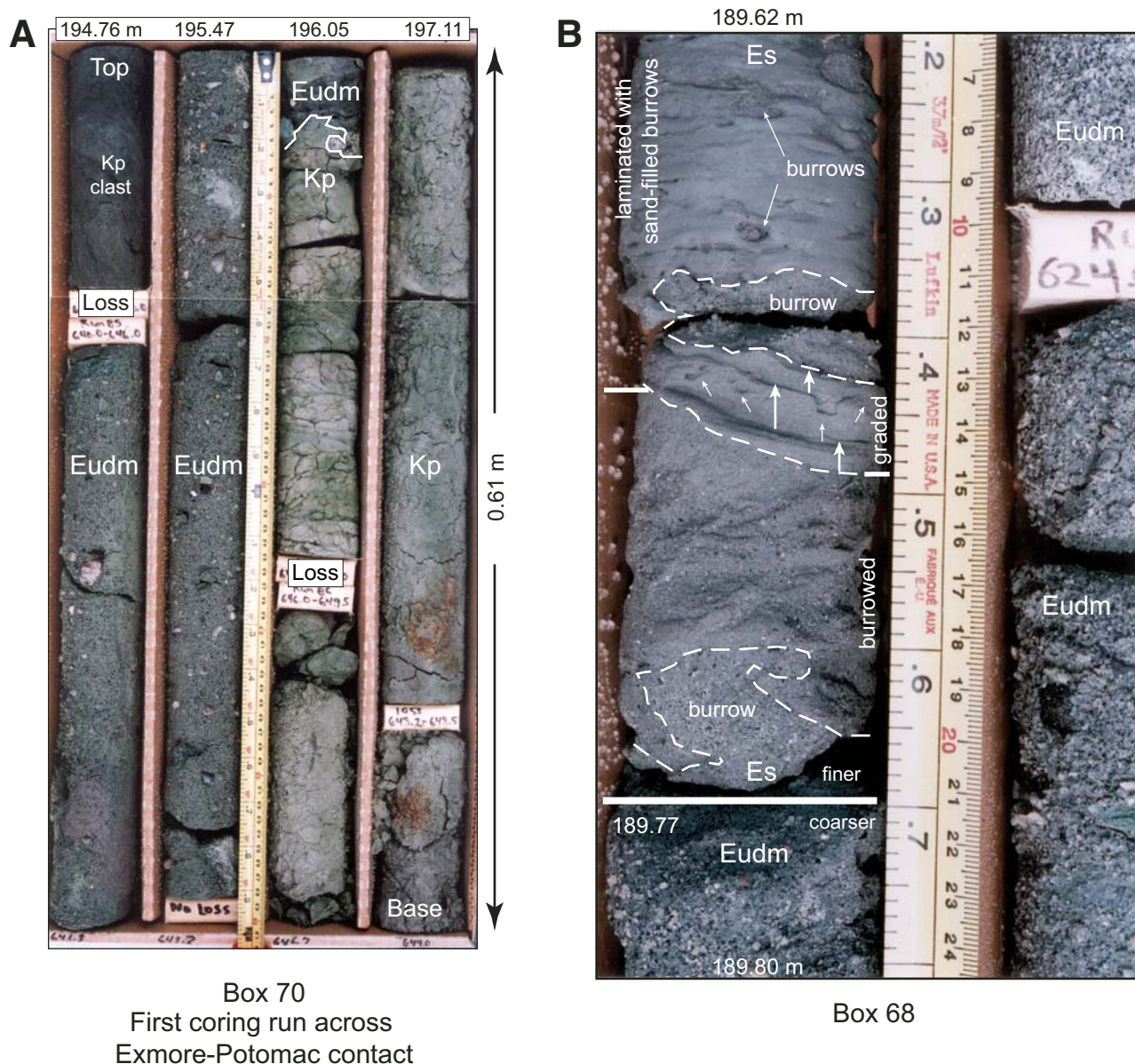


Figure 5. Geologic column for the Watkins School core showing the Potomac, Exmore, and Chickahominy Formations. The explanation also applies to Figures 8 and 12.



Box 70
First coring run across
Exmore-Potomac contact

Box 68

Figure 6. (See caption on following page.)

TABLE 1. WATKINS SCHOOL CORE: SEMIQUANTITATIVE, WHOLE-SAMPLE, X-RAY DIFFRACTION (XRD) MINERALOGY

	Sample no.	Feet	Meters	Chl/smec	Exp. phase mixed layer	Illite-glauc	Kaolinite	Zeolites	Gypsum
Chickahominy Formation									
Clay, silty & sandy	W598.5	598.5	182.4	2.13	3.67	9.52	2.68	0.00	6.97
Clay, silty & sandy	W613.9	613.9	187.1	1.73	3.62	10.10	2.13	0.00	9.81
Exmore Formation									
Clay, silty & sandy	W622.0	622.0	189.6	1.49	2.82	8.49	1.93	0.00	1.77
Sand, qtz-glauc-felds	W625.6	625.6	190.7	2.26	4.68	9.41	2.87	0.00	4.40
Sand, qtz-glauc-felds	W638.4	638.4	194.6	1.37	2.60	8.04	1.71	0.00	1.69
Potomac Formation									
Clay, silty	W652.9	652.9	199.0	1.63	16.25	7.63	3.25	0.00	0.00

Note: Gray shading—glauconite-bearing samples. Trends or anomalies in the abundances of selected minerals are shown by boxes. Chl/smec—mixed-layer chlorite/smectite; ExpPhase—mixed-layered, expandable illite/smectite; Illite-glauc—illite and (or) glauconite; Zeolites—heulandite/clinoptilolite series; K-fspr—potassium feldspar; qtz-glauc-felds—quartz-glauconite-feldspars.

Figure 6. Photographs of the Watkins School core. (A) Contact between the Potomac Formation (Kp) and the overlying upper diamict member of the Exmore Formation (Eudm). Contact is at 196.11 m depth in this initial core run across the contact. The contact is slightly deeper in deviated core run 2 at 196.63 m depth (Edwards et al., 2010). (B) Contact interval between the upper diamict member (Eudm) of the Exmore Formation and the overlying stratified member (Es) of the Exmore Formation. The member contact is at 189.77 m depth. Note the upward transition in the stratified member from basal burrowed, muddy sand to three thin graded beds (large arrows) with dewatering and associated slump features (small arrows) that are overlain by faintly laminated silty clay with sand-filled burrows.

Exmore Formation, Upper Eocene (196.63–188.84 m)

The Exmore Formation at Watkins School is nominally 7.79 m thick, although its thickness may vary by as much as ~0.5 m across short distances, as indicated by multiple redrilling efforts of its lower contact due to mechanical problems (Edwards et al., 2010). The upper contact separates variably laminated, sparingly glauconitic and microfossiliferous, clayey quartz silt at the top of the Exmore Formation from bioturbated, glauconitic, macrofossiliferous and microfossiliferous, clayey quartz silt at the base of the Chickahominy Formation.

Edwards et al. (2010) divided the Exmore Formation of the Watkins School core into two informal lithologic units of approximately member rank: the diamict unit (6.89 m) and the overlying laminated, silty unit (0.9 m). They nominally placed the intervening unit contact at 189.74 m due to core loss. Here, we refer to their diamict unit as the upper diamict member (undivided; 196.63–189.74 m) (Fig. 5). It consists of a polymict suite of sediment and rock clasts suspended in an unsorted, unstratified matrix of calcareous, muddy, feldspathic, quartz-glauconite sand and granules (Fig. 6). Glauconite typically constitutes 20%–40% of these size fractions.

Clasts in this member consist of granules, pebbles, cobbles, and sparse boulders that range from 2.0 mm to 0.76 m in diameter. The larger clasts were found in a possibly clast-supported section below 192.94 m. Maximum clast size decreases upward, and the unit is matrix supported above this basal section.

Sediments typical of the Cretaceous Potomac Formation and the Paleogene target formations (Figs. 5 and 6; Table 1) constitute the clasts in the diamict, including: gray, calcareous or noncalcareous, glauconitic or nonglauconitic muds and sands; oxidized, noncalcareous, nonglauconitic muds and sands; variably glauconitic shelly limestones and quartz sands; mollusk fragments; and quartz, quartz-feldspar, chert, and other lithic pebbles (Edwards et al., 2010).

Calcareous nannofossil assemblages were recovered from five of the larger Exmore sediment clasts located below 193.24 m. These assemblages, and the character of the clast sediments, indicate that two clasts, and probably a third clast, represent the Paleocene Aquia Formation, the fourth clast represents the Lower Eocene Marlboro Clay, and the fifth clast represents the Middle Eocene Piney Point Formation. Two clasts of Potomac sediments were barren. These seven clasts did not occur in normal stratigraphic order (Edwards et al., 2010).

Clasts of igneous rocks also are present in the upper diamict member but are less abundant than the sediment clasts. Observed rock types include aphanitic and porphyritic felsites (shocked and unshocked), shocked felsite cataclasite, and granitoids (shocked and unshocked; Edwards et al., 2010). These clasts are interpreted as impact ejecta. A sensitive high-resolution ion microprobe (SHRIMP) $^{206}\text{Pb}/^{238}\text{U}$ zircon age (weighted average of the $^{206}\text{Pb}/^{238}\text{U}$ ages) of 613 ± 4 Ma (2σ) was determined for a monomict felsite cataclasite boulder (Horton et al., 2005a), which indicates a Neoproterozoic crystallization age for this felsic volcanic rock. Rounded pebbles of quartz, quartzite, chert, and sparse diabase that lack cataclastic fabrics are considered to be recycled detrital clasts derived from disaggregated target sections of the Potomac Formation. Disaggregated quartz and feldspar grains in the diamict matrix were not examined for shock deformation.

Three samples of the diamict matrix contain mixed-age assemblages of dinoflagellate cysts derived from the Upper Cretaceous(?) and Paleogene target formations (Edwards et al., 2010). Species with ranges restricted to the Paleocene Brightseat Formation, the Lower Eocene Marlboro Clay or Nanjemoy Formation, or the Middle Eocene Piney Point Formation are consistently present. Numerous forms with ranges that include the Paleocene Aquia

Quartz	K-feldspar	Plagioclase	Calcite	Dolomite	Siderite	Pyrite	Sum	Quartz/ feldspar	Plagioclase/total feldspar	Chlorite/mixed layer
41.14	5.57	3.71	17.29	1.88	2.28	3.16	100.00	4.43	0.40	0.58
36.55	12.33	4.16	10.40	3.94	2.53	2.70	100.00	2.22	0.25	0.48
28.36	35.93	11.44	7.77	0.00	0.00	0.00	100.00	0.60	0.24	0.53
30.11	14.88	5.34	17.42	0.00	0.00	8.61	100.00	1.49	0.26	0.48
43.88	17.67	14.10	8.93	0.00	0.00	0.00	100.00	1.38	0.44	0.53
55.87	9.41	5.95	0.00	0.00	0.00	0.00	100.00	3.64	0.39	0.10

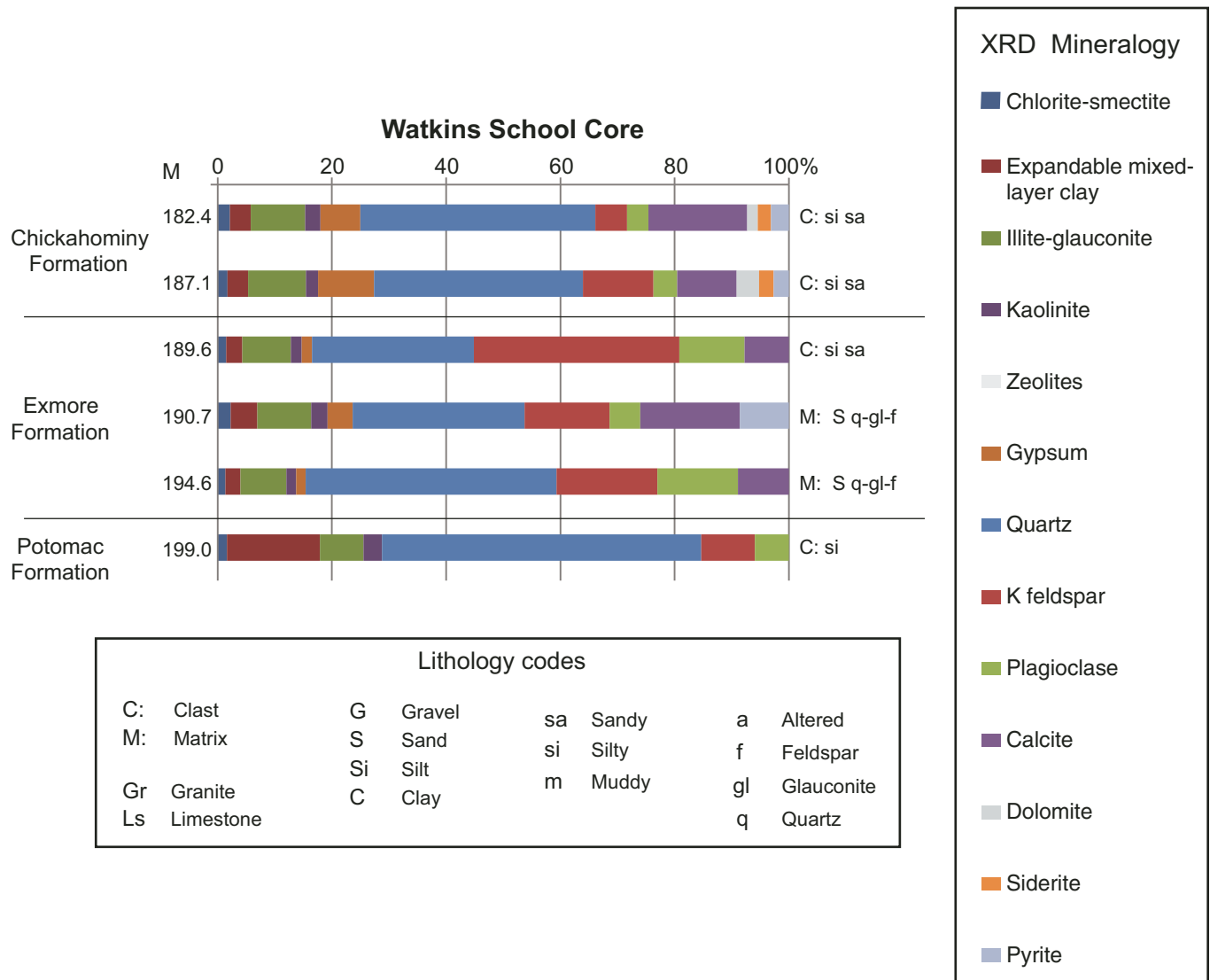


Figure 7. Mineralogic composition of core samples from the Watkins School core as determined by semiquantitative X-ray diffraction (XRD) analysis. Data are from Table 1.

Formation, but that are not restricted to the Aquia, also are present. Additional observed species that typically are not found in updip units of the Virginia Coastal Plain include: marine taxa that range from the Late Cretaceous into the Paleogene; early middle Eocene taxa; and taxa typical of Eocene strata that are younger than that of the Piney Point Formation but older than that of the Chickahominy Formation (Edwards et al., 2010).

Mixed-age assemblages of calcareous nannofossils were found in 20 samples of the diamicton matrix (Shelton et al., 2006; Self-Trail et al., 2009; Edwards et al., 2010). All samples contained species indicative of the Paleocene Brightseat Formation or Aquia Formation. Other species are indicative of the lower Eocene Marlboro Clay or Nanjemoy Formation, the middle Eocene Piney Point Formation, and possibly a pre-impact, unnamed upper Eocene unit. Late Cretaceous (Santonian–

Campanian) nannofossils were present only in seven samples from the uppermost part of the matrix at and above 190.80 m (Self-Trail et al., 2009).

The XRD analysis showed that illite and glauconite dominate over illite/smectite, kaolinite, and chlorite/smectite in the clay mineral suites of the matrix (Table 1; Fig. 7). Calcite and gypsum also are abundant, although the gypsum may be the result of evaporation of sulfate-rich pore water after core recovery. The analyzed thin sections show a clayey matrix with diagenetic calcite microspar, and pyrite, in addition to quartz and feldspars. The calcite and zeolite contents are the major compositional differences from the underlying Potomac Formation.

Here, we refer to the laminated, silty unit of Edwards et al. (2010) as the stratified member of the Exmore Formation; it is 0.90 m thick (189.74–188.84 m). The basal 6–7 cm consist of

muddy very fine to fine sand that contains numerous horizontal burrows (0.25–0.50 cm diameter) overlain by three 0.5- to 1.0-cm-thick, normally graded silt and clay beds (Fig. 6). The thickest graded bed contains several collapse structures caused by dewatering.

The upper part of the member consists of laminated clayey silt and silty clay. Burrows filled with underlying sandier sediment that was piped upward by the postimpact Chickahominy infauna are present (Fig. 6B). Irregular sand-filled burrows at the base of the member and immediately above the graded beds may represent the same population. The clay mineral suite in one XRD sample from this member is dominated by illite (glauconite included; Table 1). Feldspars are more abundant than quartz, and calcite is present, while dolomite, siderite, and pyrite are absent.

Two samples of the stratified member contained mixed-age assemblages of Paleogene dinocysts, and one also contained sparse Late Cretaceous forms (<1%). One sample from near the base of the member contained a mixed-age assemblage of Late Cretaceous and Paleogene calcareous nannofossils (Self-Trail et al., 2009; Edwards et al., 2010).

Chickahominy Formation, Upper Eocene (188.84–148.77 m)

The Chickahominy Formation at Watkins School consists of 40.06 m of compact, olive-gray, bioturbated to locally laminated, calcareous clayey silt and muddy very fine sand (Edwards et al., 2010). Its lower contact with the Exmore stratified member is sharp and conformable between massive clayey silt of the Chickahominy Formation and laminated clayey silt in the Exmore Formation.

The basal 1.52 m section of the Chickahominy Formation has scattered coarser grains, including botryoidal, black glauconite. Above the basal 1.52 m, there are three ~2-m-thick, fining-upward cycles (basal sandy silt to clayey silt to silty clay) from 187.27 to 181.26 m. Thicker fining-upward cycles are present at 181.26–167.09 m and 167.09–148.77 m. Moderate- to high-angle slickensided fractures and small-offset faults are present throughout the Chickahominy Formation in this core (Edwards et al., 2010).

The detrital sand and silt fractions of the Chickahominy sediments consist of abundant quartz and moderate amounts of K-feldspar and plagioclase, but less than in the underlying Exmore sediments. Subordinate, locally variable amounts of microfossils, macrofossil fragments, glauconite, phosphate, pyrite, and mica are present throughout the unit. The clay mineral suite is dominated by illite (including glauconite), with lesser amounts of mixed-layer illite/smectite, kaolinite, and chlorite/smectite, as indicated by XRD analysis (Table 1; Fig. 7). Calcite and gypsum are relatively abundant in the clay fraction, although the gypsum may be the result of the evaporation of sulfate-rich pore water after core recovery, as also noted for samples of the Exmore matrix. Minor dolomite, siderite, and pyrite also are present in the clay fraction.

Calcareous nannofossils from 14 samples of the Chickahominy Formation from the Watkins School core place the lower part

of the unit (samples at 169.7.0 m and below) in zone NP19/20 of late Eocene age and the upper part (samples at 165.6 m and above) in zone NP21 of late Eocene to early Oligocene age (Edwards et al., 2010). Marine dinocysts from five samples limit the age of the unit to the late Eocene (Edwards et al., 2010). Poag (2012) assigned this unit to planktonic foraminifera zones E15?, E15, and E16, which also are late Eocene.

Summary

The Watkins School core is representative of the outer margin of the brim. The principal characteristics of this section are the essentially undeformed character of the Potomac Formation and the thinness of the Exmore resurge sediments, as compared to cored sections located closer to the center of the brim (Langley) or the inner margin of the brim (Bayside).

Langley Core

Location and Stratigraphy

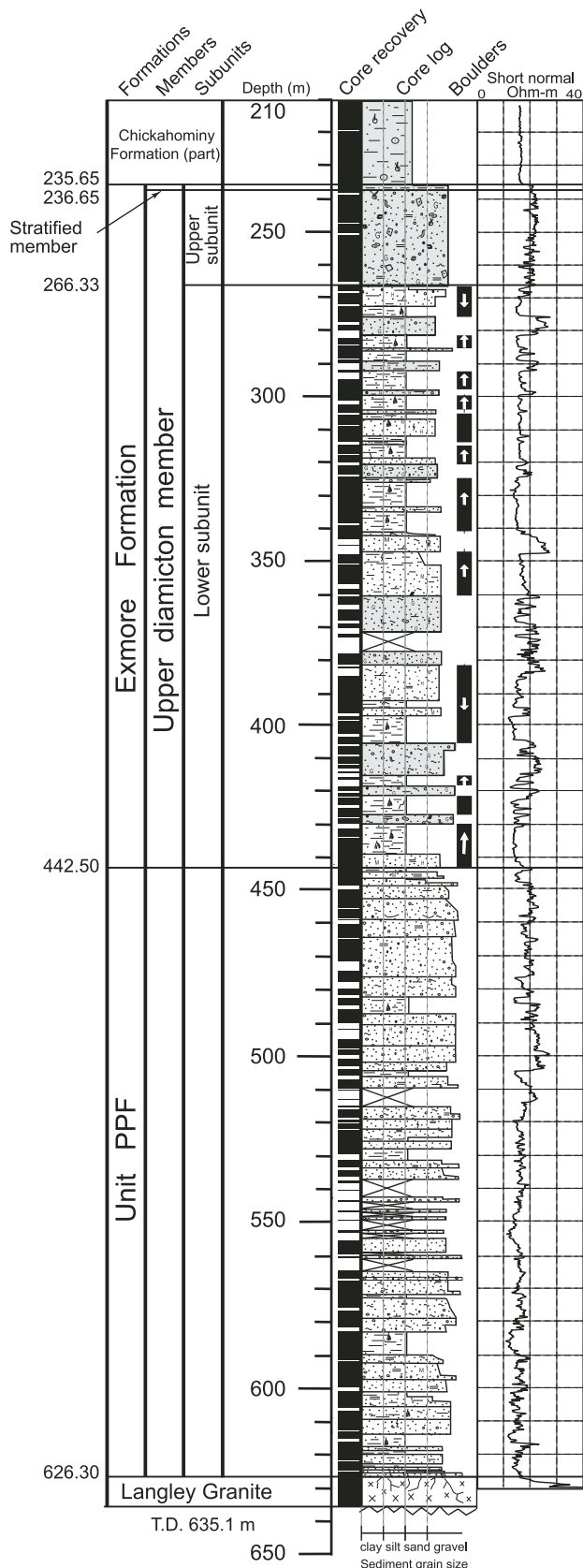
The USGS-NASA Langley core hole is located ~36 km from the center of the impact structure and ~6.5 km inside the outer margin of the brim as presently mapped (Fig. 1). It was drilled in year 2000 to a depth of 635.10 m at the NASA Langley Research Center in Hampton, Virginia. Beneath post-Eocene sediments, it successively penetrated early postimpact sediments (Chickahominy Formation), synimpact sediments (Exmore Formation), and parautochthonous sediments of the Potomac Formation (PFF unit) above an altered section of basement rock (Langley Granite; Fig. 8). Stratigraphic, petrologic, mineralogic, paleontologic, and textural analyses of this core were described in Poag et al. (2004) and several chapters in Horton et al. (2005e). Samples were taken for XRD mineralogic analysis, and the transition from the resurge sediments of the Exmore Formation to the postimpact sediments of the Chickahominy Formation was relogged. The present report adds a sedimentologic log, new sediment petrographic and mineralogic data, and stratigraphic information.

Langley Granite, Neoproterozoic (635.10–626.30 m)

The Langley Granite is a nonfoliated, medium-grained, peraluminous monzogranite consisting primarily of quartz, oligoclase, albite, microcline, and chlorite (probably pseudomorphous after biotite), as determined by thin section, XRD, scanning electron microscope, and chemical analyses (Table 2; Fig. 9; Horton and Izett, 2005; Horton et al., 2005b). Trace minerals include monazite, clinozoisite, titanite, hematite, iron-titanium oxides, apatite, and zircon. A secondary mineral assemblage of chlorite (probably pseudomorphous after biotite) + albite + clinozoisite found along fractures, faults with small displacements, and in veins suggests late magmatic hydrothermal alteration or regional greenschist metamorphism of the granite. SHRIMP ²⁰⁶Pb/²³⁸U analyses of zircons from the granite yielded a preferred Neoproterozoic crystallization age of 612 ± 10 Ma (2σ; Horton et al., 2005b).

Shock-metamorphosed minerals, impact melt, and pervasive cataclasis are absent. The ⁴⁰Ar/³⁹Ar analysis of feldspars and

Langley core



fission-track analysis of zircons and apatite yielded no evidence for Eocene impact-generated thermal effects (Horton et al., 2005b).

A distinct alteration profile is superimposed on the recovered 8.8 m section. There is a gradual downward change across ~3 m from densely fractured, mineralogically altered rock to less fractured and altered rock (Fig. 6). Chlorite is largely replaced by expandable mixed-layer clay minerals (smectite rich) in the upper part (Table 2; Fig. 9), and the feldspars are more sericitized in the highest granite sample. The chlorite is partially oxidized, and some quartz grains appear altered by partial dissolution. Pyrite is present in XRD samples of altered granite above ~630 m but absent in four samples below that depth (Table 2). Zones of iron oxides and “soapy” clay minerals are present along fractures. The highest XRD sample collected from the altered granite has a higher quartz/feldspar ratio than the deeper granite samples (Table 2; Fig. 9), which corresponds to the observed upward increase in feldspar alteration.

On a migrated, high-resolution seismic-reflection profile acquired across the Langley drill site, a high-amplitude reflection at 630–625 m depth correlates with the top of the altered granite (Catchings et al., 2005; Horton et al., 2005b). Several vertical faults that offset the top of granite basement by 10 m or less are apparent on the profile.

Parautochthonous Section of Potomac Formation (Unit PPF), Upper Eocene (626.30–442.50 m)

Stratigraphy. Gohn et al. (2005) assigned this interval to informal “crater unit A” in the Langley core. They divided the interval into two units, the “lower beds of crater unit A” and the “upper beds of crater unit A.” The intervening contact was placed at a depth of 558.1 m. Poag et al. (2004) interpreted essentially the same interval as a “detachment zone” (626.3–594.4 m) overlain by “displaced megablocks” (594.4–449.0 m).

Here, we refer to the interval from 626.30 to 442.50 m as unit PPF (Fig. 8), a parautochthonous section of Potomac Formation sediments that was internally deformed during the impact event and transported a short distance laterally (Catchings et al., 2005). We chose this nomenclature to reflect several characteristics of the unit, including: the absence of exotic sediments, fossils, and ejecta; the partially retained depositional pattern of the Cretaceous sediments; and the Eocene transportation.

Taxa in the only productive palynomorph sample, from near the top of unit PPF at 446.4 m, indicate initial deposition during the middle Albian to early Cenomanian, which is typical of the upper part of the Potomac Formation regionally (Frederiksen et



Figure 8. Geologic column for the Langley core. In the Exmore Formation, some clasts derived from the Potomac Formation are marked with arrows that distinguish upright from overturned orientations. See Figure 5 for an explanation of the symbols. Unit PPF—parautochthonous Potomac Formation. T.D.—total depth.

al., 2005). Eleven samples of various sediment types were barren or contained nondiagnostic taxa.

Description and mineralogy. An ~1.5-m-thick interval (626.3–624.8 m) of sandy, quartz-feldspar gravel, with an XRD mineralogy similar to that of the Langley Granite, nonconformably overlies the granite along a sharp contact (Fig. 8). The gravel contains subrounded to subangular clasts of altered Langley Granite that decrease upward in size (maximum 4 cm) and abundance. Dark-gray clay clasts (max. 7 cm) also are present. In the granite clasts, chlorite is largely replaced by mixed-layer clay minerals, and pyrite is present (Table 2), as also noted in the underlying altered granite. Quartz/feldspar ratios in the basal ~2 m of unit PPF (0.3–0.4) are similar to those in the altered granite (generally 0.2–0.4; Table 2). Some granitic clasts in the overlying Exmore Formation macroscopically resemble the Langley Granite, but the specific source plutons of those clasts are undetermined (Horton and Izett, 2005).

Relict Cretaceous sand-clay fining-upward units of variable thickness characterize unit PPF above the basal gravel (Fig. 8). From 624.8 to 596.9 m, each unit consists of a basal erosion surface overlain by gray, medium to very coarse, locally gravelly, feldspathic quartz sands, some with common clay intraclasts. The sands are sharply overlain in turn by reddish-gray silty clays, and dark-gray to black carbonaceous silty clays, which typically are less than 1.5 m in thickness. The abundance of mixed-layer clay minerals relative to chlorite (Table 2) in the sediments from 626.2 to 623.8 m suggests possible continued input of altered rock from the Langley Granite during the Cretaceous.

From 596.9 m to the top of the unit, some fining-upward successions show more gradual upward transitions from coarser basal sands to laminated and thinly bedded finer sands capped by gray and (or) reddish-brown oxidized clayey silts and clays. There is a general upward trend in unit PPF to thicker and more abundant oxidized clay-silt beds. A few thin coarsening-upward intervals also are present.

The XRD-determined quartz/feldspar and plagioclase/total feldspar ratios are variable in unit PPF. Differences appear to correlate primarily with variations in grain size, specifically, the relative abundance of the sand fraction (Table 2; Fig. 9). The plagioclase/total feldspar ratios in the lower part of unit PPF resemble those of the Langley Granite. The plagioclase content decreases upward, most likely reflecting an increasing degree of in situ weathering.

Stratification throughout the unit consists of cross-beds in some sand layers and sand-clay laminations and thin beds. Several root horizons, some with caliche and microfractured clay beds (blocky ped structure), are present in the upper parts of many cycles. Exotic glauconite, faunas, floras, and clasts from the Upper Cretaceous and Paleogene marine-target sediments, and ejecta clasts, are absent in unit PPF at Langley.

Features suggestive of sand liquefaction are present in the upper part of unit PPF above 558.11 m (Gohn et al., 2005). These features primarily consist of meter-scale intervals of poorly consolidated quartz-feldspar sand that lack stratification and contain randomly dispersed quartz, chert, and clay granules and pebbles

that probably were original components of the bed. Mostly unrecovered intervals of quartz-feldspar sand at 537.4–554.7 m and 559.0–563.9 m likely represent similar intervals with typically large variations in the XRD mineralogy (Table 2; Fig. 9).

Exmore Formation, Upper Eocene (442.48–235.65 m)

Members. Gohn et al. (2005) assigned the lower part of this interval to informal “crater unit B” and the upper part to the Exmore beds, with an intervening contact at 269.4 m. Poag et al. (2004) referred to this interval as a single informal unit called the “Exmore breccia.” Here, we assign this interval to the informal upper diamicton member and the overlying, informal stratified member of the Exmore Formation, following the nomenclature of Edwards et al. (2009, 2010).

Upper diamicton member (442.48–236.65 m). The upper diamicton member can be divided into two subunits at Langley. Both consist primarily of sediment clasts in a sediment matrix; however, they have contrasting maximum clast sizes, clast/matrix ratios, and diversities of clast types. A 5.0 m block of Potomac sediments that previously was included at the base of the former Exmore beds by Gohn et al. (2005) is included here at the top of the lower subunit of the upper diamicton member.

Lower subunit of the upper diamicton member (442.50–266.33 m). This subunit contains sand, clay, and sand-clay clasts derived from the Potomac Formation that vary in their apparent vertical dimensions from ~1.5 to ~22 m (coarse boulders to coarse blocks; Fig. 8). Gohn et al. (2005) referred to these clasts as “megablocks” or as “megablock zones” in places where two or more clasts are in contact without intervening matrix. The primary (pre-impact) sedimentary structures and cycles seen in unit PPF below the Exmore members at Langley, and the undisturbed Potomac Formation at Watkins School, also can be recognized within the boulders and blocks of this subunit. Dips of primary stratification within the boulders and blocks vary from horizontal to nearly vertical. Internal sedimentary structures in some clasts, primarily cross-beds, indicate that they are overturned (Fig. 8). The clasts typically are fractured and (or) folded as a result of disruption and transport. Some clasts contain water-escape structures and sand dikes that do not extend outside the clast margins, possibly indicating a pre-impact origin.

Thirteen sediment clasts were examined for pollen and spores (Frederiksen et al., 2005). Seven clasts contained Aptian, Albian, and Cenomanian assemblages typical of the Potomac Formation. These clasts were not arranged in pre-impact stratigraphic order.

Clasts of Potomac Formation sand in the lower subunit display relatively high plagioclase/total feldspar ratios that resemble those in the lower part of unit PPF and contrast with the relatively low ratios in the upper part of unit PPF at Langley (Table 2; Fig. 9). This suggests possible derivation of the sand clasts in this subunit from the lower part of the Potomac Formation or a high-low-high pattern of plagioclase abundance in the pre-impact Potomac section. The clay mineral suites in clasts of fine-grained Potomac Formation sediment in the lower subunit are dominated by illite

TABLE 2. LANGLEY CORE: SEMIQUANTITATIVE, WHOLE-SAMPLE, X-RAY DIFFRACTION (XRD) MINERALOGY

	Sample	Feet	Meters	Chlorite	Exp. phase mixed layer	Illite-glauc	Kaolinite	Zeolites	Gypsum	
Chickahominy Formation										
	Clay, silty	L760	760.0	231.6	2.12	7.49	18.13	2.65	0.00	5.39
	Clay, silty	L773	773.0	235.6	2.07	9.51	18.80	4.14	10.34	3.32
Exmore Formation										
Stratified member										
Subunit Es2	Clay, silty, sandy	L773.5	773.5	235.8	1.02	3.65	10.42	2.05	8.48	4.11
Subunit Es2	Silt, sandy	L774	774.0	235.9	0.75	2.85	6.46	1.51	8.35	5.49
Subunit Es1	Sand, qtz-glauc-felds	L774.5	774.5	236.1	0.60	2.50	5.41	1.20	4.44	3.61
Upper diamicton member										
Upper subunit	Sand, qtz-glauc-felds	L802,0	802.0	244.4	1.00	3.43	6.13	2.00	0.00	3.62
Upper subunit	Clast: sand, qtz-felds	L858	858.0	261.5	0.00	1.87	3.45	0.00	0.00	0.00
Lower subunit	Clast: silt, sandy	L890.5	890.5	271.4	1.99	3.94	30.30	3.99	0.00	0.00
Lower subunit	Clast: sand, qtz-felds	L922.7	922.7	281.2	0.92	2.92	6.40	1.83	0.00	2.75
Lower subunit	Sand, qtz-glauc-felds	L954.2	954.2	290.8	1.05	1.97	5.96	1.33	0.00	0.00
Lower subunit	Sand, qtz-glauc-felds	L1030	1030.0	313.9	0.66	1.93	3.82	1.32	0.00	0.00
Lower subunit	Clast: clay, silty, sandy	L1092,5	1092.5	333.0	0.00	5.91	19.94	4.37	0.00	0.00
Lower subunit	Clast: clay, silty	L1105	1105.0	336.8	3.49	9.38	12.62	3.49	0.00	0.00
Lower subunit	Clast: Sand, qtz-felds, muddy	L1143,2	1143.2	348.4	1.46	2.37	13.07	1.81	0.00	0.00
Lower subunit	Sand, qtz-glauc-felds	L1194,5	1194.5	364.1	0.93	1.85	3.79	1.07	0.00	2.17
Lower subunit	Sand, qtz-glauc-felds	L1236,5	1236.5	376.9	0.87	2.47	6.64	1.75	0.00	1.62
Lower subunit	Clast: Sand, qtz-felds	L1275	1275.0	388.6	0.41	1.81	4.77	0.82	0.00	0.00
Lower subunit	Sand, qtz-glauc-felds	L1331,5	1331.5	405.8	0.49	1.52	2.41	0.98	0.00	0.00
Lower subunit	Sand, qtz-glauc-felds	L1354,3	1354.3	412.8	0.33	0.75	1.48	0.67	0.00	0.00
Lower subunit	Sand, qtz-glauc-felds	L1381	1381.0	420.9	0.46	1.19	2.29	0.91	0.00	0.00
Lower subunit	Clast: clay, silty, sandy	L1394	1394.0	424.9	6.24	5.91	30.28	4.68	0.00	0.00
Lower subunit	Sand, qtz-glauc-felds	L1451,8	1451.8	442.5	0.53	1.37	2.45	1.07	0.00	0.00
Unit PPF										
	Clay, silty, sandy, lignitic	L1465	1465.0	446.5	3.20	5.92	15.14	3.36	0.00	0.00
	Sand, qtz-felds	L1489,2	1489.2	453.9	1.15	0.53	1.27	2.29	0.00	0.00
	Clay, silty, sandy	L1594	1594.0	485.9	1.88	6.31	32.01	1.91	0.00	0.00
	Sand, qtz-felds	L1694,5	1694.5	516.5	1.12	1.65	2.04	2.25	0.00	0.00
	Gravel, qtz, clay-silt	L1853	1853.0	564.8	0.92	1.29	2.07	0.92	0.00	0.00
	Sand, qtz-felds	L1886,7	1886.7	575.1	0.33	1.47	3.05	0.43	0.00	0.00
	Sand, qtz-felds	L1898	1898.0	578.5	0.55	0.95	1.54	1.10	0.00	0.00
	Sand, qtz-felds	L1942	1942.0	591.9	0.40	3.82	5.40	0.80	0.00	0.00
	Sand, qtz-felds	L1952	1952.0	595.0	0.44	3.49	3.51	0.88	0.00	0.00
	Sand, qtz-felds	L1986	1986.0	605.3	0.94	2.89	2.09	1.89	0.00	0.00
	Sand, qtz-felds	L1993	1993.0	607.5	0.54	4.07	1.42	1.09	0.00	0.00
	Sand, qtz-felds	L2000,6	2000.6	609.8	1.04	0.00	1.67	1.24	0.00	0.00
	Sand, qtz-felds	L2027,6	2027.6	618.0	0.72	1.13	2.27	1.44	0.00	0.00
	Clay, silty, sandy	L2046,5	2046.5	623.8	2.15	13.35	5.88	2.36	0.00	0.00
	Clay, silty, sandy	L2048,2	2048.2	624.3	1.50	8.55	7.16	1.72	0.00	0.00
	Gravel, qtz-felds	L2053.2	2053.2	625.8	0.80	5.69	3.47	0.91	0.00	0.00
	Gravel, qtz-felds	L2054.6	2054.6	626.2	1.24	7.68	3.75	1.24	0.00	0.00
Langley Granite										
	Granite, altered	L2055	2055.0	626.4	1.00	5.95	8.21	1.12	0.00	0.00
	Granite, altered	L2058	2058.0	627.3	1.24	10.99	2.58	1.42	0.00	0.00
	Granite, altered	L2059	2059.0	627.6	0.78	6.30	3.37	0.86	0.00	0.00
	Granite, altered	L2060	2060.0	627.9	0.50	3.48	1.43	0.50	0.00	0.00
	Granite	L2065	2065.0	629.4	5.30	2.74	3.38	1.91	0.00	0.00
	Granite	L2066	2066.0	629.7	6.16	1.74	3.11	1.79	0.00	0.00
	Granite	L2068.7	2068.7	630.5	3.84	4.10	2.40	2.00	0.00	0.00
	Granite	L2073.6	2073.6	632.0	10.18	0.55	1.60	1.32	0.00	0.00
	Granite	L2079.5	2079.5	633.8	12.19	0.73	2.30	1.71	0.00	0.00
	Granite	L2083.5	2083.5	635.1	9.17	0.00	1.10	1.19	0.00	0.00

Note: Gray shading—glaucinite-bearing samples. Trends in the abundance of selected minerals are shown by boxes. Chl/smec—mixed-layer chlorite/smectite; ExpPhase—mixed-layered, expandable illite/smectite; Illite-glauc—illite and (or) glauconite; Zeolites—heulandite/clinoptilolite series; K-fspr—potassium feldspar; qtz-glauc-felds—quartz-glaucinite-feldspars. Unit PPF—parautochthonous Potomac Formation.

Quartz	K-feldspar	Plagioclase	Calcite	Dolomite	Siderite	Pyrite	Sum	Qtz/ feldspar	Plagioclase/ total feldspar	Chlorite/ mixed layer	
<u>Chickahominy Formation</u>											
20.08	11.76	3.80	22.86	0.00	1.75	3.96	100.00	1.3	0.2	0.3	
16.07	6.77	7.74	12.90	0.00	2.56	5.77	100.00	1.1	0.5	0.2	
<u>Exmore Formation</u>											
<u>Stratified member</u>											
20.33	11.42	14.83	15.22	1.86	1.90	4.71	100.00	0.8	0.6	0.3	Subunit Es2
16.40	31.36	10.54	9.57	1.15	1.33	4.23	100.00	0.4	0.3	0.3	Subunit Es2
18.12	29.36	21.68	8.28	0.00	1.20	3.61	100.00	0.4	0.4	0.2	Subunit Es1
<u>Upper diamicton member</u>											
26.06	34.90	5.74	11.49	1.91	1.78	1.95	100.00	0.6	0.1	0.3	Upper subunit
53.94	8.99	24.67	3.34	3.74	0.00	0.00	100.00	1.6	0.7	0.0	Upper subunit
30.30	17.13	6.86	2.03	1.98	0.00	1.48	100.00	1.3	0.3	0.5	Lower subunit
44.16	26.48	10.78	1.67	2.09	0.00	0.00	100.00	1.2	0.3	0.3	Lower subunit
48.61	26.23	9.94	1.36	1.44	1.12	0.99	100.00	1.3	0.3	0.5	Lower subunit
48.63	27.87	12.22	1.84	1.70	0.00	0.00	100.00	1.2	0.3	0.3	Lower subunit
21.83	43.74	2.91	0.00	0.00	1.30	0.00	100.00	0.5	0.1	0.0	Lower subunit
49.41	6.64	6.68	4.71	0.00	3.59	0.00	100.00	3.7	0.5	0.4	Lower subunit
20.16	16.39	40.10	1.40	1.66	0.89	0.69	100.00	0.4	0.7	0.6	Lower subunit
27.51	42.52	15.63	1.30	2.29	0.93	0.00	100.00	0.5	0.3	0.5	Lower subunit
25.14	46.23	13.05	1.23	0.00	1.00	0.00	100.00	0.4	0.2	0.4	Lower subunit
37.31	28.60	22.76	1.97	1.56	0.00	0.00	100.00	0.7	0.4	0.2	Lower subunit
53.76	31.63	6.23	1.36	1.61	0.00	0.00	100.00	1.4	0.2	0.3	Lower subunit
44.22	25.50	23.33	2.23	1.50	0.00	0.00	100.00	0.9	0.5	0.4	Lower subunit
45.82	41.43	4.37	1.32	1.34	0.87	0.00	100.00	1.0	0.1	0.4	Lower subunit
21.83	9.89	12.36	2.68	2.19	1.99	1.96	100.00	1.0	0.6	1.1	Lower subunit
63.23	22.83	4.00	1.35	1.95	1.20	0.00	100.00	2.4	0.1	0.4	Lower subunit
<u>Unit PPF</u>											
44.43	9.05	6.15	3.69	3.17	3.32	2.56	100.00	2.9	0.4	0.5	
21.26	70.22	1.55	0.75	0.98	0.00	0.00	100.00	0.3	0.02	2.2	
29.77	15.04	4.61	3.00	1.74	1.83	1.90	100.00	1.5	0.2	0.3	
45.50	40.45	3.45	1.75	1.78	0.00	0.00	100.00	1.0	0.1	0.7	
42.77	46.72	2.52	1.46	1.31	0.00	0.00	100.00	0.9	0.1	0.7	
12.96	77.41	2.75	0.70	0.55	0.34	0.00	100.00	0.2	0.0	0.2	
25.82	58.00	4.66	0.74	0.70	0.00	5.94	100.00	0.4	0.1	0.6	
15.32	66.86	5.22	0.81	0.86	0.49	0.00	100.00	0.2	0.1	0.1	
29.56	35.95	21.57	1.76	1.71	1.12	0.00	100.00	0.5	0.4	0.1	
29.19	40.18	16.68	2.38	2.63	1.13	0.00	100.00	0.5	0.3	0.3	
27.67	49.11	12.45	1.78	1.87	0.00	0.00	100.00	0.4	0.2	0.1	
43.91	38.98	8.07	1.84	1.66	0.92	0.67	100.00	0.9	0.2	No mixed-layer clay	
46.06	25.54	17.03	1.96	2.67	1.20	0.00	100.00	1.1	0.4	0.6	
36.38	17.50	14.19	3.20	2.84	2.16	0.00	100.00	1.1	0.4	0.2	
21.19	22.17	31.69	1.68	1.85	1.39	1.10	100.00	0.4	0.6	0.2	
21.95	30.73	31.61	1.45	1.62	0.97	0.78	100.00	0.4	0.5	0.1	
20.63	35.42	23.71	1.91	2.01	1.29	1.11	100.00	0.3	0.4	0.2	
<u>Langley Granite</u>											
22.88	19.39	3.96	2.44	2.75	1.88	1.42	100.00	1.0	0.2	0.2	
18.41	3.76	56.22	1.88	2.12	0.00	1.38	100.00	0.3	0.9	0.1	
21.03	30.87	29.50	2.33	2.47	1.42	1.07	100.00	0.3	0.5	0.1	
14.36	21.03	54.40	1.17	1.65	0.86	0.63	100.00	0.2	0.7	0.1	
19.34	23.36	38.18	1.36	2.21	1.19	1.04	100.00	0.3	0.6	1.9	
12.26	26.93	44.17	0.92	1.63	0.78	0.52	100.00	0.2	0.6	3.5	
21.89	24.59	34.09	2.09	3.49	1.50	0.00	100.00	0.4	0.6	0.9	
12.15	28.36	43.75	0.82	1.27	0.00	0.00	100.00	0.2	0.6	18.5	
15.46	19.27	43.70	1.29	2.23	1.12	0.00	100.00	0.2	0.7	16.7	
5.11	31.59	50.35	0.58	0.91	0.00	0.00	100.00	0.1	0.6	No mixed-layer clay	

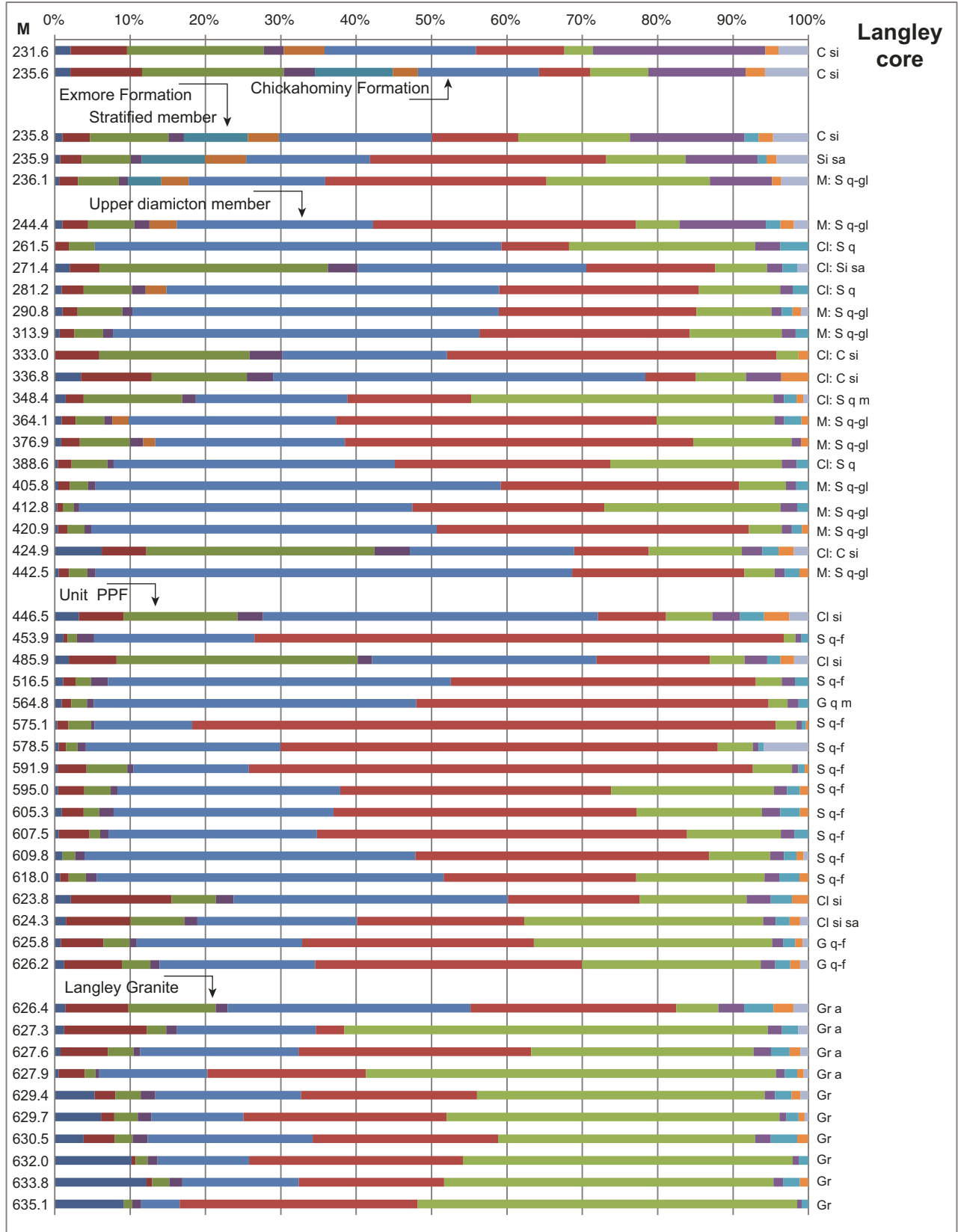


Figure 9. Mineralogic composition of Langley core samples as determined by semiquantitative X-ray diffraction (XRD) analysis. Data are from Table 2. See Figure 7 for legend. Unit PPF—parautochthonous Potomac Formation.

(macroscopic and microscopic glauconite is absent; Table 2; Fig. 9). The same dominance is present in clays near the top of unit PPF at Langley. A quartz-rich sample at 338.8 m depth likely represents a sand clast.

In most places, the clasts of Potomac sediment in the lower subunit are separated by intervals of unsorted, unstratified, spar-

ingly fossiliferous, sparingly calcareous, muddy, feldspathic, quartz-glaconite sand and granules, plus smaller Potomac clasts (Figs. 10, 11E, and 11F). Gohn et al. (2005) referred to these intervals as “matrix zones.” These zones vary from a few centimeters to ~23 m in apparent thickness and typically are matrix supported. Three matrix samples contained mixed-age, early Paleo-

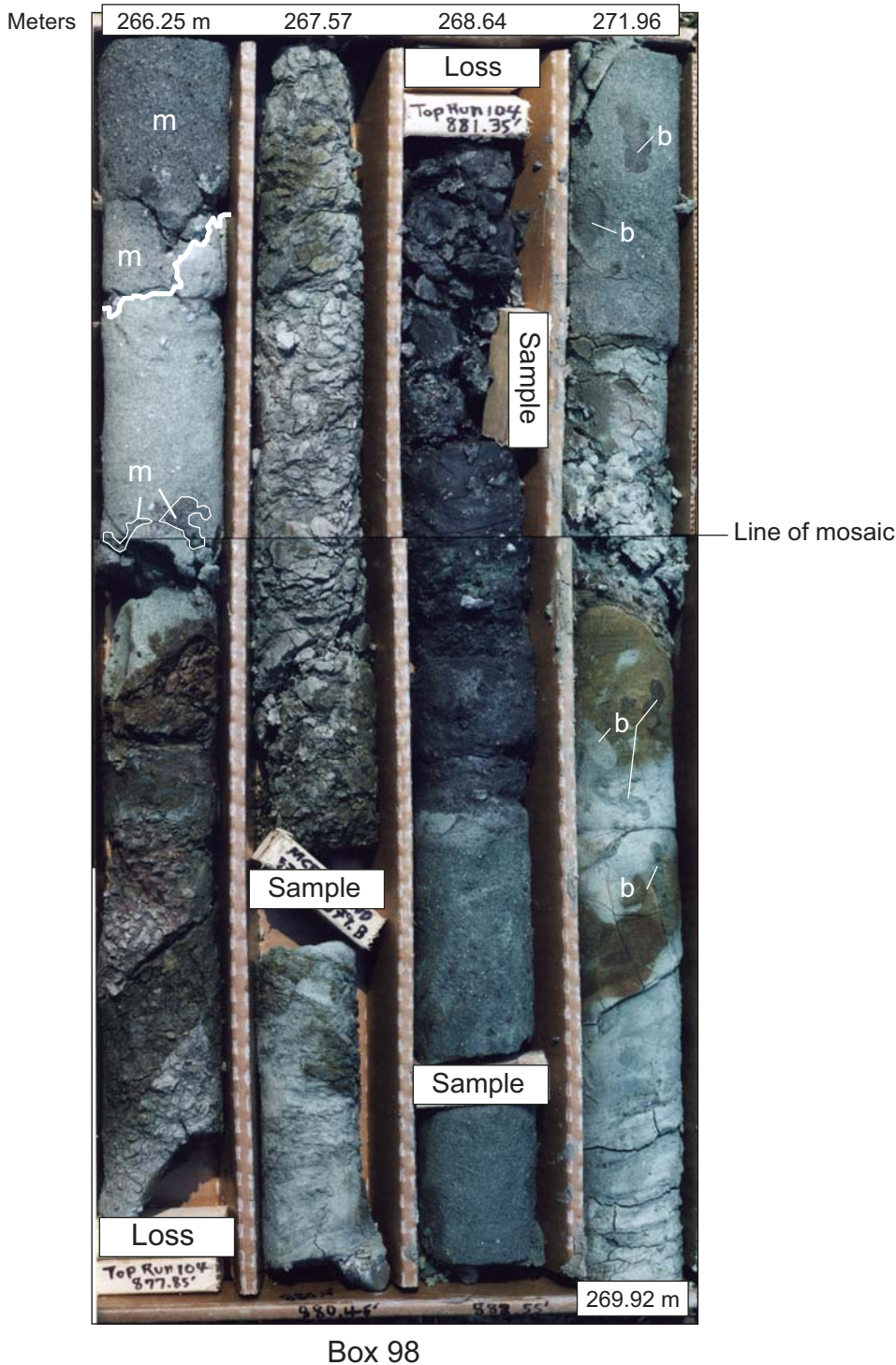


Figure 10. Section of the lower subunit of the Exmore Formation upper diamicton member in the Langley core. Clasts derived from the Potomac Formation include dark-gray to black, lignitic sands and clays and mottled medium-gray and grayish-red clays that locally contain burrows (b) (freshwater crustaceans?). Glauconitic resurge matrix (m) is present at the top of the section.

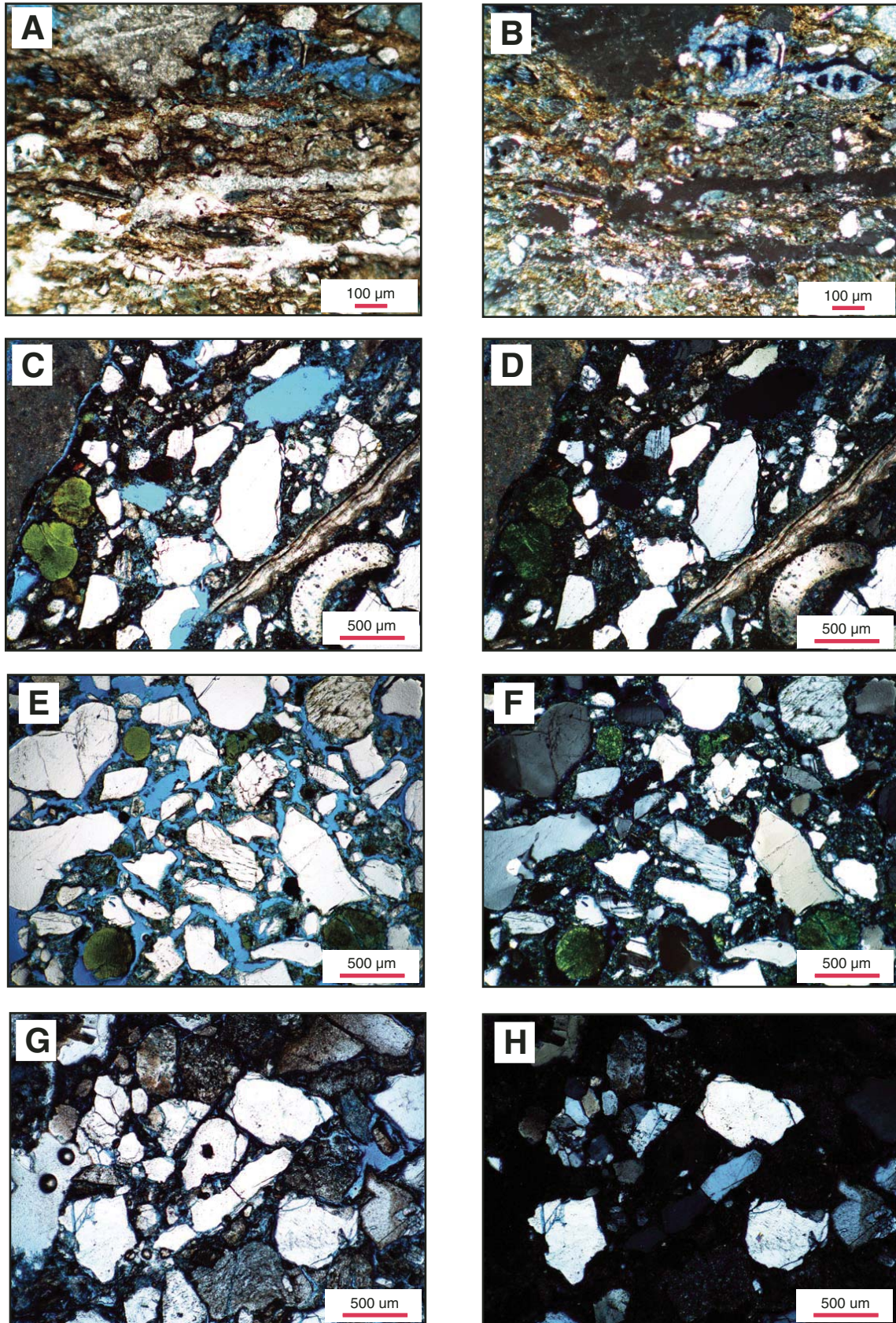


Figure 11.

gene dinocyst assemblages, and one matrix sample at 298.5 m contained a mixed-age, early Paleogene calcareous nannoflora (Frederiksen et al., 2005; Edwards et al., 2010, their figures 11 and 26). Two calcareous nannofossil samples from the matrix in the lower subunit from above 298.5 m, and eight samples from below that depth, were barren.

The matrix in the lower subunit of the upper diamicton member is atypically poor in carbonate minerals, as compared to sections of this unit in the Bayside core and the resurge diamictons in general (Tables 2 and 3). Calcareous macrofossil fragments and microfossils are present only in the 298.5 m matrix sample near the top of the lower subunit. Four samples taken between 414.3 m and 278.4 m in the lower subunit were processed for dinocysts but did not react to HCl in the laboratory. A sample from the base of the lower subunit (442.45 m) had a mild reaction to HCl.

Clasts in the matrix zones of the lower subunit vary from granules to medium boulders (2 mm to 1.0 m) and also consist entirely of Potomac sands and clays. These clasts are internally fractured and distorted, and their margins vary from embayed and sharp (clays) to diffuse (sands). Well-rounded quartz, chert, and quartzite pebbles in the matrix are multicycle sediments from the Potomac Formation gravels. Sparse, rounded igneous and metamorphic lithic pebbles in the matrix lack cataclastic fabrics and also were derived from the Potomac gravels (Horton and Izett, 2005). However, one 22 cm cobble of cataclastic felsite containing shocked quartz is present at 275.8 m depth (Horton and Izett, 2005).

No definite clasts of Upper Cretaceous and Paleogene marine-target sediments were observed in the matrix zones of the lower subunit, although some clasts of noncalcareous, greenish-gray muds and sands could represent those units. However, disaggregated sediments from the marine units are well represented by the variably abundant glauconite in all matrix zones.

Upper subunit of the upper diamicton member (266.33–236.65 m). This diamicton primarily consists of sediment clasts in an unstratified sediment matrix and is poorly sorted and matrix supported. The XRD-determined mineralogy of this subunit is similar to that of the units below and above (Table 2; Fig. 9). Sparse ejecta particles vary in size from sand grains to 22 cm and include: individual shocked quartz grains and dinocysts; and

clasts of aphanitic, porphyritic, or spherulitic felsite, felsite cataclasite and breccia, and granodiorite (Horton and Izett, 2005). Some felsite clasts contain shocked quartz and (or) pseudotachylite veins.

In contrast to the lower subunit, the upper subunit contains sediment clasts from most of the pre-impact formations, some of which contain age-diagnostic microfossils (Gohn et al., 2005; Frederiksen et al., 2005). Clasts representing the pre-impact Potomac Formation (Albian–Cenomanian), Aquia Formation (Paleocene), and Marlboro, Nanjemoy, and Piney Point formations (Eocene) are present (Fig. 2). The various types of clasts appear to be randomly distributed and do not occur in their pre-impact stratigraphic order.

The sediment clasts range in size from granules to fine cobbles (2–128 mm) throughout the member. Coarse cobbles and fine boulders (128–512 mm) that consist only of Potomac Formation sediments are present only below ~254.5 m. Clasts from at least two Eocene units that are not presently recognized in the Virginia Coastal Plain also are present (post-Nanjemoy–pre-Piney Point unit, and post-Piney-Point–pre-Chickahominy unit; Frederiksen et al., 2005). No clasts from the Upper Cretaceous marine units were recognized.

Biostratigraphic age determinations using pollen and spores indicated a middle Albian(?) age for one clast of Potomac sediments, and an early Cenomanian age for four Potomac clasts from the upper subunit (Frederiksen et al., 2005). One additional clast contained pollen and spores indicative of an age near the Paleocene–Eocene boundary.

Calcareous nannofossils indicated unique ages for 11 clasts from the upper subunit that ranged from late Paleocene to late Eocene, inclusive (Frederiksen et al., 2005). Six clasts had mixed ages that may indicate contamination during the impact or during drilling. Nine clasts that were barren of calcareous nannofossils probably represent the Potomac Formation. The studied clasts from the upper subunit were not distributed in normal biostratigraphic order by depth.

The matrix supporting the clasts consists of calcareous, macrofossiliferous and microfossiliferous, muddy, gravelly, feldspathic, quartz–glauconite sand, with shocked quartz. Centimeter-scale zones defined by size segregation of sand grains, clustering of pebbles, and locally by weakly developed vertical alignment of elongate grains, resemble water-escape pipe/pillar and pocket structures (Lowe, 1975; Postma, 1983). These zones are particularly well developed above ~247 m. Thermal and physical damage of some dinocysts and calcareous nannofossils, including fused clumps of dinocysts, has been attributed to the impact (Edwards and Powars, 2003; Self-Trail, 2003; Frederiksen et al., 2005).

Some pollen and spores in one sample of the matrix from the upper subunit are compatible with a late Eocene age, but an abundance of long-ranging taxa suggests a mixed-age assemblage (Frederiksen et al., 2005). Twenty-nine samples of the matrix from the upper subunit contained mixed-age assemblages of Late Cretaceous and Paleogene calcareous nannofossils. The




Figure 11. Photomicrographs of thin sections from samples of the Langley and Bayside cores. (A) Langley core, sample 760 (231.6 m), Chickahominy Formation. Finely laminated, silty clay rich in organic matter. Note foraminifera in upper-right corner. (B) Same as A, cross polarized. (C) Bayside #1 core, sample 999 (394.5 m), upper diamicton member of the Exmore Formation. Poorly sorted, fossiliferous sand. Note glauconite grains in lower-left corner. (D) Same as C, cross polarized. (E) Langley core, sample 1194 (363.9 m), upper diamicton member of the Exmore Formation. Several grains of glauconite are seen in the poorly sorted, quartz-feldspar sand. (F) Same as E, cross polarized. (G) Bayside 2 core, sample 2275 (693.5 m), gravel and sand unit (unit GS). Angular quartz and feldspar grains occur in a moderately to poorly sorted sand. (H) Same as G, cross polarized.

TABLE 3. BAYSIDE CORE: SEMIQUANTITATIVE, WHOLE-SAMPLE, X-RAY DIFFRACTION MINERALOGY

	Sediment/rock	Sample no.	Feet	Meters	Chl/smec	Exp. phase mixed layer	Illite-glauc	Kaolinite	Zeolites	Gypsum
<u>Chickahominy Formation</u>										
	Clay, silty	B895.6	895.6	273.0	0.00	12.82	13.72	3.17	0.00	3.47
	Clay, silty	B911	911.0	277.7	0.00	8.55	9.98	2.61	7.36	2.73
<u>Exmore Formation</u>										
<u>Stratified member</u>										
Subunit Es2	Clay, silty-sandy	B915.5	915.5	279.0	2.75	3.93	14.41	3.54	11.86	3.14
Subunit Es2	Clay, silty sandy	B917.5	917.5	279.7	2.40	3.03	10.20	3.03	13.60	2.87
Subunit Es1	Sand, qtz-glauc-felds	B927.1	927.1	282.6	1.92	2.60	6.87	2.85	4.15	6.01
Subunit Es1	Sand, qtz-glauc-felds	B930	930.0	283.5	0.00	0.00	3.00	1.82	1.36	1.27
Subunit Es1	Sand, qtz-glauc-felds	B959.8	959.8	292.5	0.68	0.84	2.91	1.21	0.00	1.00
<u>Upper diamicton member</u>										
Upper subunit	Sand, qtz-glauc-felds	B989.5	989.5	301.6	4.04	4.59	44.57	8.77	0.00	5.15
Upper subunit	Sand, qtz-glauc-felds	B999	999.0	304.5	0.00	1.17	3.58	1.48	0.00	5.80
Upper subunit	Sand, qtz-glauc-felds	B1020	1020.0	310.9	1.09	0.00	3.98	1.45	0.00	3.08
Upper subunit	Sand, qtz-glauc-felds	B1027	1027.0	313.0	4.32	0.00	12.96	0.00	0.00	25.18
Upper subunit	Clast: limestone	B1057.1	1057.0	322.2	0.00	0.00	0.77	0.00	0.00	0.00
Upper subunit	Clast: sand, calcareous	B1095	1095.0	333.8	0.00	0.00	4.32	1.76	0.00	3.85
Lower subunit	Clast: clay, sandy-silty	B1128.9	1129.0	344.1	0.00	2.23	4.98	2.40	0.00	0.00
Lower subunit	Clast: sand, qtz-felds	B1135.1	1135.0	346.0	0.00	0.00	3.14	0.57	0.00	0.00
Lower subunit	Sand, qtz-glauc-felds	B1663	1663.0	506.9	0.00	0.00	1.72	0.83	0.00	0.00
Lower subunit	Sand, qtz-glauc-felds	B1707	1707.0	520.3	0.00	0.00	1.64	0.82	0.00	0.00
Lower subunit	Clast: sand, qtz-felds	B1718.8	1719.0	523.9	0.00	0.58	2.29	3.10	0.00	0.00
Lower subunit	Sand, qtz-glauc-felds	B1731.5	1732.0	527.8	0.00	0.00	2.09	0.87	0.00	0.00
Lower subunit	Sand, qtz-glauc-felds	B1753	1753.0	534.3	0.00	0.00	1.27	0.82	0.00	0.00
<u>Block-dominated member</u>										
	Clast: sand, qtz-felds	B1787.3	1787.0	544.8	0.00	0.00	3.36	1.90	0.00	0.00
	Clast: sand, qtz-felds	B1988.5	1989.0	606.1	0.00	0.00	12.68	4.60	0.00	0.00
	Clast: sand, qtz-felds	B2082.6	2083.0	634.8	0.00	0.00	0.42	0.56	0.00	0.00
<u>Lower diamicton member</u>										
	Clast: sand, qtz	B2143.1	2143.0	653.2	0.00	0.52	1.05	0.79	0.00	0.00
<u>Unit PPF</u>										
	Sand, qtz-felds	B2213	2213.0	674.5	0.00	0.12	0.23	0.52	0.00	0.00
	Clay, sandy-silty	B2248.6	2249.0	685.4	0.00	6.03	3.07	1.38	0.00	0.00
<u>Unit GS</u>										
	Sand, qtz-felds	B2268.2	2268.0	691.3	0.00	4.00	2.89	3.00	0.00	0.00
	Sand, qtz-felds	B2275.1	2275.0	693.5	0.00	0.15	0.61	0.27	0.00	0.00
	Clay, sandy-silty	B2285.8	2286.0	696.7	0.00	3.94	1.62	1.54	0.00	0.00
	Sand, qtz-felds	B2299	2299.0	700.7	0.00	2.08	2.23	1.35	0.00	0.00
	Sand, qtz-felds	B2307	2307.0	703.2	0.50	2.34	1.18	0.97	0.00	0.00
	Gravel, sandy, qtz-felds	B2325.1	2325.0	708.7	2.12	6.29	4.79	0.36	0.00	0.00
<u>Granite</u>										
	Granite, altered	B2329.2	2329.0	709.9	0.00	4.98	1.74	0.35	0.00	0.00
	Granite	B2370	2370.0	722.4	0.46	0.00	2.06	1.39	0.00	0.00

Note: Gray shading—glaucinite-bearing samples. Trends in the abundance of selected minerals are shown by boxes. Chl/smec—mixed-layer chlorite/smectite; ExpPhase—mixed-layered, expandable illite/smectite; Illite-glauc—illite and (or) glauconite; Zeolites—heulandite/clinoptilolite series; K-fspr—potassium feldspar; qtz-glauc-felds—quartz-glaucinite-feldspars. Unit PPF—parautochthonous Potomac Formation; Unit GS—gravel and sand unit.

Quartz	K-feldspar	Plagioclase	Calcite	Dolomite	Siderite	Pyrite	Sum	Quartz/ feldspar	Plagioclase/ total feldspar	Chlorite-smectite/ mixed layer	
<u>Chickahominy Formation</u>											
15.99	5.58	4.37	31.07	2.72	2.41	4.67	100.00	1.61	0.44	0.00	
15.32	5.34	4.16	36.70	0.00	2.73	4.51	100.00	1.61	0.44	0.00	
<u>Exmore Formation</u>											
<u>Stratified member</u>											
14.67	13.36	8.38	17.16	0.00	3.67	3.14	100.00	0.67	0.39	0.70	Subunit Es2
14.93	16.53	13.13	15.17	0.00	2.20	2.90	100.00	0.50	0.44	0.79	Subunit Es2
27.99	17.46	10.22	17.09	0.00	0.00	2.85	100.00	1.01	0.37	0.74	Subunit Es1
21.45	19.18	8.27	43.64	0.00	0.00	0.00	100.00	0.78	0.30	--	Subunit Es1
7.27	66.77	13.02	4.07	0.84	0.89	0.50	100.00	0.09	0.16	0.81	Subunit Es1
<u>Upper diamicton member</u>											
16.57	3.90	6.41	2.37	0.00	1.81	1.81	100.00	1.61	0.62	0.88	Upper subunit
23.71	27.60	2.44	28.47	0.00	4.32	1.42	100.00	0.79	0.08	0.00	Upper subunit
16.59	43.47	20.14	9.02	0.00	0.00	1.18	100.00	0.26	0.32	--	Upper subunit
18.41	7.39	6.38	13.15	6.77	0.00	5.44	100.00	1.34	0.46	--	Upper subunit
1.46	0.63	0.58	96.56	0.00	0.00	0.00	100.00	1.21	0.48	--	Upper subunit
22.16	33.38	5.95	28.58	0.00	0.00	0.00	100.00	0.56	0.15	--	Upper subunit
28.21	40.91	11.83	5.40	2.49	0.00	1.54	100.00	0.53	0.22	0.00	Lower subunit
10.57	62.73	22.47	0.54	0.00	0.00	0.00	100.00	0.12	0.26	--	Lower subunit
23.29	66.49	6.92	0.22	0.53	0.00	0.00	100.00	0.32	0.09	--	Lower subunit
24.88	52.29	14.32	5.05	0.99	0.00	0.00	100.00	0.37	0.21	--	Lower subunit
22.60	56.39	14.24	0.33	0.48	0.00	0.00	100.00	0.32	0.20	0.00	Lower subunit
26.86	53.53	12.82	2.98	0.84	0.00	0.00	100.00	0.40	0.19	--	Lower subunit
14.62	75.83	4.48	1.46	1.52	0.00	0.00	100.00	0.18	0.06	--	Lower subunit
<u>Block-dominated member</u>											
19.25	68.13	5.83	0.63	0.90	0.00	0.00	100.00	0.26	0.08	--	
22.22	51.90	7.25	0.80	0.55	0.00	0.00	100.00	0.38	0.12	--	
46.06	47.15	3.76	0.63	1.43	0.00	0.00	100.00	0.90	0.07	--	
<u>Lower diamicton member</u>											
27.43	63.84	4.20	1.39	0.77	0.00	0.00	100.00	0.40	0.06	0.00	
<u>Unit PPF</u>											
28.67	45.08	22.90	1.27	1.21	0.00	0.00	100.00	0.42	0.34	0.00	
25.27	28.63	32.08	0.64	2.90	0.00	0.00	100.00	0.42	0.53	0.00	
<u>Unit GS</u>											
34.33	39.21	13.79	0.47	2.30	0.00	0.00	100.00	0.65	0.26	0.00	
13.28	50.28	33.78	0.51	1.12	0.00	0.00	100.00	0.16	0.40	0.00	
34.76	48.28	7.23	0.85	1.79	0.00	0.00	100.00	0.63	0.13	0.00	
30.22	32.59	30.28	0.00	1.25	0.00	0.00	100.00	0.48	0.48	0.00	
32.16	46.68	14.57	0.00	1.59	0.00	0.00	100.00	0.53	0.24	0.21	
28.48	26.36	29.65	0.52	1.44	0.00	0.00	100.00	0.51	0.53	0.34	
<u>Granite</u>											
12.75	24.17	54.98	0.00	1.03	0.00	0.00	100.00	0.16	0.69	0.00	
10.00	17.79	66.63	0.67	1.00	0.00	0.00	100.00	0.12	0.79	No mixed layer clay	

Late Cretaceous species indicate Santonian and Campanian ages and are present only above 242.22 m. The Paleogene species indicate early and late Paleocene ages and early, middle, and late Eocene ages. Three samples of the matrix from the upper subunit contained mixed-age Paleocene–Eocene dinocyst assemblages.

Trends in the distributions of dinocysts and calcareous nanofossils in the upper subunit suggest temporal changes in provenance during the impact event. Dinocysts from the older Paleogene source sediments are more common in the lower part of the subunit, whereas specimens from the younger Paleogene sediments are more common in the upper part. Late Cretaceous calcareous nanofossil assemblages occur only at and above 242.22 m and increase in diversity and abundance upward, as also noted in the comparable subunit in the Watkins School core. Trends in the mineralogic composition of samples from this subunit may reflect these fossil trends (Figs. 7 and 9).

Stratified member (~236.65–235.65 m). The stratified member (1.0 m thick) consists of two informal subunits, designated Es1 and Es2 in the Langley core, following the nomenclature used by Edwards et al. (2009) for this member in the Eyreville core. Lower subunit Es1 is ~0.75 m thick, extending from a provisional basal contact at ~236.65 m to an upper contact at 235.65 m. However, the basal contact may lie in an unrecovered 1.28-m-thick interval below 236.65 m. Subunit Es1 consists of muddy, calcareous, glauconitic, quartz-feldspar sand. The sand fraction ranges from very fine to very coarse. In contrast to the sediments of the underlying upper diamicton member, the gravel fraction in subunit Es1 is significantly less abundant, and pebbles are the largest clasts. The percentage of muddy matrix also is relatively reduced in Es1, and unlined, subvertical (escape?) burrows are present locally in this otherwise massive section.

Upper subunit Es2 (0.27 m thick) extends from 235.92 m to 235.65 m. It consists of three layers at Langley as recognized, with minor variations, by Poag (2002), Poag and Norris (2005), Poag et al. (2004), Gohn et al. (2005), and Powars et al. (2005, their figure 9g). From base to top, they are: (1) a basal clayey silt between 235.92 and 235.87 m; (2) a layer of similar silt containing pyritic microstructures (“pyrite lattices”) between 235.87 and 235.84 m; and (3) finely laminated, pyritic clayey silt and muddy very fine sand between 235.84 and 235.65 m. XRD samples from subunits Es1 and Es2 contain clinoptilolite/heulandite, which is absent in all other XRD samples from the Langley core (Table 2; Fig. 9). The presence of zeolites with calcite and pyrite in units Es1 and Es2 distinguishes them from all lower units in the core.

One dinocyst sample and six calcareous nanofossil samples from subunit Es1 of the stratified member contained mixed-age assemblages of Late Cretaceous, Paleocene, and Eocene taxa (Frederiksen et al., 2005). One dinocyst sample and two calcareous nanofossil samples from subunit Es2 contained similar assemblages. The dinocyst specimens typically were fragmented, and the whole specimens were typically folded, corroded, or curled due to impact heating (Edwards and Powars, 2003). In contrast, the calcareous nanofossil specimens were typically whole, except for the rosette forms of the genus *Discoaster*. Poag (2002)

and Poag and Norris (2005) found no indigenous microfossils, but some reworked taxa, in the stratified member. They referred to layer 3 of subunit Es2 as a postimpact biologic “dead zone.”

Chickahominy Formation, Upper Eocene (235.65–183.28 m)

The Chickahominy Formation in the Langley core consists of 52.37 m of compact, olive-gray, bioturbated to locally laminated or massive, calcareous, silty clay, clayey silt, and muddy very fine sand (Powars et al., 2005). Massive silty clay at the base of the Chickahominy overlies laminated clayey silt and very fine sand of the Exmore Formation along a sharp and conformable boundary. The Oligocene Drummonds Corner beds overlie the Chickahominy Formation at Langley along a heavily burrowed contact at 183.28 m depth (Powars et al., 2005; Edwards et al., 2005).

The XRD-determined mineral composition of the Chickahominy sediments is similar to that of the Chickahominy section at Watkins School. Both contain calcite and illite-glaucinite. The sand fraction of the Chickahominy sediments at Langley consists of variable amounts of quartz, feldspar, microfossils, macrofossil fragments, glauconite, phosphate, pyrite (grains, nodules, and filled shells), and mica (Figs. 11A and 11B; Powars et al., 2005). The clay fraction is dominated by illite (including glauconite) with lesser amounts of expandable mixed-layer clay and chlorite/smectite (Table 2; Fig. 9). Clinoptilolite/heulandite is present in the lowest Chickahominy XRD sample taken at 235.61 m depth, which is 4 mm above the top of the Exmore Formation (Table 2; Fig. 9).

A moderately dipping normal fault is present in the Chickahominy at ~229.94 m depth. A 1.5-cm-wide, pyritic fault gouge separates the hanging wall and footwall (Poag and Norris, 2005, their figure F16; Poag et al., 2004, their figure 7.10; Powars et al., 2005, their figure G10). Several other moderately dipping slickensided fractures or small-displacement normal faults are present elsewhere in the unit at Langley.

Calcareous nanofloras indicate an age range from late Eocene to early Oligocene (zones NP 19–20 and NP 21) for the Chickahominy section at Langley (Edwards et al., 2005). However, planktonic foraminifer (zones E15?, 15, and E16) and dinocyst assemblages restrict its age to late Eocene (Edwards et al., 2005; Poag, 2012; Poag and Norris, 2005). Age-depth plots for the Langley core suggest a rapid minimum-sediment-accumulation rate for the Chickahominy section (Edwards et al., 2005). Initial postimpact benthic foraminiferal assemblages include species that typically are found in low-oxygen and high-nutrient environments (Poag, 2012; Poag and Norris, 2005).

Summary

The Langley core is representative of the central part of the brim. The principal characteristics of this section include the presence of unshocked Neoproterozoic granite below deformed, parautochthonous target sediments of the Potomac Formation (unit PPF). This unit is sedimentologically and mineralogically similar to the Potomac Formation in the Watkins School core. However, these units differ significantly in the greater degree

of impact disruption at Langley. The overlying Exmore resurge sediments at Langley are significantly thicker than the correlative section at Watkins School.

There is a gradual transition in the XRD-determined mineralogy from the lower part to the altered upper part of the Langley Granite that continues into the sediments of unit PPF. The XRD mineralogy of unit PPF resembles that of the Potomac Formation at Watkins School, and the mineralogy of the Exmore members at Langley is similar to the equivalent units at Watkins School and Bayside (see next section).

Bayside Cores 1 and 2

Location and Stratigraphy

Two USGS core holes were drilled to a combined depth of 728.47 m at Bayside in southern Mathews County, Virginia, in 2001 (Figs. 1, 12A, 12B and 13). The site is located in the brim, ~25 km from the crater's center and ~18 km inside the outer margin of the brim (Fig. 1). The core holes penetrated postimpact sediments, synimpact sediments of the Exmore Formation, a parautochthonous section of Potomac Formation sediments (unit PPF), a unique section of interbedded gravel and sand (unit GS), and bottomed in granitic rock. The Bayside core was briefly described by Poag et al. (2004) and Horton et al. (2005a, 2006, 2008).

Granite, Neoproterozoic (728.47–708.87 m)

Nonfoliated, pale-red, medium-grained, variably altered monzogranite to granodiorite was encountered in the basal 19.6 m of the Bayside #2 core hole (Figs. 12A and 13A). The recovered granite in the upper 2.26 m is mineralogically altered, densely fractured, and friable, and it spontaneously disaggregates in water. The uppermost 6 cm are medium gray and contain clay-filled fractures. The gray color may be the result of iron reduction by groundwater. The altered section is separated from distinctly less-altered granite by two unrecovered intervals at 718.26–716.13 m and 715.82–711.13 m (Fig. 10A). Only broken pieces of minimally altered granite (~2–7 cm) were recovered from the bit at the base of the deeper interval, possibly suggesting a zone of highly fractured rock that plugged the bit and prevented core recovery. The lower, less-altered part of the granite is mineralogically comparable to the less-weathered section of the Langley Granite (Tables 2 and 3; Figs. 7 and 14).

Borehole logs show a generally downward increase in electrical resistivity in the granite section (Fig. 12A), presumably as a result of decreasing clay-mineral content and rock porosity. The logs indicate that minimally altered granite is present below a depth of ~715 m and that the strongly altered granite is no more than ~6.1 m thick. An interval of anomalously low resistivity in the upper part of the unrecovered interval likely indicates a washout zone of increased borehole diameter in highly altered or highly fractured rock.

The dominant minerals in the minimally altered granite are plagioclase, K-feldspar, quartz, and chlorite (after biotite), in decreasing order of abundance, with minor illite/sericite, kaolinite,

epidote or clinozoisite, and traces of relict biotite (Table 3; Fig. 14; Horton et al., 2005a). Numerous veins, fractures, and minor faults contain epidote or clinozoisite, albite, chlorite, quartz, and calcite. Plagioclase/total feldspar ratios in the granite are significantly higher than those of the overlying gravel and sand sediments (unit GS). SHRIMP $^{206}\text{Pb}/^{238}\text{U}$ zircon data indicate a Neoproterozoic crystallization age of 625 ± 11 Ma (2σ), which is similar to the age of the Langley Granite (Horton et al., 2002a).

Shocked minerals were not found in thin sections of six samples of the minimally altered granite ranging in depth from 727.53 to 719.48 m. Fission-track ages of zircons and apatites did not indicate any impact-related (Eocene) thermal disturbance of the granite (Horton et al., 2002b).

In the upper section of altered granite, igneous and metamorphic minerals such as feldspars, micas, and chlorite pseudomorphs after biotite are partly replaced by expandable mixed-layer smectite-illite and kaolinite (Table 3; Fig. 14). These clay minerals also fill abundant, variably oriented dilational fractures accentuated by iron-oxide stains. The presence of these clay minerals in significant amounts distinguishes the altered granite from its fresh equivalent and suggests low-temperature chemical weathering.

Shocked minerals were not observed in thin sections of five samples of the altered granite that range in depth from 711.07 m to 709.24 m. However, three of these thin sections exhibit brittle faults that locally contain microbreccia or gouge. These faults are more conspicuous and apparently more abundant in the altered granite than in the granite below ~715 m depth.

Veinlets of polygonal quartz in a thin section from 710.98 m depth occur along some fault segments and crosscut other faults at gentle to high angles. The crystallization of sericitic white mica and polygonal quartz along fault surfaces in this thin section resembles late Paleozoic and early Mesozoic faults in the region (e.g., Bobyarchick and Glover, 1979) and may predate the alteration features in the granite that are consistent with chemical weathering. However, the clay-matrix gouge that fills dilational cracks and microfaults in the thin section from 710.98 m depth is a relatively late feature that, considering the location, may represent minor, impact-induced fractures and faults. In summary, although the granite at Bayside shows no evidence for shock metamorphism or an impact-related thermal disturbance, the uppermost part contains minor faults that may be impact related.

Gravel and Sand Unit (Unit GS), Age Uncertain (708.87–688.82 m)

The gravel and sand unit is 20.05 m thick (Fig. 12A). Its basal contact between underlying medium-gray, altered granite and fine to very coarse sand and granules that lack a basal pebble lag is sharp and horizontal. The upper contact is placed at the top of the highest occurrence of lithic gravel at 688.82 m. Unit GS is a distinctive unit that does not resemble any known pre-impact sedimentary units in the target region.

The gravel and sand unit consists of several sediment types (Figs. 12A and 13B), including: (1) varicolored,

A Bayside cores 1 and 2

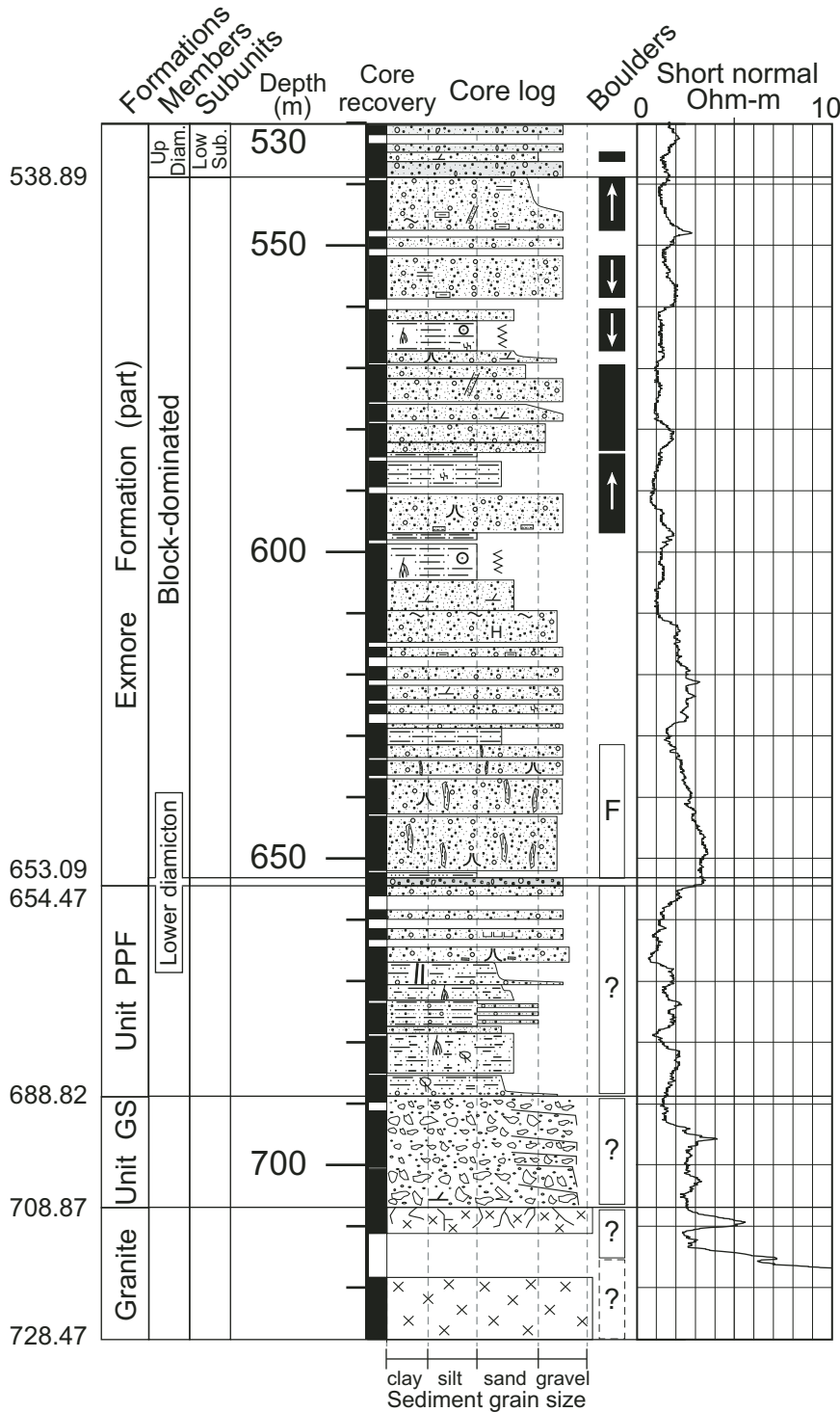


Figure 12 (Continued on facing page). Geologic columns for the Bayside core. In the Exmore Formation, some clasts derived from the Potomac Formation are marked with arrows that distinguish upright from overturned orientations. (A) Stratigraphic column for the granite, gravel and sand unit (unit GS), parautochthonous Potomac Formation (unit PPF), and the lower diamicton and block-dominated members of the Exmore Formation. See Figure 5 for an explanation of symbols.

B Bayside cores 1 and 2

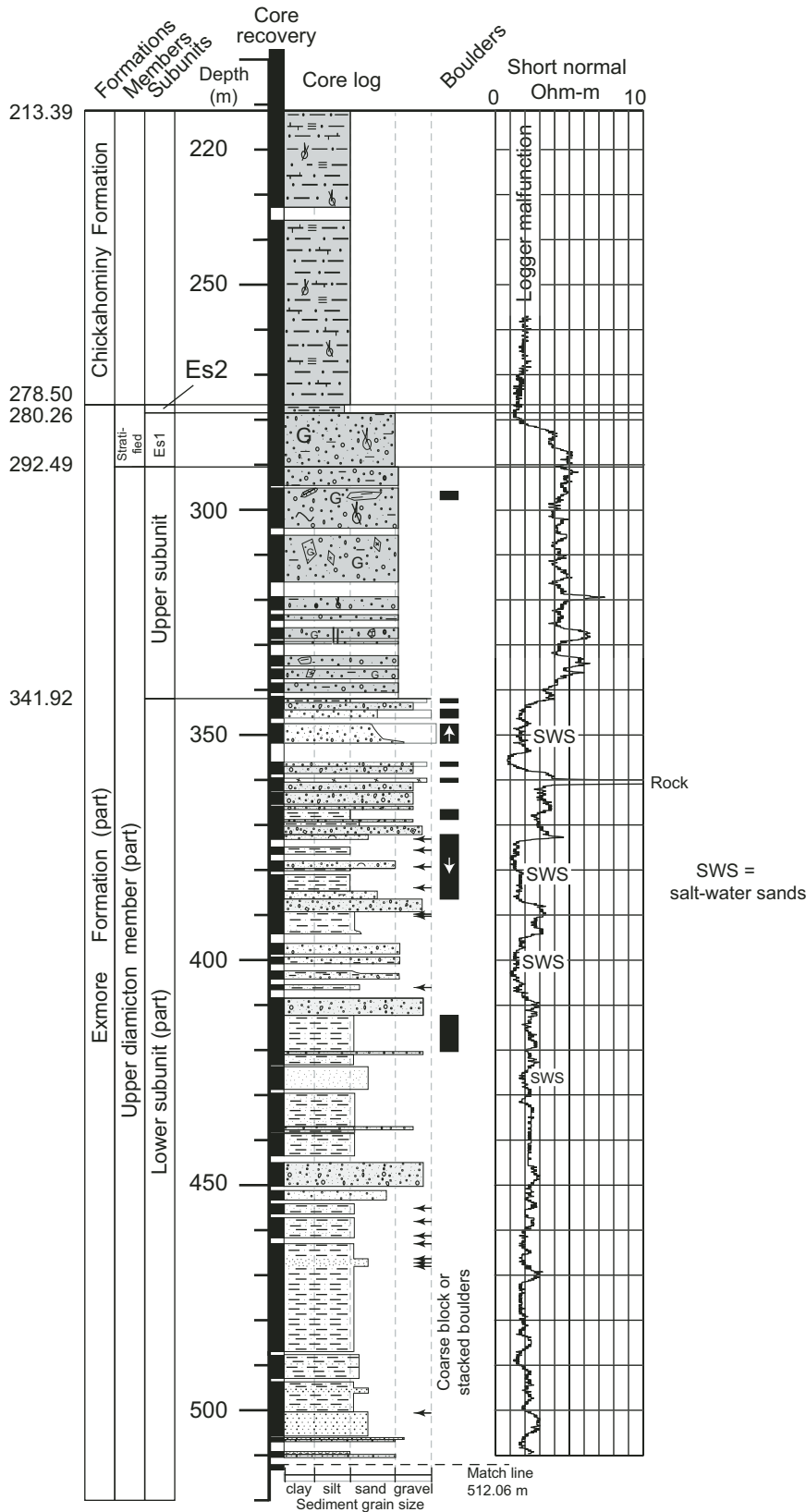


Figure 12 (Continued). (B) Stratigraphic column for the upper diamiction and stratified members of the Exmore Formation and the Chickahominy Formation. The locations of low-resistivity, salt-water-bearing sands (SWS) are indicated (McFarland and Bruce, 2005).

SWS = salt-water sands

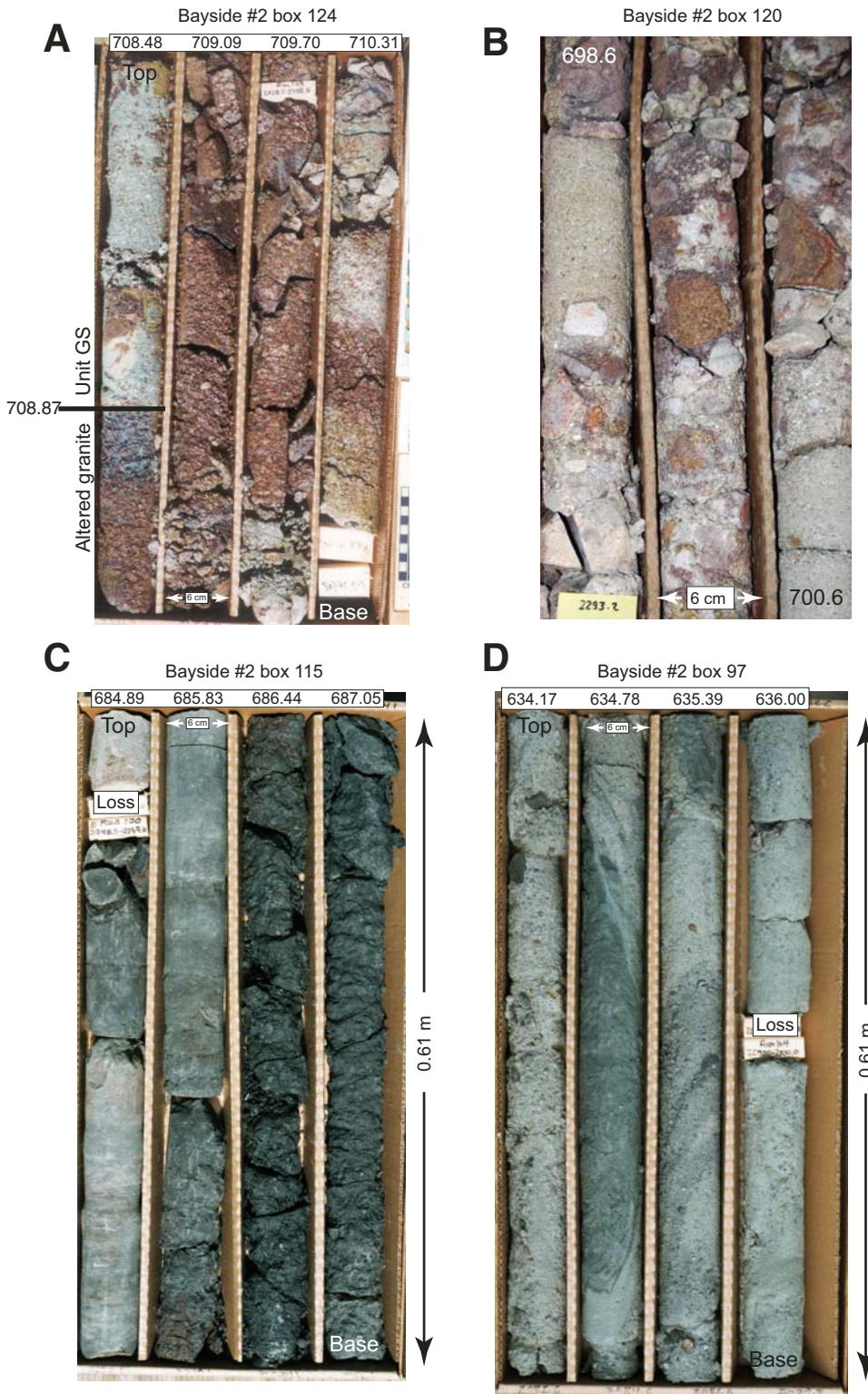


Figure 13. Photographs of the Bayside core. Granite, gravel and sand unit (unit GS), parautochthonous Potomac Formation (unit PPF), and the block-dominated member of the Exmore Formation. (A) Boundary between the altered granite and overlying unit GS at a depth of 708.87 m. Note the centimeter scale at the lower right. (B) Intervals of sandy gravel, pebbly sand, sand with granules, and dark muddy sand in unit GS. Note the polymict clasts and grain-supported texture in the gravels. Centimeter scale at bottom. (C) Fine- to medium-grained quartz sands and dark carbonaceous clays in unit PPF. Note the light-gray root casts in the sand and clay layers and horizontal laminations in some sand layers. (D) Steeply inclined sand-clay clasts in a matrix of liquefied sand in the block-dominated member of the Exmore Formation.

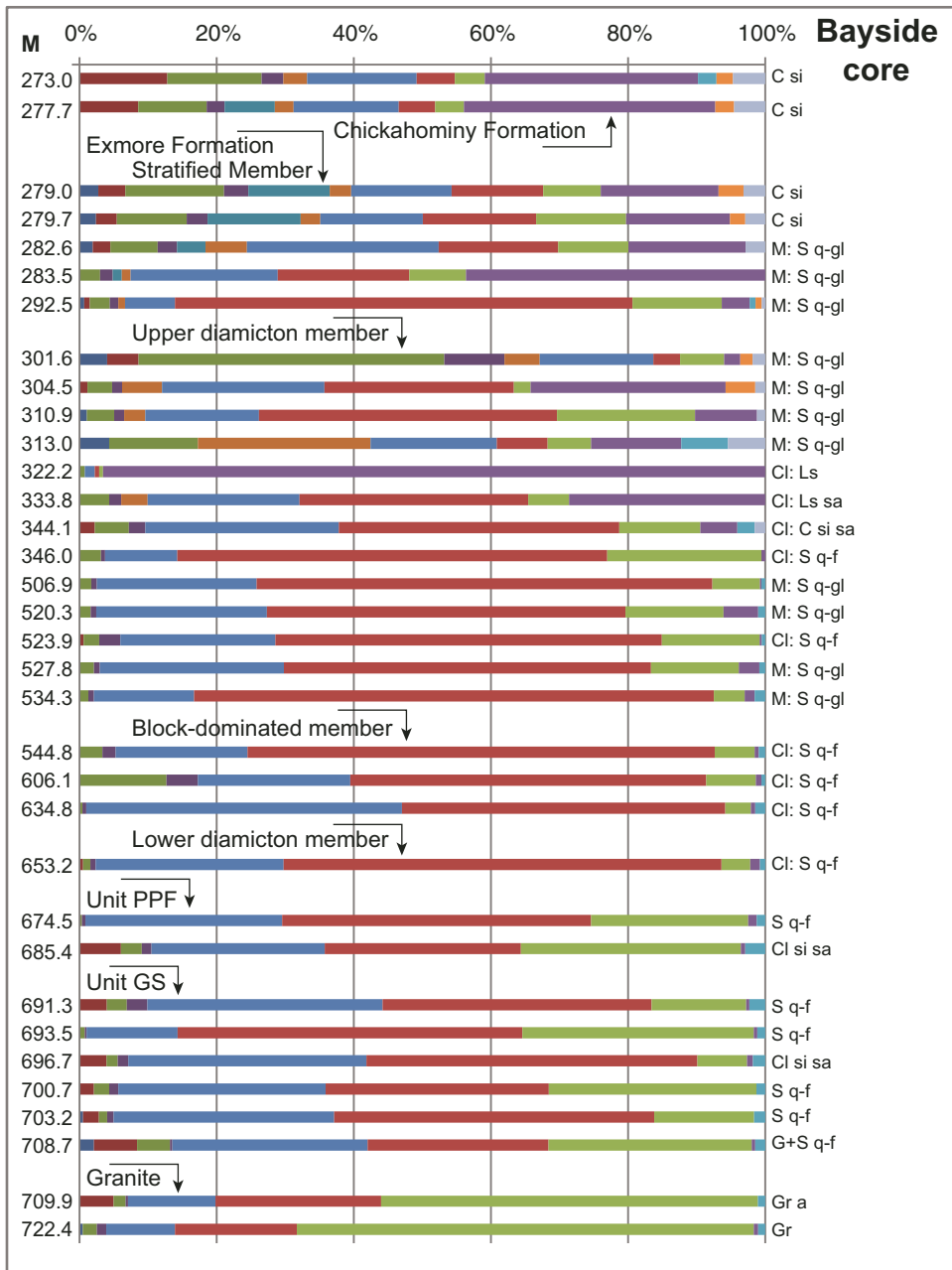


Figure 14. Mineralogical composition of stratigraphic units in the Bayside core as determined by semiquantitative X-ray diffraction (XRD) analysis. Data are from Table 3. See Figure 7 for mineral color code and lithologic letter code. Unit abbreviations: unit GS—gravel and sand unit, unit PPF—parautochthonous Potomac Formation.

sandy, granule-pebble-cobble gravel; (2) light-gray, gravelly (varicolored granules and pebbles), very fine to very coarse sand (Figs. 11G and 11H); (3) light-gray or medium-brownish-gray, silty, very fine to very coarse sand with granules; and (4) dark-gray, slightly to moderately carbonaceous, variably muddy, very fine to very coarse sands.

The sand fractions are feldspathic in all layers, but plagioclase/total feldspar ratios are lower than in the fresh granite below, possibly reflecting selective plagioclase weathering or sediment derived from different source material, as in the Langley core (Table 3; Fig. 14). The clay mineral suite is similar to that of the altered granite, with expandable mixed-layer clay being rela-

tively more abundant than illite and kaolinite. Traces of calcite and dolomite in the XRD samples likely represent contamination by carbonate minerals acquired higher in the drill hole by the drilling mud. Calcareous and (or) glauconitic clasts, and disaggregated calcareous and glauconitic sediments from the Upper Cretaceous and Paleogene marine-target sediments are absent.

XRD analyses of the matrix in unit GS indicate compositions that are comparable to the parautochthonous Potomac Formation samples at Bayside (Fig. 14).

The gravel layers in unit GS are primarily clast supported. A majority of the sand-rich layers contain “floating” rock and sediment clasts. These large clasts range in size from granules

to pebbles and fine cobbles (2–128 mm), except for a single small boulder (280 mm) of fine-grained leucogranite (691.38–691.10 m). The clasts are angular to subrounded.

The polymict clast suite includes: aphanitic and porphyritic (but not cataclastic) varieties of felsite; fine-grained leucogranite; altered clasts of the underlying granite; gray sandy clay; mafic metavolcanic rock; and chert in approximately decreasing order of abundance. Clasts that resemble the underlying granite are present only in the lower 5.4 m of unit GS. Most of these granite clasts, and some of the felsite clasts, are oxidized to red and brown colors, and some have light-gray alteration rinds. Poag et al. (2004, p. 171, their figure 6.4) suggested that the rinds may represent shock alteration and therefore that these clasts represent fallback ejecta. However, we find that the redox rinds on the rock clasts in unit GS do not contain glassy or recrystallized glassy material.

Alternating intervals of sand and gravel in the core may be beds or they may be clasts (see Discussion). Rounded quartz and

quartz-feldspar pebbles typical of the Potomac Formation are not present in unit GS.

No shocked minerals were observed in thin sections of seven pebble-sized clasts (2.7–5.8 cm) of felsite and leucocratic granite from unit GS. Quartz and feldspar grains in residues of five clay-sand samples from depths of 708.39 m to 689.27 m that were subjected to HCl and HF etching prior to further processing for dinocyst analysis also did not show shock deformation features.

The gravel-poor sand layers typically are massive, but a few display parallel laminations and centimeter-scale beds that are defined by variations in grain size and low-angle dips (<10°). Some sand layers change upward by the gradual addition of pebbles into gravel layers, whereas other gravel-over-sand and sand-over-gravel contacts are sharp. Sand-over-gravel contacts have up to 2 cm of relief produced by pebbles and cobbles that protrude from the gravel into the sand. Sand-over-sand contacts are complex and interpenetrating.

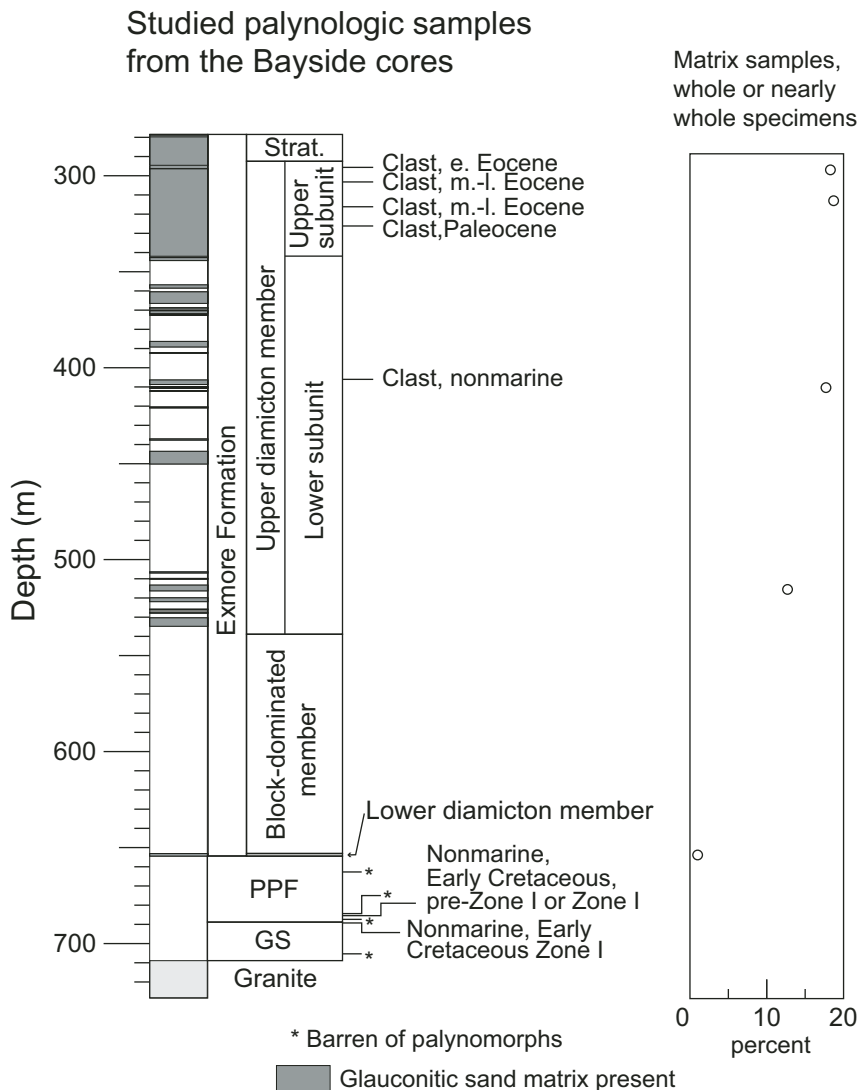


Figure 15. Simplified stratigraphic column of the Exmore Formation, gravel and sand unit (unit GS), and parautochthonous Potomac Formation (unit PPF) recovered from Bayside #1 and #2 cores showing palynological results. For illustrations of fossils and discussion, see Appendix A (dinoflagellate cysts) and Appendix B (nonmarine palynomorphs). Note that clasts are not in normal stratigraphic order, and that even the best-preserved matrix samples contain less than 20% whole or nearly whole dinocyst specimens. Abbreviations: Strat.—stratified member of the Exmore Formation; e.—early; m.—middle; l.—late.

A palynomorph sample (carbonaceous muddy sand) from 689.29 m depth in the upper part of unit GS (Fig. 15; Table 4) was assigned to pollen zone I of Brenner (1963), Doyle and Robbins (1977), and Bebout (1981). This zone is Aptian to early Albian in age (Hochuli et al., 2006; Doyle et al., 2008) and is found regionally in the lower part of the Potomac Formation. An additional sample taken at 705.34 m was barren. However, unit GS does not display the fluvial, typically finer-grained, fining-upward cycles of the subsurface Potomac Formation or the underlying Lower Cretaceous Waste Gate Formation (Hansen and Doyle, 1982) of the Mid-Atlantic region.

Unit GS presently lies above altered Neoproterozoic granite and below the parautochthonous section of the Potomac Formation (unit PPF; Figs. 2 and 12A). This unit's stratigraphic position and palynologic age would be consistent with an in-place section of Lower Cretaceous sediments nonconformably overlying a basement granite. Alternatively, if unit GS at Bayside consists of a transported section of disaggregated basement rock and Lower Cretaceous sediments that was redeposited during the impact event, then a late Eocene age would be appropriate.

Parautochthonous Section of the Potomac Formation (Unit PPF), Upper Eocene (688.82–654.47 m)

Unit PPF is 34.35 m thick in the Bayside core, where it overlies unit GS and underlies the thin lower diamicton member of the Exmore Formation (Fig. 12A). Unit PPF consists entirely of continental sediments comparable to those found regionally in the Cretaceous Potomac Formation (Fig. 13C). Glauconitic clasts and disaggregated sediments from the Upper Cretaceous and Paleogene marine-target sediments, and ejecta clasts were not observed in this unit.

The lower 18.29 m section of unit PPF consists of alternating sand and carbonaceous clay beds that vary in thickness from 0.1 to 3 m within fining-upward cycles. Two sand types are present: light- to medium-gray, laminated to variably bioturbated, silty very fine to fine sands; and mottled light-gray and red-brown, feldspathic, very fine to very coarse sands with 5%–20% granules. Laminations typically are horizontal or have very low-angle dips. Root structures and fine-grained plant material are common to locally abundant in both types. Ripple cross-stratification and dewatering structures are present but sparse, and pebbles and cobbles are absent, except at the base of the unit. The carbonaceous clays vary from medium gray to very dark gray and to mottled dark gray and reddish brown. The clays contain common to abundant root structures and black, particulate plant material. XRD-determined mineral compositions in unit PPF are similar to those in unit GS and in unit PPF at Langley.

The plagioclase/total feldspar ratio is significantly higher in unit PPF than in clasts of the Potomac Formation in the overlying Exmore Formation (Table 3; Fig. 14), suggesting that different parts of the pre-impact Potomac Formation are represented in unit PPF than in the basal part of the Exmore Formation. This may reflect selective plagioclase alteration or sediment derived from different source material. Petrographic analysis of quartz and feldspar

grains in residues of samples from 684.37 m and 682.87 m that were subjected to HCl and HF etching prior to further processing for dinocysts did not find evidence of shock deformation features.

Fining-upward, gravel-sand-clay cycles that vary from 0.1 to 3.0 m in thickness are present in the upper 16.06 m above 670.53 m depth (Fig. 12A). These cycles contain basal gravel layers that contain sparse cobbles and common subrounded to rounded pebbles of quartz, quartz-feldspar, chert, and dark lithic fragments. The sands are feldspathic and indistinctly laminated. Lamination dip angles are typically low to horizontal. The ratio of sand to silt-clay beds is distinctly higher above 670.5 m than below.

A sample of gray, muddy, fine sand from 685.46 m depth in the lower part of unit PPF contained a moderately diverse but numerically sparse assemblage of pollen and spores (Fig. 15). Palynologic samples taken at 687.40, 684.38, and 662.70 m were barren. The mostly wide-ranging taxa in the productive sample limit its likely age only to Early Cretaceous (Valanginian–Hauterivian to Albian, but perhaps not late Albian). An Aptian–early Albian age determination for the underlying palynomorph sample in unit GS suggests that the sample from unit PPF also represents pollen zone I of Aptian–early Albian age, but only if the two samples are in their original relative stratigraphic positions. Therefore, unit PPF physically, mineralogically, and palynologically resembles the lower part of the pre-impact Potomac Formation. However, as noted for unit GS, if these Cretaceous sediments were disaggregated and transported during the impact, or if they were transported together as a large block, we would consider the age of unit PPF to be late Eocene.

Exmore Formation, Upper Eocene (654.47–278.50 m)

Members. The 375.97-m-thick Exmore Formation in the Bayside cores is assigned to four members on the basis of three criteria: (1) contrasting proportions of clasts and disaggregated sediments derived from the Cretaceous Potomac Formation versus those derived from the Upper Cretaceous and Paleogene marine-target sediments; (2) contrasting clast size distributions; and (3) the presence or absence of stratification. From the base upward, these units are the lower diamicton member, the block-dominated member, the upper diamicton member, and the stratified member, following the nomenclature of Edwards et al. (2009); see also Figure 12.

Lower diamicton member (654.47–653.09 m). This thin member consists of 1.38 m of unsorted and unstratified, matrix-supported, muddy, glauconitic, quartz-feldspar sand. Sparse pebbles and fine cobbles (max. 8.5 cm) of sand and dark carbonaceous clay, as well as subrounded to rounded quartz, quartz-feldspar, and chert pebbles, are dispersed throughout the member. The carbonaceous clay clasts resemble similar clays interbedded with sands in underlying unit PPF. A mixed-age assemblage of early, middle, and late Eocene dinocysts is present in a sample from 653.63 m. Nearly all specimens are poorly preserved fragments (but without evidence of impact heating), and taxa of other ages could be present but are not identifiable (Horton et al., 2005a, their figure 12e).

TABLE 4. PALYNOLOGICAL SAMPLES FROM THE BAYSIDE #1 AND BAYSIDE #2 CORES (SEE APPENDICES A AND B)

Palynological samples	Core	Depth (ft)	Midpoint (m)	Sample type	Matrix (300 counts)		Age	Formation(?)	Clasts
					% whole	% frag			
<u>Unit</u>									
	#1								
Chickahominy Formation	R6190F	895.0–895.4	272.86	Clayey silt					
Exmore upper diamicton member	R6190BF	969.8–970.1	295.64	Clast				Marlboro	
Exmore upper diamicton member	R6190E	974.1–974.5	296.97	Matrix-counted	18.3	81.7			
Exmore upper diamicton member	R6190C	994.8–994.9	303.23	Clast			m–l Eoc.	Unnamed ls	
Exmore upper diamicton member	R6190C	1026.4–1026.8	312.91	Matrix-counted	18.7	81.3			
Exmore upper diamicton member	R6190B	1037.2–1037.3	316.15	Clast			m–l Eoc.	Unnamed ls	w/ matrix contam.
Exmore upper diamicton member	R6190A	1070.0–1070.2	326.17	Clast				Aquia	w/ matrix contam.
	#2								
Exmore upper diamicton member (lower subunit)	R6190DC	1332.1–1332.4	406.07	Clast					Nonmarine
Exmore upper diamicton member (lower subunit)	R6190CC	1345.8–1346.1	410.25	Matrix-counted	17.7	82.3			
Exmore upper diamicton member (lower subunit)	R6190CA	1690.7–1691.0	515.37	Matrix-counted	12.7	87.3			
Exmore upper diamicton member (lower subunit)	R6190CE	1924.4–1924.7	586.60	Barren					
Exmore lower diamicton member	R6190CD	2144.1–2144.8	653.63	Matrix-counted	1.0	99.0			
PPF	R6190DB	2174.0–2174.4	662.70	Barren					
PPF	R6190HH	2245.3–2245.4	684.38	Barren					Discussed in Appendix B on pollen
PPF	R6190BA	2248.8–2249.0	685.46	Barren					
PPF	R6190DA	2255.1–2255.4	687.40	Barren					Discussed in Appendix B on pollen
GS	R6190HE	2261.4–2261.25	689.27	Barren					
GS	R6190HB	2314.1–2314.25	705.34	Barren					

Note: frag—fragment; m–l Eoc—middle to late Eocene; ls—limestone; contam.—contamination; PPF—parautochthonous Potomac Formation; GS—gravel and sand unit.

Block-dominated member (653.09–538.89 m). At Bayside, this 114.2-m-thick interval consists entirely of sediments derived from the Potomac Formation. However, its position above the glauconitic sediments of the Exmore lower diamicton member requires assignment to the block-dominated member of the Exmore Formation.

The block-dominated member consists of variably deformed intervals of typical Potomac Formation sediments in the form of blocks or disaggregated sediments that display a general upward decrease in deformational intensity (e.g., dewatering structures). Glauconite is absent, and the small percentages of calcite and dolomite shown on Table 3 and Figure 14 likely represent down-hole contamination. XRD analysis of one Potomac Formation sand clast from the lower diamicton member and three from the block-dominated member display low plagioclase/total feldspar ratios and little or no expandable mixed-layer clays, as compared to the units underlying the Exmore Formation. This suggests pre-impact plagioclase weathering or derivation of the sediment from a higher part of the Potomac Formation.

The basal interval from 653.09 to 628.74 m consists primarily of massive, gravelly (granules-pebbles, 2–64 mm), feldspathic quartz sand that locally contains dewatering structures. Domains in this interval that are the size of fine to medium boulders (0.25–1 m) have diffuse boundaries and relict Cretaceous sand-clay bedding inclined at high to vertical angles (Fig. 13D). The next higher interval (628.74–604.60 m) was poorly recovered but also consists of massive gravelly sand that contains relict bedding inclined at moderate angles in its upper ~3 m.

The uppermost interval from 604.60 m to 538.89 m consists of internally coherent sediment megaclasts (some overturned) of typical Potomac Formation sediments. Within the megaclasts, meter-scale beds of dark-gray or mottled red-gray silty clay alternate with locally burrowed, planar- and cross-bedded, feldspathic quartz sands and sandy granule-pebble gravels containing quartz, lithic, and silty clay clasts. Ripple and dune cross-bed sets that dip less than 25° and root structures occur commonly throughout the interval.

Upper diamicton member (538.89–292.49 m). This 246.40-m-thick member consists of two subunits, as also noted in the Langley core. Both are diamictons that contain clasts (granules to blocks) as well as disaggregated sediments from the Cretaceous continental Potomac Formation and the Upper Cretaceous(?) and Paleogene marine formations. The subequal mixture of these two groups of target sediments contrasts with the dominance of Potomac Formation sediments in the underlying block-dominated member. Ejecta clasts are present in both subunits of the upper diamicton member.

Lower subunit (538.89–341.92 m). This diamicton contains abundant sediment clasts and sparse crystalline-ejecta clasts distributed in an unsorted and unstratified matrix of sparingly calcareous, muddy, feldspathic quartz-glauconite sand and granules (Figs. 16A and 16B). The sediments are locally grain or matrix supported. Clasts of Potomac Formation sediment range from granules to boulders and small blocks (2 mm to 8.2 m), whereas

clasts of the younger marine-target sediments range only from granules to fine cobbles (2–128 mm).

Fining-upward intervals containing laminations, cross-laminations, and root structures typical of the pre-impact Potomac Formation sediments are present within many Potomac sediment clasts. Sand dikes, dewatering structures, and convolute bedding are common within these clasts and most likely represent pre-impact liquefaction, since they were not observed in the matrix. The orientations of cross-laminations and fining-upward intervals within some Potomac clasts indicate that they are overturned.

The 48.7 m interval from 506.4 to 457.7 m consists of red-brown-gray-mottled Potomac Formation sands and clays interrupted at a few places by centimeter-scale stringers of glauconitic sediment. Bedding in this interval dips at moderate to steep angles. Three other long intervals that consist of similar sediments also occur at 437.1–420.9 m, 406.4–392.4 m, and 386.3–372.1 m. Each of these four intervals may consist individually of a single, largely intact, but internally fractured boulder or block, or they may be groups of stacked boulders of Potomac sediments.

The plagioclase/total feldspar ratios in samples of Potomac sand clasts from the lower subunit are higher than those in samples of Potomac sand clasts from the upper subunit. This change suggests that different parts of the pre-impact Potomac Formation are included in those subunits, respectively (Table 3; Fig. 14). The higher ratios suggest less-weathered or different source material.

The clasts of crystalline-rock ejecta in the lower subunit include granitic rocks and lesser amounts of felsite that are variably overprinted by cataclastic fabrics. The largest of these clasts is a boulder of polymict cataclasite, which extends (including core loss) from 360.4 m to 359.5 m depth, where the top was lost during drilling. The polymict cataclasite consists mainly of brecciated but cohesive leucogranite with sparse fragments (<2 cm length) of mafic igneous rock. A $^{40}\text{Ar}/^{39}\text{Ar}$ age spectrum of muscovite from the leucogranite indicated a radiometric age of 616–606 Ma (Neoproterozoic) for cooling through the closure temperature for argon (~350 °C) without discernible impact heating (Horton et al., 2005a, p. 157–162). A 7 cm clast of smectite interpreted to represent altered impact melt glass is present at 410.1 m depth.

Two matrix samples from the lower subunit at 515.37 and 410.25 m contained mixed-age assemblages of late Paleocene and early, middle, and late Eocene dinocysts. Most specimens (82%–87%) were variably preserved fragments, some with evidence of impact heating.

Upper subunit (341.92–292.49 m). The sediments of this 80.1-m-thick subunit are similar in most respects to those of the underlying lower subunit of the upper diamicton member, but there are somewhat larger variations in the XRD mineralogy of the upper subunit. The upper subunit also is a diamicton with clasts supported by an unstratified and unsorted matrix of fossiliferous, muddy, feldspathic, quartz-glauconite sand and granules (Figs. 12B and 16C). Unlike the lower subunit, cobbles (<0.25 m) are the largest recovered clasts in the upper subunit, with one

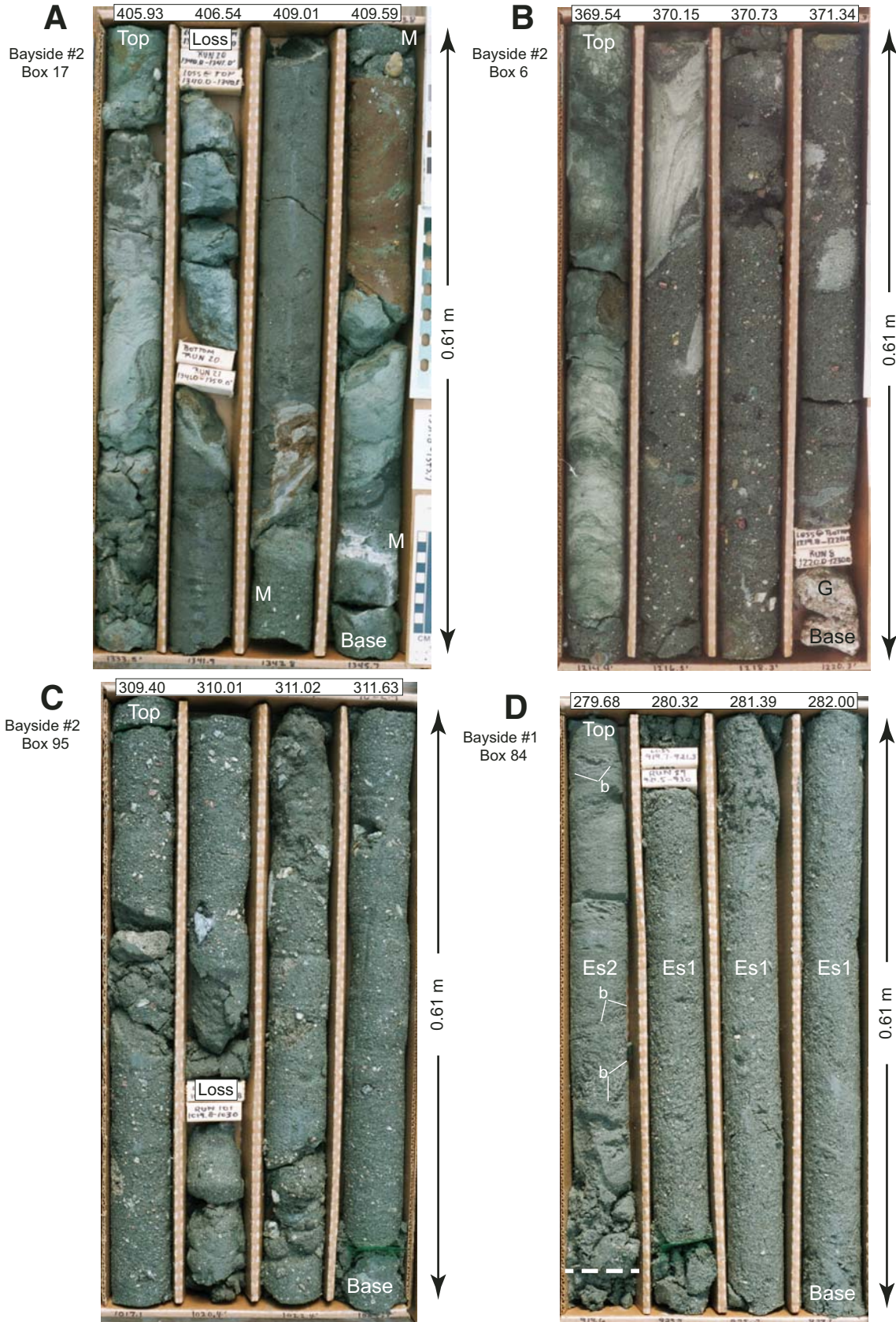


Figure 16.

exception, a 1.86 m boulder of gray silty clay derived from the Eocene Marlboro Clay (296.4–294.6 m).

This subunit's polymict suite of sediment granules, pebbles, and cobbles represents most or all of the Cretaceous and Paleogene target-sediment formations, including: clasts of Potomac Formation gravel, sand, silt, and clay in variable proportions; cemented, glauconitic, bioclastic limestone and shelly quartz sand; cemented, sparingly glauconitic limestone; indurated, shelly quartz-glaucanite sand; and indurated, glauconitic silty and sandy clay. Shell fragments and typically rounded quartz, quartz-feldspar, quartzite, chert, and phosphate pebbles also are present. The larger clasts primarily consist of Potomac Formation sediments. The upper subunit also contains ejecta clasts dominated by aphanitic to porphyritic felsite and by granitoids (e.g., monzonite at 320.41 m).

Four clasts and two matrix samples from the upper subunit were examined for dinoflagellate cysts (Fig. 15, Appendix A). A carbonate-cemented, shelly, glauconitic sandstone clast at 326.17 m contained late Paleocene dinocysts and is thus identified as being derived from the Aquia Formation. Two gray limestone clasts (316.15, 303.23 m) contained latest middle to early late Eocene dinocyst assemblages and are thus derived from an as-yet-unidentified formation. A fine-grained clast from 295.64 m depth contained an early Eocene assemblage that represents the Marlboro Clay. Matrix samples from 312.91 and 296.97 m included mixed-age Paleocene and Eocene assemblages. Most specimens were fragments (81%–82%); preservation was highly variable and included textures indicative of impact melting.

XRD analyses of samples from the upper diamicton member vary considerably because of the compositional and grain-size heterogeneity of its sediments (Table 3; Fig. 14), as noted above for the underlying block-dominated member. The amounts of calcite, siderite, and pyrite in the upper subunit of the upper diamicton member are distinctly greater than those in the lower subunit. These differences correspond to the increase in macrofossils and microfossils, and secondary pyrite and iron minerals

observed in hand samples and thin sections of the upper subunit (Figs. 16C).

Stratified member (292.49–278.50 m). The stratified member of the Exmore Formation is 13.99 m thick in the Bayside core. It is divided into lower subunit Es1 and upper subunit Es2 (Figs. 12B and 16D), which also are recognized in the Langley and Eyreville cores. The two subunits are differentiated by the presence of pebbles and granules in Es1 and their near absence in Es2 at Bayside. No biostratigraphic data were collected from this member at Bayside.

Subunit Es1 (292.49–280.26 m). This unit is 12.23 m thick and consists of poorly sorted, muddy, calcareous, glauconitic, quartz-feldspar sand and gravelly sand. The sand fraction ranges from very fine to very coarse, and the gravel fraction consists of granules and pebbles smaller than ~1.0 cm. Repetitions of pebble concentrations, massive intervals, and indistinctly burrowed intervals may indicate depositional units with thicknesses of 1–3 m (Fig. 16D).

The clay mineral suite consists primarily of illite and minor glauconite with secondary kaolinite and expandable mixed-layer clay (Table 3; Fig. 14). Siderite and pyrite are locally present, and calcite is common to abundant. Heulandite/clinoptilolite is present in two samples from the upper part of the subunit.

Subunit Es2 (280.26–278.50 m). This subunit is a 1.76-m-thick, fining-upward section of muddy, calcareous, glauconitic quartz-feldspar sand and overlying finer-grained sediments. Below ~278.82 m, the maximum sand size decreases upward from very coarse to very fine. This interval is characterized by subhorizontal, sand-filled burrows (~1 cm diameters) with thick clayey walls that decrease in abundance upward (Fig. 16D). Sparse, centimeter-scale massive intervals also are present. Above ~278.82 m, the (silt + clay)/sand ratio rapidly increases to the degree that the unit becomes a wavy-laminated section of clayey silt and muddy very fine sand. The mineralogy of the clay-sized fraction is similar to that of subunit Es1. Heulandite/clinoptilolite is present in two XRD samples from Es2 (Table 3; Fig. 14).

Chickahominy Formation, Upper Eocene (278.50–213.39 m)

The Chickahominy Formation is 65.11 m thick at Bayside, where it consists of typical brownish-gray to olive-gray, bioturbated (e.g., *Terebellina*) to locally parallel-laminated, calcareous, fine-grained sediments similar to those in the Chickahominy sections in the Watkins School and Langley cores. Quartz, K-feldspar, plagioclase, glauconite, pyrite, mica, microfossils, and macrofossil fragments are present in the sand fraction. The clay mineral suite is dominated by illite (including glauconite) with secondary expandable mixed-layer clay and kaolinite (Table 3; Fig. 14). XRD analysis also indicates abundant calcite and common siderite and pyrite. Heulandite/clinoptilolite is present in three XRD samples from the basal 2 m of the unit.

The XRD-determined mineral compositions of the Exmore Formation in the Bayside cores are similar to those in the equivalent units of the Langley core. The compositions of the uppermost

←

Figure 16. Photographs of the Bayside core, upper diamicton and stratified members of the Exmore Formation. (A) Matrix-poor, clast-supported section of the lower subunit of the upper diamicton member of the Exmore Formation containing contorted clasts of sediments from the Potomac Formation. M—matrix. Note the centimeter scale at lower right. (B) Section of contorted sediment clasts, predominantly from the Potomac Formation, in typical matrix of calcareous, glauconitic, muddy, quartz-feldspar sand and granules derived from the Cretaceous and Paleogene target sediments. Note the cataclastic granite clast (G) at the lower right. Lower subunit of the upper diamicton member of the Exmore Formation. (C) Sediment and rock pebbles in typical diamicton matrix. Upper subunit of the upper diamicton member of the Exmore Formation. (D) Contact interval between the lower subunit (Es1) and upper subunit (Es2) of the stratified member of the Exmore Formation. Es1 consists of massive, muddy, fine to very coarse quartz-feldspar sand with sparse pebbles. Es2 consists of locally massive or laminated, muddy finer-grained sand. Several burrows (b) are marked in subunit Es2.

part of the upper diamicton member and the stratified member at Bayside also are similar.

Poag (2012) assigned the Chickahominy section at Bayside to late Eocene planktonic foraminiferal zones E15?, E15, and E16. Marine dinocysts from a sample in the lower part of the Chickahominy Formation also indicate a late Eocene age. Sparse impact-damaged dinocyst specimens are present, and radiolarians, diatoms, silicoflagellates, sponge spicules, and pollen also were observed.

Summary

The Bayside core is representative of the inner part of the brim. The principal characteristics of this section include the presence of unshocked Neoproterozoic granite below the coarse sediments of enigmatic unit GS (see Discussion), which are overlain by deformed, parautochthonous sediments of unit PPF (see Discussion). The granite is mineralogically, petrologically, and chronologically similar to the Langley Granite. Both granites were minimally affected by the impact event. Unit PPF is similar to unit PPF at Langley with regard to pre-impact sedimentation and synimpact deformation. The lower diamicton and block-dominated members of the Exmore Formation at Bayside are absent at Langley, resulting in a thicker Exmore section at Bayside than at Langley. The stratigraphy and composition of the Exmore Formation at Bayside are similar to the stratigraphy and composition of the Exmore Formation in the Eyreville core in the central crater.

DISCUSSION: IMPACT STAGES AND PROCESSES IN THE BRIM

Lateral Correlations and Impact Processes

The results of this study, when integrated with previous work, provide insights into the complex interaction of the temporally overlapping processes that occur in the target-sediment layer of a large marine impact structure. Large variations in the style and magnitude of impact deformation and material transport were observed in the cores from the outer margin of the brim toward the central crater (Fig. 17). These parameters also change vertically as functions of the pre-impact depth and composition of the target materials.

Here, we discuss the succession of impact effects on the uppermost basement rocks and the target-sediment layer of the brim and relate them to the transport of these target layers toward and into the central crater (Figs. 17 and 18). Central-crater sedimentation in the Chesapeake Bay impact structure (Eyreville core), and other marine-target impact structures, has been discussed at length by Gohn et al. (2009b), Dypvik and Kalleson (2010), and Azad et al. (2015).

The succession of impact effects is discussed using the frequently cited, temporally overlapping stages in the evolution of an impact event (Melosh, 1989). Therefore, the inherent processes of a hypervelocity impact are briefly reviewed for each stage.

Contact and Compression Stage

Processes

During this nearly instantaneous stage, the kinetic energy of the projectile is transferred to the target and the impactor as shock waves (Melosh, 1989, 2013; Osinski and Pierazzo, 2013). The shock wave is reflected as a rarefaction wave from the upper surface of the impactor, resulting in the melting and (or) vaporization of the projectile. A shock wave and subsequent rarefaction wave also result in fragmentation, shock metamorphism, melting, and (or) vaporization of the target. These direct effects are primarily limited to the target volume that becomes the transient cavity in the following excavation stage. Only tensile fragmentation and near-surface spallation of target materials extend outside the boundary of the excavated transient crater (Melosh, 1984, 1989, 2013).

Target Fragmentation

In the Chesapeake Bay impact structure, tensile fragmentation of target sediments during the compaction and compression stage may be indirectly represented by variations in the size of postimpact clasts relative to sediment type. The larger clasts observed in the Exmore resurge sediments typically consist of the most coherent and oldest target sediments, specifically clay-dominated Potomac Formation beds. Less-coherent Potomac sands and Upper Cretaceous–Paleogene marine sediments from the upper part of the target-sediment layer are represented primarily by smaller clasts and disaggregated grains in the matrix. These variations in grain size may represent a differential response to tensile fragmentation by stronger and weaker (older and younger) target sediments, in part, but they also represent the effects of subsequent seismic shaking (Melosh, 1989, section 12.6) and resurge erosion and transport. The undeformed character of the Potomac Formation sediments in the Watkins School core suggests that this location was outside the zone of intense tensile fragmentation.

The dilational cracks and small-offset faults filled with microbreccia or gouge in the altered granite at Bayside likely were impact induced. However, the fractures, faults, and veins that are filled or coated with greenschist-facies minerals in the least-altered granites at Langley and Bayside formed at higher temperatures and pressures, and over longer durations, typical of late magmatic hydrothermal fluids or Paleozoic greenschist-facies regional metamorphism (Horton et al., 2005a, 2005b).

Shocked Minerals and Impact Melt

Impact melt particles and shocked minerals found as individual grains and in rock ejecta in the Exmore Formation record passage of the shock wave in the evolving transient crater prior to their ejection, fallback, and redistribution by the resurge flows. In the brim, shocked minerals and impact melt were not observed in the Neoproterozoic granites, unit GS at Bayside, unit PPF at Langley and Bayside, or in the Potomac Formation at the Watkins School site. Shocked minerals and impact melt also are absent in

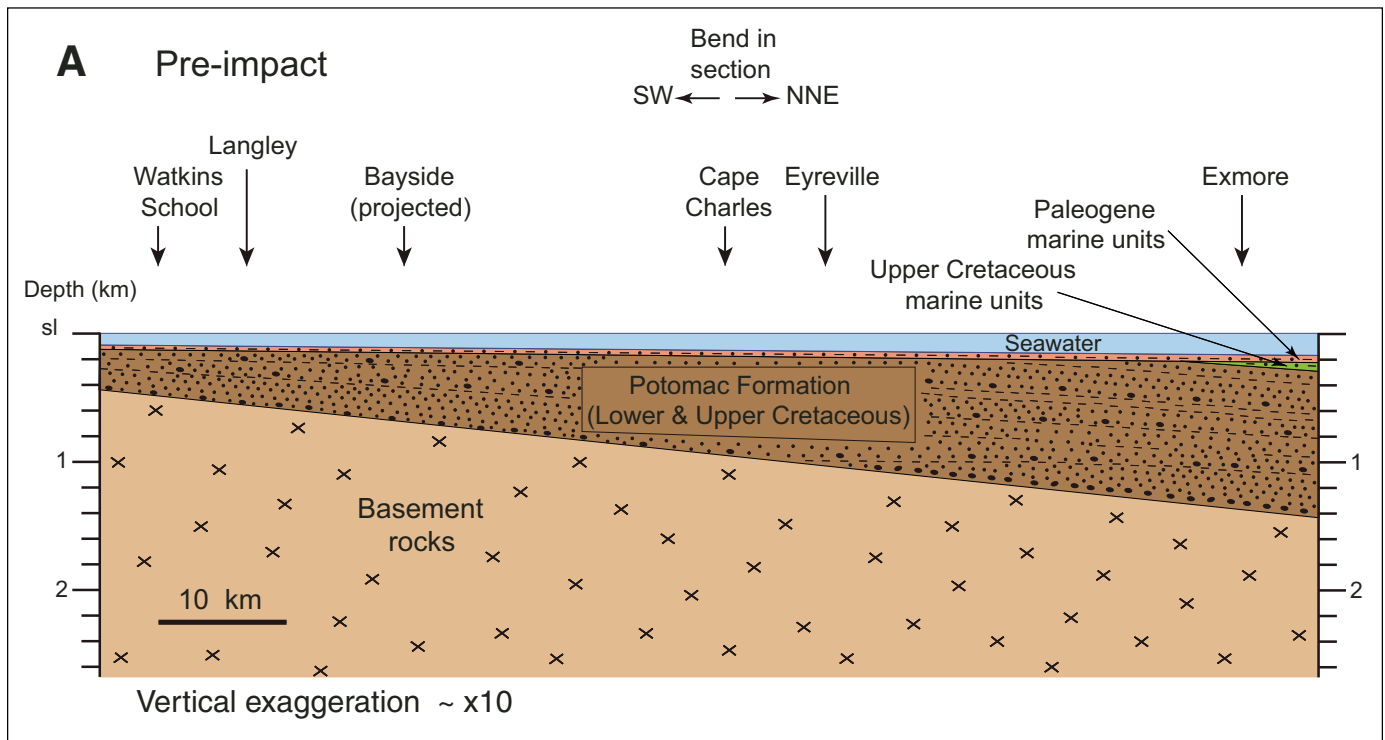
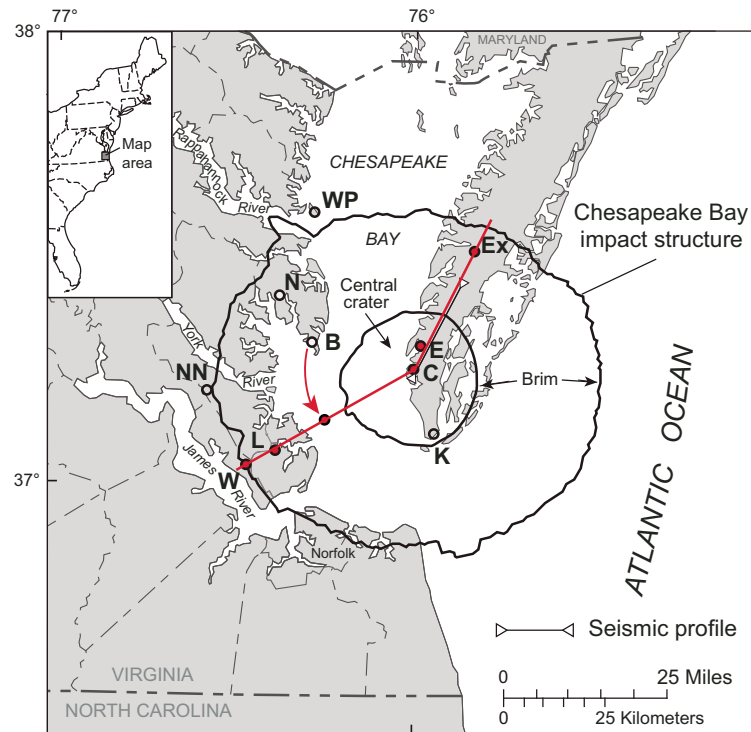


Figure 18 (Continued on following pages). Schematic time-series cross sections for the development of the Chesapeake Bay impact structure (line of section is shown on the location map; see Fig. 1 for acronyms on map). Vertical exaggeration is 10×. (A) Pre-impact target stratigraphy; sl—sea level. Note the multilayered seawater-sediment-rock target. The basement is shown as an undifferentiated section; however, various target basement rocks were observed as excavated clasts in the studied cores, in addition to the Neoproterozoic granites in the Langley and Bayside cores.

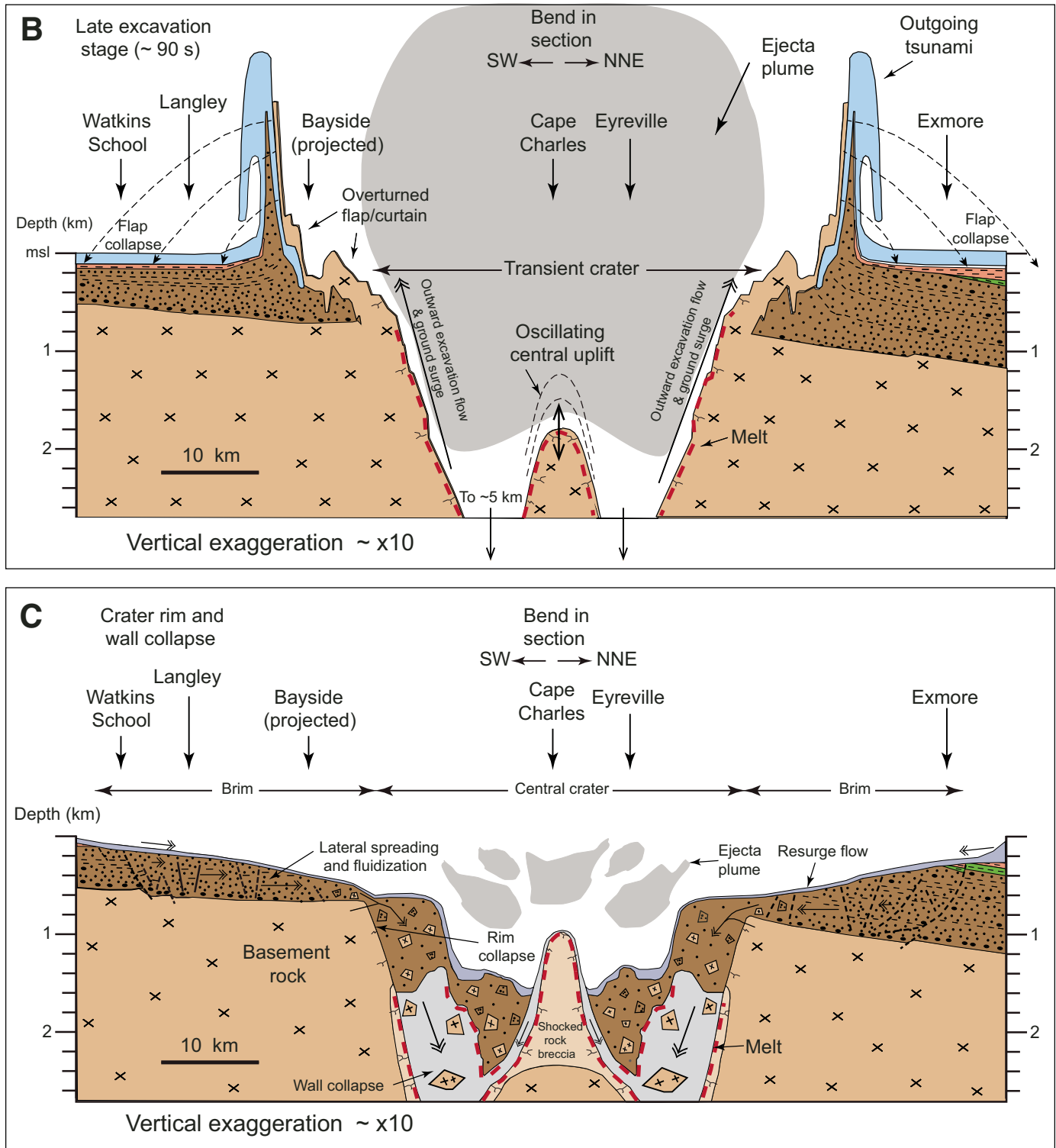


Figure 18 (*Continued*). (B) Late excavation stage; msl—mean sea level. Principal features include: ground surge and excavation flow; an oscillating (and later collapsing) central uplift in the open transient crater; the imminent collapse of the overturned flap and ejecta curtain; a radially outgoing tsunami; and an ejecta plume. The configuration of the impact structure is based on: the Collins et al. (2008b) hydrocode model at a model time of ~90 s; figure 5B of Kenkmann et al. (2009), which also represents an elapsed time of ~90 s after impact; and data presented in this report. (C) Crater rim and wall collapse. Outward and upward movement of material has transitioned to inward and downward collapse of the transient-crater wall and rim and inward movement of target sediments in the brim due to seismic shaking and seawater resurge. The configuration of the impact structure is based on the Collins et al. (2008b) hydrocode model at a model time of ~530 s.

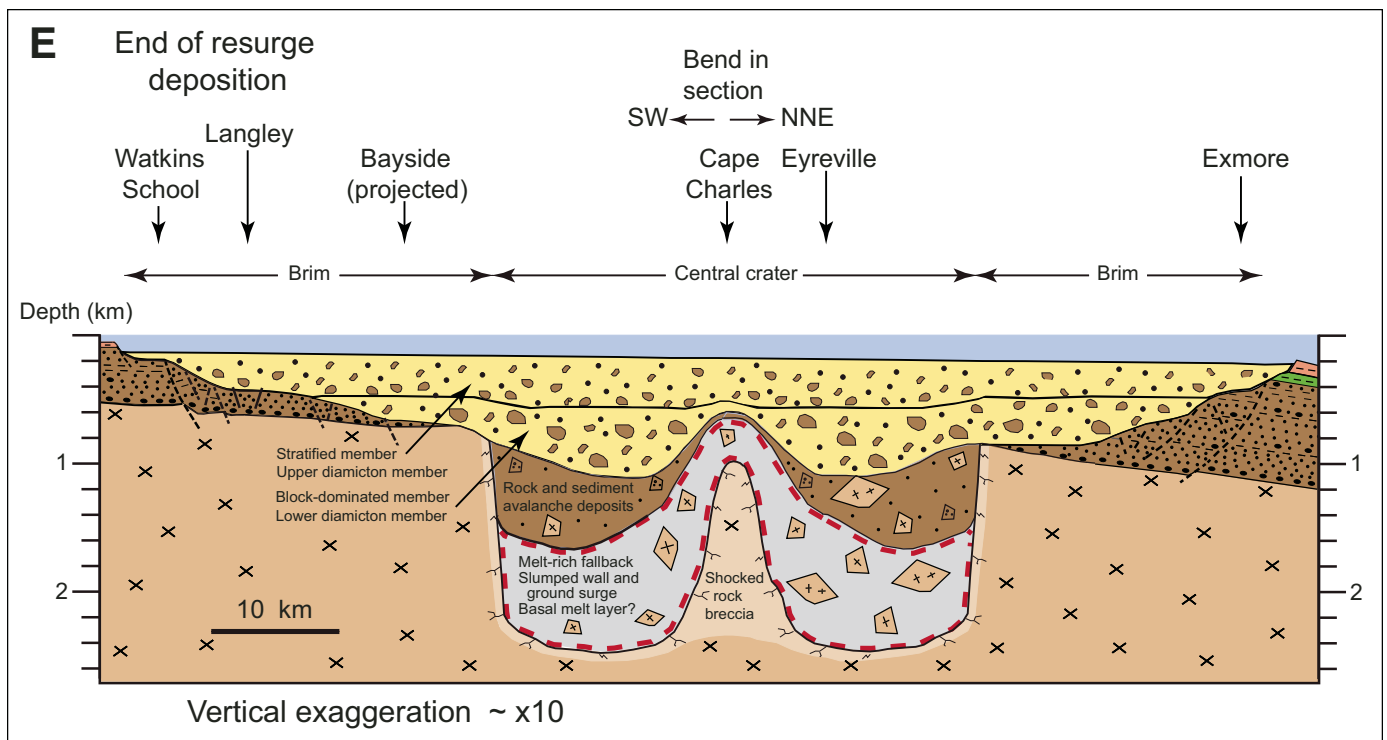
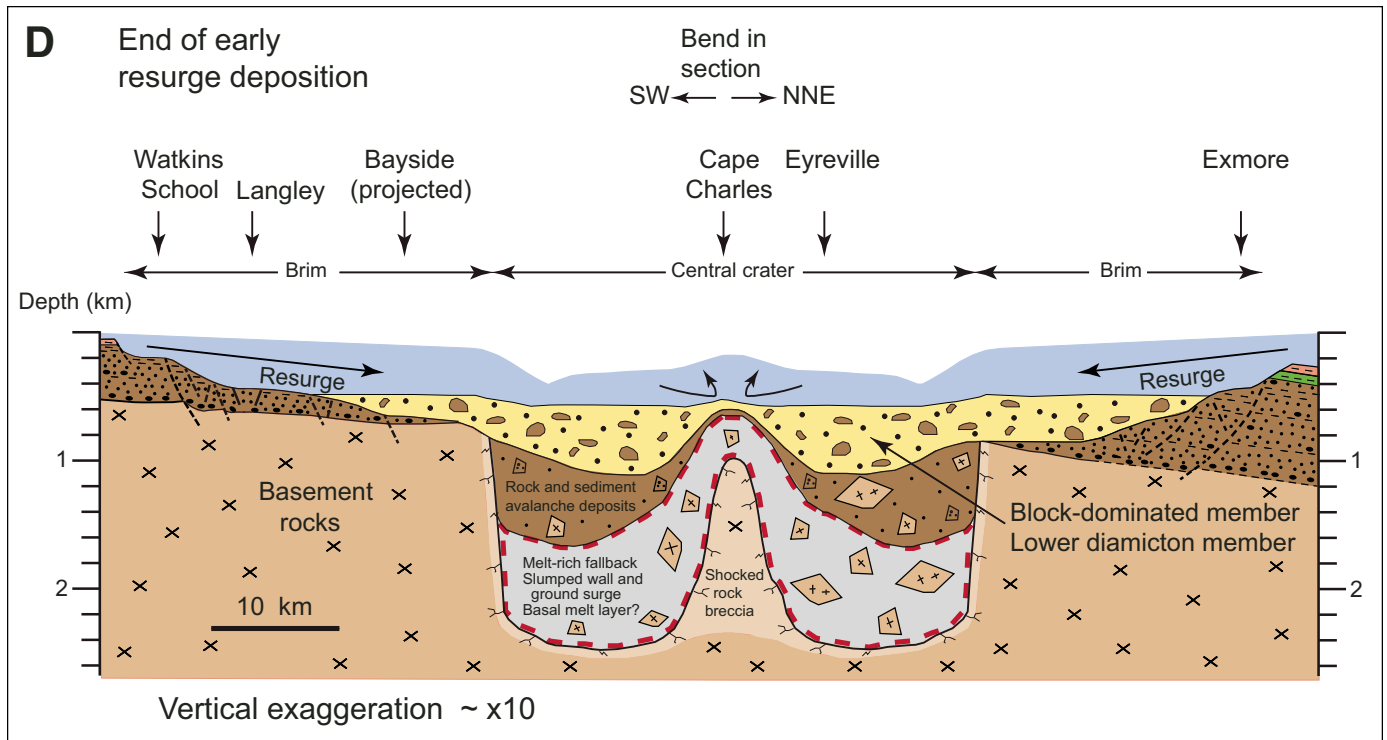


Figure 18 (*Continued*). (D) End of early Exmore Formation resurge deposition. Inward transport of sediment derived from the brim and the area outside the brim by seawater resurge is ongoing. Deposition of the upper diamicton member of the Exmore Formation is in progress. The configuration of the central crater in D, E, F, and G is based on the seismic-reflection and -refraction survey of Catchings et al. (2008) and data presented in this report. (E) End of Exmore resurge deposition and the transition to normal shelf sedimentation. Deposition of resurge sediments has ended, and deposition of sediments suspended by the impact in the water column is ongoing at rates greater than typical shelf sedimentation.

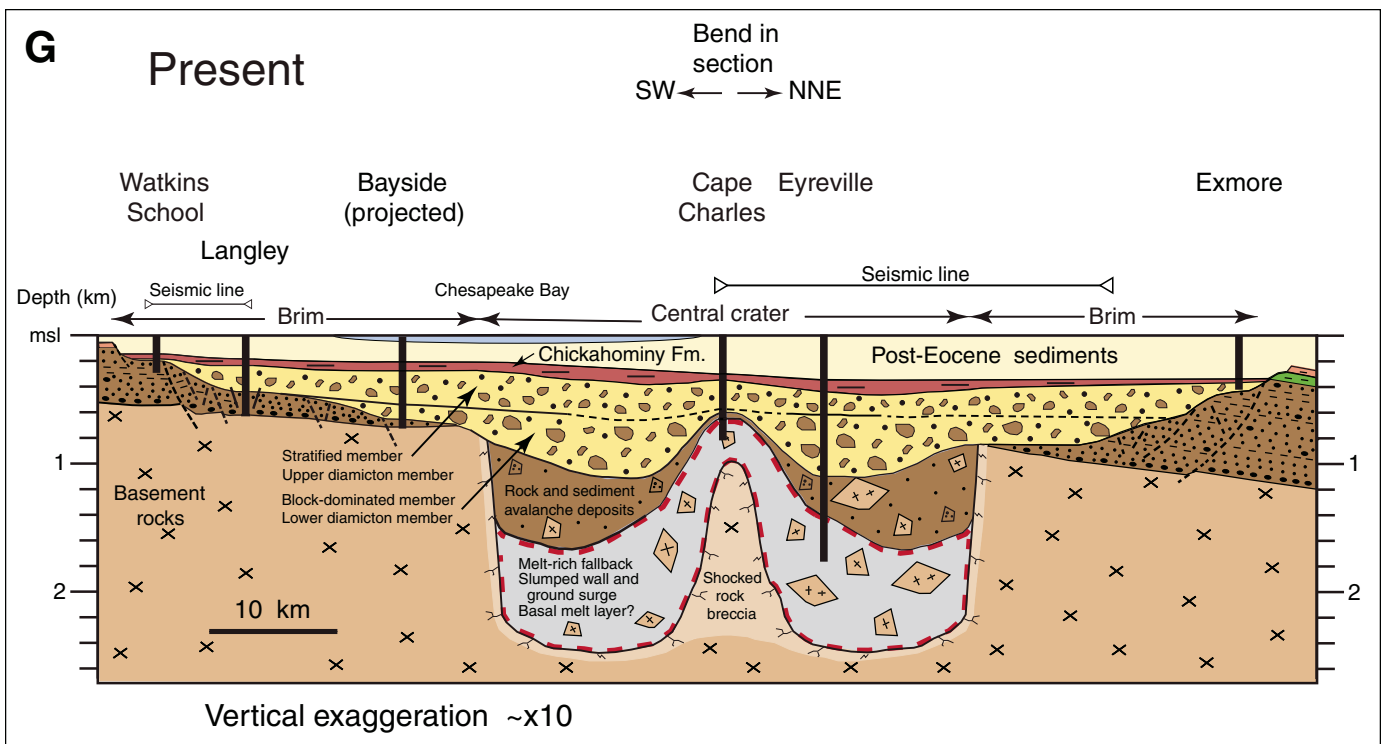
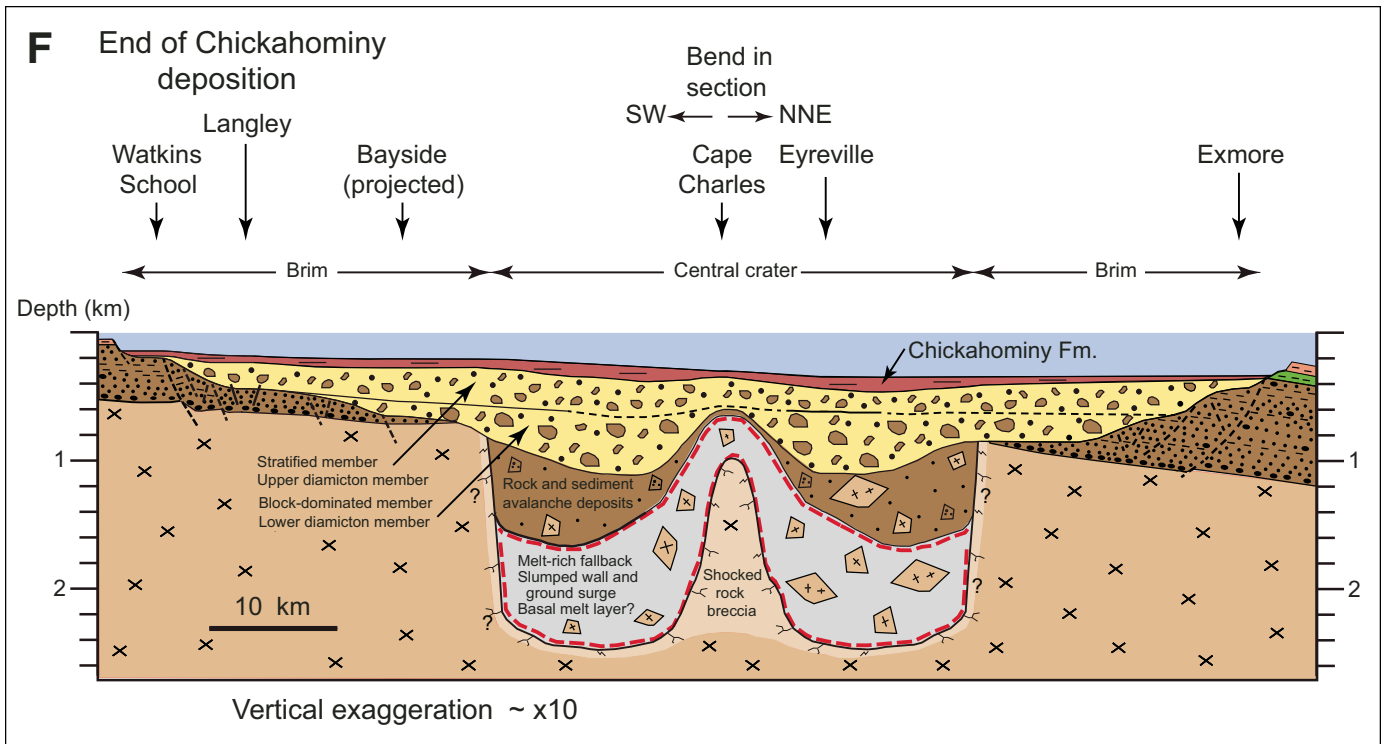


Figure 18 (Continued). (F) End of early postimpact shelf deposition of the Chickahominy Formation. (G) Present configuration of the impact structure. The locations and depths of the studied core holes are indicated.

the granite megablock in the Eyreville core that was transported from the brim's inner margin into the collapsing transient crater. Fission-track studies of zircon and apatite from the granites at Langley and Bayside did not detect any Eocene thermal event (Horton et al., 2005b). Shocked and unshocked metamorphic and igneous rocks, suevitic and lithic impact breccias, and impact melt rocks derived from a variety of target basement rocks are present below allochthonous rock and sediment breccias in the collapsed transient crater, as seen in the Eyreville core (Horton et al., 2009a, 2009b) and in the Cape Charles core (Horton et al., 2004, 2005c, 2008).

Excavation Stage

Processes

The hemispherical shock wave produced at the point of impact expands outward and interacts with the downward-traveling rarefaction wave produced by reflection of the shock wave at the target surface (Melosh, 1989; Osinski and Pierazzo, 2013; Osinski et al., 2013). Their interaction produces an excavation flow (ejection and spallation) of target material that moves radially outward and opens the transient cavity. Target materials below the zone of excavation flow are displaced downward and outward, resulting in allochthonous, variably shocked breccias that primarily remain in the transient crater above parautochthonous rocks of the crater floor.

Excavation Flow, Overturned Flap, Ejecta Curtain, and Outgoing Tsunamis

Excavation flow of target materials did not occur in the brim outside the transient cavity in the Chesapeake Bay impact structure. However, the brim was affected directly by the results of excavation flow in the transient cavity. Loading of the target sediments by the collapsing overturned flap and ejecta curtain caused additional fragmentation and vertical mixing of rocks and sediments in the inner part of the brim (Fig. 18B; Collins et al., 2008b; Kenkmann et al., 2009, their figure 5b). An outgoing tsunami ("rim wave" of Wünnemann et al., 2010) produced by collapse of the overturned flap caused additional dynamic loading in the central and outer parts of the brim and beyond (Fig. 18B; and between Figs. 18B and 18C). The effects of overturned-flap collapse may be recorded in the lower part of the Bayside core (see Modification Stage). However, except for the presence of ejecta in the resurge deposits, the effects of these early processes cannot be differentiated in drill cores from the concurrent and subsequent effects of seismic shaking and inward seawater-resurge flow, discussed below.

Ejecta Fallback and Possible Plume Interaction

Shocked and unshocked lithic clasts, shocked mineral grains, and sparse impact melt clasts are present as entrained fallback ejecta in resurge sediments of the Exmore Formation across the entire impact structure (Horton and Izett, 2005; Horton et al., 2002a, 2002b, 2005a, 2008, 2009b; Ormö et al., 2009; Reimold

et al., 2009). An example of interaction between the vapor-rich impact plume and resurge sediments possibly is represented in the lower subunit of the Exmore upper diamicton member in the Langley core. The anomalous paucity of calcareous fossils in the matrix of this unit suggests local contact with acidic and (or) hot vapor of the plume at a considerable distance from the transient crater (e.g., Kenkmann et al., 2009, their figure 5).

Modification Stage

Processes

Gravity-driven collapse of the transient crater starts as the energy transferred from the impactor to the target begins to wane (Melosh, 1989; Melosh and Ivanov, 1999; Osinski and Pierazzo, 2013; Kenkmann et al., 2013). Inward and upward movement of the cavity's floor produced a central peak in the transient crater of the Chesapeake Bay impact structure, which was followed closely by downward and inward collapse of the cavity wall. In the inner brim, target materials were moved as avalanches and other mass flows toward and into the transient cavity by rim collapse, seismic shaking, and ocean resurge. Ocean resurge initially eroded target sediments within and outside the brim, but later resurge erosion was limited to the area outside the brim after target sediments in the brim were covered by initial resurge sediments (Figs. 17 and 18C–18G).

Transient Crater Rim Collapse

Evidence for the transport of unshocked basement rocks as megaclasts across significant distances near the rim of the transient crater is provided by a 13.32-m-thick block of amphibolite in the sand and crystalline block unit (unit SCB) and the 275.37-m-thick granite megablock recovered in the Eyreville core (Figs. 17 and 18C; Horton et al., 2009b; Townsend et al., 2009). High-resolution seismic lines across the Eyreville drill site suggest that the granite megablock has lateral dimensions of a few hundred meters (W-E) to at least 1 km (NE-SW; Powars et al., 2009).

The absence of shocked minerals and melt rock in the granite megablock indicates that it was originally located outside the zone of shock pressures during the first minute of the impact event. We concur with interpretations that it subsequently moved due to seismic shaking and gravity-driven collapse of the transient crater rim and slid into the central crater, where it is now encased in variably disaggregated Cretaceous target sediments (Gohn et al., 2009b; Horton et al., 2009b). Kenkmann et al. (2009, their figure 5) placed its initial location at the hinge of the overturned flap and indicated an inward transport distance of ~6 km.

The lowest ~7 m of the granite megablock at Eyreville are red, pervasively altered, and contain dilational fractures filled with quartz, sericitic white mica, and chlorite, similar to the dilational mineralized fractures in the altered granite at Bayside. Further study is needed to determine if this zone of alteration in the Eyreville granite megablock was inherited from the pre-impact basement, produced during the impact event, or caused by

postimpact hydrothermal activity as documented in the underlying sand (Malinconico et al., 2009; Horton et al., 2009b).

The sediment boulders and sand unit (SBS; 1095.70–867.43 m) overlies the granite megablock in the Eyreville core (Fig. 17). It consists of blocks, boulders, and smaller clasts of Potomac Formation sediments separated by zones of fluidized Potomac sand. Upper Cretaceous and Paleogene glauconitic sediments occur only in a few centimeter-scale veins near the top of the unit, and shocked material and melt clasts are absent.

The carbonaceous character of the clays in unit SBS is similar to that of clays in unit PPF at Langley and Bayside. Pollen and spore assemblages from samples of unit SBS indicate Aptian–Albian and Albian ages that are typical of the lower to middle part of the pre-impact Potomac Formation. However, the clasts with these ages are not present in normal stratigraphic order (Self-Trail et al., 2009, their figure 12). Therefore, unit SBS represents mass transport of sediments from the lower part of the pre-impact Potomac Formation in the inner brim to the collapsing transient crater.

These sediments moved as one or more transported megaclasts due to seismic shaking (Edwards et al., 2009; Gohn et al., 2009b). The near absence of exotic materials in the unit suggests that the megaclast(s) remained relatively coherent during transport until it (they) reached the rim of the transient crater and then moved downslope as catastrophic sediment avalanche and density flows.

Pollen and spore assemblages from two samples of the sand matrix that surrounds rock boulders and blocks in unit SCB below the granite megablock at Eyreville (Fig. 17) suggest that they are (?)Berriasian to Barremian (Self-Trail et al., 2009, their figure 12). This age is older than the Aptian to middle Albian ages of samples from unit SBS (transported Potomac Formation) above the granite megablock at Eyreville and the Aptian–early Albian age indicated by the pollen and spore assemblage in unit GS at Bayside. The sediments in unit SCB may represent material collapsed from the downdip (eastern) part of the transient-crater rim, where older Cretaceous sediments are known to be present in the subsurface of the Delmarva Peninsula (Hansen, 1982).

Remnant Target Sediments at Watkins School and Langley

Remnant sections of the Cretaceous Potomac Formation are present above the basement rocks and below the resurge sediments in the Watkins School and Langley cores (Figs. 17 and 18). Their thicknesses decrease toward the central crater, primarily as a result of the inward-increasing depth of resurge erosion and earlier extensional slumping.

In the Watkins School core, the typical depositional cycles of the Potomac Formation remain intact, and no downward mixing of Upper Cretaceous and Paleogene target sediments and fossils, or shocked and (or) cataclastic ejecta, occurred (Fig. 6). Stratification in the Potomac sediments is not rotated, and liquefaction of sediments is minimal and probably occurred during their original Cretaceous deposition. Pervasive fracturing and faulting were not observed. These characteristics suggest that the Potomac

sediments at Watkins School could have spread laterally with minimal disruption and rotation for only a short distance as part of a large, upright, coherent megaclast during the impact event.

In the Langley core, the pattern of Cretaceous deposition remains largely intact in unit PPF, with limited rotation of bedding and no vertical mixing of ejecta clasts and Cretaceous and Paleogene marine fossils and sediments (Fig. 8). Poag et al. (2004, their figure 6.3A) referred to the lower subunit of unit PPF (626.3–594.4 m) at Langley as a décollement zone. Although core samples are not conducive to documenting such a zone, we did not observe structural evidence for a horizontal décollement, or for listric normal faults caused by lateral spreading, in this interval. We attribute certain local disruptive features observed in this interval to be the result of pre-impact processes (e.g., clay intraclasts, sediment load structures, and pedogenic structures).

Seismic Shaking and Lateral Spreading

Fragmentation of the target sediments by the rarefaction event, discussed above, was followed closely by seismic shaking, which is apparent in animations produced from *iSALE* hydrocode models of the Chesapeake Bay impact event (Collins and Wünnemann, 2005; Collins et al., 2008b; Kenkmann et al., 2009). Gohn et al. (2005) and Horton et al. (2006, 2008) suggested that this shaking produced the observed sediment liquefaction and inward-directed lateral spreading of the target-sediment layer in the brim in a manner similar to earthquake-generated lateral spreading of susceptible near-surface sediments. Lateral spreading is defined as the finite, lateral movement of gently to steeply sloping, saturated soil or sediment deposits caused by earthquake-induced liquefaction (Kramer, 2013). The initiation of lateral spreading likely proceeded in a headward manner outward from the transient cavity.

Liquefaction is the transformation of a saturated granular material from a solid to a liquefied state as a consequence of increased pore-water pressure; it can be induced by gravity loading, seismic shaking, nonseismic vibrations, or wave-induced shear stresses (Obermeier, 1996; Obermeier et al., 2001). Liquefaction occurs in sediments that lack cohesion, most commonly in sands of uniform grain size, where shear strain causes an increase in pore-water pressure and a temporary transfer of grain support to the pore fluid (Obermeier et al., 2001). Sediments remain in a liquefied state only during the active disturbance. Fluidization (distinct from liquefaction) of sediment is the result of upward fluid flow, and sediment can remain fluidized as long as external fluid is pumped into it (Allen, 1984). It can be caused by processes such as liquefaction or dewatering by compaction of underlying layers. The liquefaction features and extensional structures observed in drill cores and seismic images from the annular trough or brim resemble those of lateral spreads triggered by rapid ground motion during earthquakes, where mass movement on gentle to horizontal slopes is caused by liquefaction of saturated, cohesionless sediments, and the dominant movement is lateral extension (Horton et al., 2008, and references therein). Lateral spreading is consistent with the numerical modeling of

Collins and Wünnemann (2005) and Collins et al. (2008b), which reproduced the Chesapeake Bay impact structure “inverted sombrero” morphology by gravitational collapse and inward spreading of weak sediments across the annular trough and slumping into the collapsed transient crater. To our knowledge, liquefaction-induced lateral spreading has not yet been suggested for other “inverted sombrero” impact structures.

A high-resolution seismic-reflection profile acquired across the Langley drill site shows that collapse of the target-sediment layer due to lateral extension was greater there than in adjacent areas of the survey (Catchings et al., 2005; Horton et al., 2008). Numerous short, high-angle faults and apparent bedding dips up to $\sim 20^\circ$ define a synformal structure that was penetrated near its center by the Langley core hole. This collapse structure is stratigraphic in unit PPF between depths as great as ~ 540 m and as shallow as ~ 250 m and does not affect the underlying granite, the lower part of unit PPF, or the base of the upper subunit of the Exmore upper diamicton member.

Relief on individual bed reflections across the structure at the level of the lower subunit of the Exmore upper diamicton member is as large as ~ 70 m. The apparent width of the structure decreases downward from ~ 540 m at the level of the lower subunit of the Exmore upper diamicton member to ~ 370 m at the level of the upper part of unit PPF. Similar collapse structures within the brim are apparent on marine seismic profiles that cross the Chesapeake Bay structure (e.g., Poag et al., 1999, their figures 6, 8–9; Powars and Bruce, 1999, their plate 3, C–C'). In some cases, normal faults at the margins of these structures extend into the basement (Powars et al., 2002).

Seismic reflections that represent unit PPF are nearly horizontal below ~ 550 m on the Langley seismic profile. This pattern is consistent with the nearly horizontal bedding seen in the PPF section of the Langley core. The seismic profile also shows that unit PPF is broken into minimally rotated blocks at a scale of tens of meters. Some of the contacts observed in unit PPF of the core may represent such block boundaries, but the high dip angles of the block boundaries and the small diameter of the core are not conducive to recognizing these features.

The collapse zone seen on the Langley seismic image is located laterally between two relatively coherent megaclasts (dimensions of $\sim 10^2$ to 10^3 m) of Potomac sediments (Catchings et al., 2005; Horton et al., 2008). By way of comparison, the Oligocene(?) Otay Mesa lateral spread in southern California is a well-exposed example of similar features at a somewhat smaller scale in an earthquake-induced lateral spread (Vanderhurd et al., 2011, particularly figures 5 and 6). The basal slip surface in the Otay Mesa example is a bentonite bed, but movement of the Potomac sediments likely occurred along multiple impact-generated zones of sand liquefaction (Gohn et al., 2005).

Lower Section of Rocks and Sediments at Bayside—In Place or Transported?

Transport of basement rocks. Until the recovery of the 275.37-m-thick, unshocked granite megablock in the Eyreville

core (Horton et al., 2009b; Townsend et al., 2009), the unshocked granite sections at the bottoms of the Langley and Bayside cores were considered to be in-place or nearly in-place basement rocks. The demonstrated transport of the granite megablock into the collapsing transient crater at Eyreville raised the possibility that other transported basement-rock megaclasts may be present elsewhere in the structure. Consequently, we considered three possibilities for the transport history of the granite at Bayside.

First, the lower part of the Bayside core, and the underlying uncored section, may contain one or more megaclasts of unshocked basement rocks that fell from the overturned flap. The location of the Bayside site in the inner part of the brim places it within the numerically modeled zone of flap collapse (Collins et al., 2008b; Kenkmann et al., 2009; Wünnemann et al., 2010). Rock megaclasts from the flap are seen in these models to sink through the partially fluidized and otherwise strongly disrupted target-sediment layer of the inner brim while simultaneously being transported toward the transient-crater rim by seismic shaking. The modeled transport distances of individual megaclasts vary from ~ 1 to 3 km and increase with smaller clast size and with closer proximity to the rim upon reentry. Also, a section of stacked high-amplitude reflections seen at the top of the basement rock on a nearby marine seismic profile (Powars et al., 2009, their figure 2a) suggests the presence of rock from the overturned flap overlying basement rocks of the brim within ~ 10 km of the Bayside site but at a shorter radial distance (~ 5 km less) from the structure's center.

Second, the Bayside granite may represent basement rocks initially located beneath the target-sediment layer in the brim that were disrupted and transported laterally as megaclasts by seismic shaking. However, transport of locally derived basement rocks within the brim is not apparent in the cited numerical models. Therefore, third, the Bayside granite may represent basement rocks of the brim that remained in place, or nearly so, in a manner similar to that inferred for the Langley Granite.

An additional complication is that the three identified granite transport histories are not mutually exclusive. It is possible that neither rock megaclasts from the overturned flap nor transported rock megaclasts generated within the brim by seismic shaking completely covered autochthonous basement rocks in the brim. Therefore, a single core hole could have encountered one category of rock but missed nearby rocks having a different transport history.

The principal characteristics of the cored granite at Bayside do not provide compelling reasons for choosing among the three transport histories, including: its Neoproterozoic crystallization age and monzogranitic to granodioritic composition, greenschist minerals in veins and along fractures, the absence of shocked minerals and melt, and fission-track ages that do not indicate Eocene heating. Microbreccia-filled, dilational fractures and microfaults seen in thin sections of the altered granite at Bayside likely are impact-generated features, but these minor structures also do not distinguish between an in-place versus a transported origin. Low-temperature mineralogic alteration (e.g., expandable, mixed-layer smectite-illite) at the top of the cored granite section would be

consistent with Cretaceous or older subaerial chemical weathering but also with pre- and postimpact diagenesis.

Transport of brim target sediments—unit GS. Unit GS is present above the Neoproterozoic granite and below unit PPF at Bayside (Figs. 12A and 14). A single productive sample contains an Aptian–early Albian palynomorph assemblage (zone I) that is typical of the lower part of the Potomac Formation regionally. Similar sediment units with abundant and petrologically diverse rock clasts are not known to occur in the other studied core holes located in the Chesapeake Bay impact structure, nor are similar Cretaceous lithofacies recognized in Mid-Atlantic coastal plain sections outside the impact structure (Anderson et al., 1948; Owens and Gohn, 1985; Powars and Bruce, 1999; Powars et al., 2016; Poag et al., 2004).

A significant obstacle to understanding unit GS is the absence of information about the lateral extent of the unit, and its individual components outside the core. The alternating intervals of muddy sand, sand, sand with minor gravel, and sandy rock-clast gravels may represent sand clasts and rock clasts in a sandy matrix within a diamicton, assuming limited lateral extent and continuity of each interval. In contrast, the alternating intervals also may be viewed as stratification, assuming substantial lateral extent and continuity of each interval. Therefore, we considered two possibilities for the transport history of unit GS.

First, unit GS may represent an impact-generated mass flow consisting of rock and sediment clasts in a sandy matrix, using the assumption that the sand and clayey sand intervals are cobbles and small boulders and not laterally continuous sedimentary beds. This diamicton would therefore consist of basement rocks and Cretaceous sediments from the brim that were disrupted during the impact and transported laterally by seismic shaking as a single, unsorted mass. The Early Cretaceous palynomorphs found in one sample also would have been transported. The wide variety of rock types in the unit indicates that they were not derived entirely, or even mostly, from a regolith developed on the Bayside granite. Instead, they would represent several different rock types that were present at the top of the pre-impact basement section.

Unit GS bears some resemblance to unit SBS (sediment boulders and sand) of the Eyreville core, which, as noted, is an avalanche/density flow–generated diamicton of Potomac Formation sediments that collapsed into the transient crater from its rim (Fig. 14; Gohn et al., 2009b). Both units consist of Potomac Formation sediments and have Aptian–Albian palynomorph assemblages (Self-Trail et al., 2009; this report), and both display local interpenetrating clast contacts (Fig. 13B). Differences in maximum clast size (~15 m in SBS, ~1 m in GS), abundance and composition of rock clasts (possible sparse recycled Potomac pebbles in SBS; abundant, diverse suite in GS), and presence or absence of liquefaction features (present within and outside clasts in SBS, absent in GS) serve to differentiate these units.

Second, unit GS may represent stratified, size-sorted sediments that were deposited nonconformably on the granite at Bayside during the late Early Cretaceous but were minimally disrupted and moved during the Eocene impact. The inferred

stratification and observed sorting would suggest repeated temporal variation in processes, which is typical of long-term alluvial-fluvial deposition, but contrasts with the catastrophic character of impact-induced deposition, which primarily results in poorly stratified, poorly sorted deposits. The similar XRD mineralogy of the GS matrix and the underlying granite is consistent with a short distance of sediment transport.

The alternation of sandy gravels with pebbly, massive, and less common laminated sands in unit GS resembles the gravel-sand couplets produced by hyperconcentrated flows and shallow-water flows in laterally unconfined sheetfloods, and flows in incised channels on alluvial fans (Blair and McPherson, 1994, 1999, 2009; Deynoux et al., 2005; Kar et al., 2014), primarily those with mud-poor source areas (Blair, 1999). The presence of sparse low-angle planar stratification in a few sand beds, and very sparse cross-stratification suggest upper-flow-regime deposition, which is consistent with the indicated sedimentary processes (Blair and McPherson, 1994). Other pre-impact alluvial or fluvial models might prove to be preferable to this model if the larger-scale geometries of the layers become known.

The palynoflora in unit GS indicates deposition in a terrestrial, low-energy environment within a subtropical or tropical setting (~15°N–30°N). The abundance and diversity of ferns and other lower vascular plants (using fossil spore evidence) likely are not consistent with original deposition in a dominantly arid climate. However, the presence of charcoal, without a correlative and proportional increase in thermal alteration of palynomorphs, indicates fires and at least occasional or seasonal aridity in the original depositional environment. Quaternary alluvial fans are known from tropical and subtropical areas with seasonably variable (monsoonal) rainfall, some of which contain lithofacies similar to those of unit GS (e.g., Brierley et al., 1993; Leier et al., 2005; North and Davidson, 2012; Kar et al., 2014).

Transport of brim target sediments—unit PPF. Unit PPF overlies unit GS and underlies Exmore resurge sediments at Bayside. This PPF section resembles the lower part of the PPF section at Langley in that it consists of fining-upward cycles with basal gravels, feldspathic sands and silts, and carbonaceous clays. The PPF sections in both cores also have similar XRD mineralogic compositions. Carbonaceous clays are uncommon in the upper part of the Potomac Formation in the Watkins School core. Also, unit PPF has similar XRD mineralogic compositions at Langley and Bayside. Laminations in the sands and silts typically are horizontal, suggesting minimal tilting of unit PPF. One Bayside sample contained a sparse assemblage of Early Cretaceous palynomorphs for which the discernible biostratigraphic age range (Valanginian–Hauterivian to early[?] Albian) overlaps that of the lower part of the Potomac Formation.

The general retention of the primary depositional characteristics of the Cretaceous Potomac Formation sediments that constitute unit PPF at Bayside places constraints on the magnitude of its disruption and movement histories. The absence of evidence for impact-generated erosion and subsequent redeposition (as considered for unit GS), and for rotation of the unit suggests that

unit PPF at Bayside moved as a relatively coherent megaclast of large but uncertain dimensions (34.35 m vertically in core) due to seismic shaking.

Combined movement histories—granite, unit GS, unit PPF. Having considered individual movement histories and mechanisms for the granite, unit GS, and unit PPF at Bayside, several scenarios appear possible for their combined history. The possibilities extend from an entirely allochthonous scenario to an entirely parautochthonous scenario.

In all scenarios, movement of these units occurred before the arrival of the Exmore oceanic resurge currents. Above PPF, the block-dominated member of the Exmore Formation consists almost entirely of variably tilted blocks, and liquefied sections, of Potomac Formation sediments that overlie the glauconitic resurge sediments of the Exmore lower diamicton member (Fig. 17). The similarity of the Potomac clasts and megaclasts in unit PPF and the Exmore block-dominated member suggests that both units first moved in a similar fashion by seismic shaking until the upper part of this section was overtaken by, reworked, and incorporated into the resurge flow (Figs. 17 and 18C–18D).

If the cored granite at Bayside, or just its upper part, is considered to be allochthonous, in the form of a flap megaclast or a laterally transported block from the brim's basement, then all material above the granite must be allochthonous. Transported granite (and perhaps sediments) also could be present below the bottom of the Bayside core hole and above autochthonous granite.

Both models for unit GS remain relevant in this context. Either this unit is an impact-generated diamicton that resulted from disruption, mass transport, and redeposition of brim target sediments and basement rocks, or it is a relatively coherent megaclast of Early Cretaceous sediments that was transported largely intact for an uncertain distance by seismic shaking. Unit PPF would be a largely intact megaclast of the lower part of the Potomac Formation that also moved due to seismic shaking.

If the cored granite at Bayside is considered to be parautochthonous, units GS and PPF could be interpreted to be parautochthonous or allochthonous. In the parautochthonous case, units GS and PPF would be megaclasts of sediments initially located in the brim that retained their initial stratigraphic order, as presently observed in the core, and that did not move large distances. This interpretation would be similar to the interpretation of the granite and unit PPF at Langley, where the PPF (Potomac Formation) sediments may have moved laterally for short distances (approximately tens to hundreds of meters) due to seismic shaking and resulting lateral spreading. In the allochthonous case, unit GS could again be viewed as an impact-generated diamicton, or as a transported megaclast of Cretaceous sediments, and unit PPF would again be a transported megaclast.

Support for substantial transport distances for the pre-resurge sediments presently above the granite in the inner brim is provided by the cited hydrocode models and by marine seismic surveys. The models show impact deformation of the full thickness of the target-sediment layer and lateral transport distances of several kilometers in the inner part of the brim within ~35 km of

ground zero (Collins et al., 2008b; Kenkmann et al., 2009). This transport could have been in the form of redeposited sediments (unit GS) and (or) transported megaclasts (units GS and PPF).

The seismic profiles typically show that the sedimentary section above the top of the basement and below the upper part of the Exmore upper diamicton member is not seismically reflective across the brim's inner 8–9 km (e.g., Powars and Bruce, 1999; Poag et al., 2004), which includes the Bayside core site located ~8 km from the central crater rim (Powars et al., 2009). This general absence of layered seismic reflections suggests thorough disruption and significant transport of the target-sediment layer in that area.

Seawater-Resurge Erosion and Deposition

The Exmore Formation is a key stratigraphic unit for establishing the erosional and depositional history of the brim and for interpreting the different phases of crater filling from the brim to the central crater (Figs. 17 and 18C–18E). Seawater-resurge currents eroded variably deformed target sediments outside and within the brim and transported them as various density flows toward and into the collapsing transient crater. Earlier disruption and erosion of the sediment layer by outgoing tsunamis likely occurred, but the record of those events was completely erased by the inward resurge flow. The resurge diamictons also contain fallback ejecta, including shocked and cataclastic rock clasts and mineral grains, melt particles, and thermally and physically altered microfossils (Edwards and Powars, 2003; Self-Trail, 2003; Horton and Izett, 2005; Ormö et al., 2009; Reimold et al., 2009; Edwards et al., 2010). Stratigraphic continuity of the Exmore Formation across the brim and into the central crater is well established.

The depth of resurge erosion in the brim increases toward the central crater but is variable locally, as seen on marine seismic profiles (Powars and Bruce, 1999; Poag et al., 2004). In the studied cores, the base of resurge erosion increases in depth by 457.84 m from 196.63 m at Watkins School to 654.47 m at Bayside (Fig. 17), and the thickness of underlying modified pre-impact Cretaceous sediments decreases accordingly.

The large volume of resurge sediments within the collapsed transient crater (Figs. 17 and 18) indicates that the raised rim and overturned flap of the collapsed transient crater were not significant impediments to the resurge flow. Hydrocode models indicate that inward flow began within the brim at ~2–3 min into the event and reached the center of the structure in ~6–8 min (Collins and Wünnemann, 2005; Kenkmann et al., 2009).

Early resurge flow and its interaction with lateral spreading. The distances to which target sediments were extended by lateral spreading increased inward across the brim with increasing proximity to the free surface at the rim of the transient crater. The depth to which target sediments were eroded and incorporated into the resurge concomitantly increased inward.

These effects are illustrated by the final configuration of the remnant part of the target Potomac Formation (Figs. 17 and 18D). The Potomac Formation is relatively thick and minimally disturbed at Watkins School, and unit PPF is moderately

extended and locally collapsed at and near Langley. The internally disrupted but somewhat coherent megaclasts of lower Potomac Formation sediments in liquefied Potomac-sand matrix in the Exmore block-dominated member were transported as mass flows by the resurge at Bayside and Eyreville. Only a remnant section of the basal Potomac sediments (PPF, GS?) may be present at Bayside. Paleogene and Upper Cretaceous target sediments were removed across the entire brim and for an uncertain distance outside the impact structure.

The thin Exmore resurge section and thick remnant Potomac section at Watkins School indicate that, in that sector of the outermost part of the brim, resurge currents removed only the Paleogene sediments (and Upper Cretaceous sediments if present) and perhaps the uppermost Potomac target sediments (Fig. 17). This resulted from the greater induration of the Potomac sediments, as compared to that of the Paleogene sediments, and from the minimal lateral extension in that area. However, local erosion (resurge gullies) or lateral extension (localized grabens) followed by resurge sedimentation have been demonstrated in two places outside the outer margin of the brim on the western side of the structure (Powars et al., 2016, their figures 5 and 11).

At Langley, significant lateral extension is indicated by the collapse structure in the lower part of the Potomac section (unit PPF). This section was not significantly eroded and transported by resurge, however, even though uppermost Potomac and younger sediments were removed and replaced by resurge diamictons. At some point between the Langley and Bayside core sites, and presumably at similar radii from the structure's center elsewhere, the amount of lateral extension was sufficient to allow ready incorporation and transport of lower Potomac sediments as relatively coherent but internally disrupted megaclasts in the resurge flow, as represented by the Exmore block-dominated member in the Bayside and Eyreville cores (Fig. 17). At Bayside, Potomac clasts in typical glauconitic resurge matrix with mixed-age fossil assemblages in the lower diamicton member below the block-dominated member confirm the role of resurge mass flow in moving Potomac clasts that were produced initially by lateral extension in the middle to inner part of the brim.

Late resurge transport and sedimentation. The upper diamicton member of the Exmore Formation is the record of late resurge sedimentation. It overlies minimally disrupted Potomac sediments at Watkins School, laterally extended Potomac sediments (unit PPF) at Langley, and the resurge-transported Exmore block-dominated member at Bayside and Eyreville (Figs. 17, 18D, and 18E).

The lower subunit of the upper diamicton member shows the combined effects of lateral spreading and resurge erosion and transport at Langley, Bayside, and Eyreville (Fig. 17). Boulders and blocks of Potomac sediments initially disrupted by lateral extension became engulfed in typical glauconitic resurge matrix containing mixed-age fossil assemblages, smaller clasts of Potomac and Paleogene target sediments, and minor fallback ejecta. Hydrocode models suggest that transport distances of the lower subunit increased from hundreds of meters to a few kilo-

meters from Langley to Bayside and up to tens of kilometers at Eyreville (Collins et al., 2008b).

The upper subunit of the upper diamicton member represents the final phase of resurge transport and resedimentation of target sediments in the brim (Figs. 17, 18D, and 18E). Maximum clast size in this diamicton is distinctly smaller than in the lower subunit, and there is a more nearly equal ratio of Potomac and post-Potomac sediment clasts. These trends resulted from the limited availability of clasts from the remnant Potomac sections in and near the brim, which were now covered by earlier resurge sediments. Instead, material in this member primarily was derived from outside the brim. The Langley and Eyreville high-resolution seismic profiles show overlapping layers in the uppermost part of the upper subunit that likely represent debris and perhaps turbidity flows derived from slumps of individual sectors of the outer brim margin during waning resurge flow (Catchings et al., 2005; Powars et al., 2009).

Microfossil distribution patterns in the upper diamicton member also suggest temporal changes in the dominant direction of resurge sediment transport (Self-Trail et al., 2009). The best example involves the Upper Cretaceous marine-target sediments, which are present today only in the areas south, east, and northeast of the outer margin of the impact structure (Fig. 1; Powars and Bruce, 1999; Powars, 2000; Poag et al., 2004). This distribution suggests that these sediments also were present only in the eastern part of the impact target during the Eocene. Late Cretaceous calcareous nannofossils and dinoflagellates occur throughout the Exmore resurge section in the Eyreville core (Self-Trail et al., 2009), but their abundances increase upward, reaching maximum values in the uppermost part of the upper diamicton member (Self-Trail et al., 2009). To the west at Langley and Watkins School, Late Cretaceous marine fossils also do not appear below the uppermost part of the upper diamicton member (Frederiksen et al., 2005; Self-Trail et al., 2009).

This distribution pattern indicates that significant volumes of eroded Upper Cretaceous target materials in the east were not transported to the western part of the evolving impact structure until late in the resurge event.

Deposition of Post-Resurge Transported Sediments and Suspended Sediments

The stratified member of the Exmore Formation in the Watkins School core consists of a 0.90-m-thick section of locally burrowed or graded, muddy very fine sands and overlying laminated, muddy very fine sands and clayey silts (Fig. 6B). At Langley (1.00 m thick) and Bayside (13.99 m thick), the member includes the lower subunit Es1, which consists of muddy, calcareous, glauconitic, quartz-feldspar sand (pebbly, very fine to very coarse) that is typically massive but locally burrowed, and the upper subunit (Es2) consists of burrowed, muddy, calcareous, glauconitic, quartz-feldspar sand (very fine to medium) that grades upward into laminated, muddy very fine sands, clayey silts, and silty clays.

The stratified member is 7.06 m thick in the Eyreville core and generally resembles the comparable section at Bayside

(Edwards et al., 2009; Gohn et al., 2009b; Poag, 2009). However, ~0.5-m-thick, fining-upward intervals defined primarily by alternations of pebbly sand and massive to burrowed sand are present in subunit Es1 (Gohn et al., 2009a, 2009b; Dypvik and Kalleeson, 2010). Similar intervals are present in Es1 at Bayside.

The stratified member records the change from seawater-resurge deposition (upper diamicton member) to sediment reactivation and redeposition by locally generated sediment flows, and finally to settling of the fine-grained sediments suspended in the water column during the impact event (Figs. 17 and 18E). The presence of reworked pre-impact microfossils, and the absence of indigenous biota indicate that deposition of this member preceded the local recovery of the biota (e.g., Poag, 2002, 2012; Edwards et al., 2009). Poag (2002, 2012) referred to the uppermost beds of subunit Es2 as a postimpact shelf “dead zone” on this basis. Poag (2012, table 1) suggested a period of months to years for deposition of subunit Es1 (“flow-in deposit”) and <0.1 m.y. for subunit Es2 (settling from suspension; “dead zone”).

The impact structure consisted of a partially filled shelf basin following the cessation of resurge flow and the re-establishment of the pre-impact sea level. Benthic biofacies in several cores indicate that outer neritic to upper bathyal water depths were present in this midshelf basin at the start of postimpact Chickahominy Formation deposition and presumably during deposition of the Exmore stratified member. Inferred paleodepths vary from ~70 m on the shelf adjacent to the western (updip) edge of the shelf basin to ~200 or 300 m in the shelf basin and ~130 m on the shelf adjacent to the eastern (downdip) edge of the basin (Browning et al., 2009; Poag, 2012). Therefore, the modeled relief from the outer edge to the central part of the shelf basin was ~175 m along an atypically high ~10° slope at the end of impact-induced sedimentation (Poag, 2012).

Much of this relief occurred at inward-facing escarpments at the outer margin of the brim and at the margin of the collapsed transient cavity, resulting in slope angles on the basin floor that were lower than the model numbers. Inward increases in the preserved thickness of the Exmore stratified member in the shelf basin, as seen in the studied cores (Fig. 17), suggest that the shelf basin was segmented into a deeper central subbasin above the collapsed transient crater and a shallower outer subbasin above the brim (Kulpecz et al., 2009).

The thinness of the stratified member and the absence of its subunit Es1 at Watkins School are consistent with this core hole’s location at or near the outer margin of the shelf basin (i.e., brim), which the resurge flow bypassed with only minor net sedimentation. The accommodation space produced there by resurge erosion of the Paleogene target sediments near the basin margin primarily was filled by postimpact Chickahominy sediments (Fig. 17). The thin graded beds near the base of the stratified member in the Watkins School core (Fig. 6) suggest a brief period of episodic resuspension of fine sediments, perhaps by bottom currents. Originally, thin sections of subunit Es2 likely were present outside the shelf basin (impact structure) but were removed during Oligocene and later cycles of erosion. Relatively thin inter-

vals of units Es1 and Es2 at Langley near the center of the brim are intermediate in thickness between the thin Watkins School section and the thicker sections located near (Bayside) and above (Eyreville) the collapsed transient cavity.

The sandy sediments of subunit Es1 were moved from the edge toward the center of the shelf basin as sediment gravity flows (possibly concentrated density flows; see Mulder and Alexander, 2001; Pickering and Hiscott, 2016) produced by slumping of unstable basin slopes and (or) by reactivation produced by oscillation waves within the shelf basin and (or) storm waves. The fining-upward intervals of sandy sediments in subunit Es1 at Eyreville, and probably at Bayside, represent these density flows. Winnowing of the source resurge sediments is indicated by the absence of oversized clasts in the Es1 sections. The presence of burrows in Es1 suggests that living macrofauna taxa were transported in these flows and that, presumably, they were initially transported in the earlier seawater-resurge flow.

The sandy lower part of subunit Es2 represents one or more sediment density flows that resemble those of unit Es1 but are finer grained and more heavily burrowed. This part of Es2 corresponds primarily to the core-hole sections characterized by Poag et al. (2004) and Poag (2007, 2009, 2012) as flow-in deposits (small-scale turbidity flows) in the Bayside and Eyreville cores.

The laminated, pyritic, fine-grained upper part of subunit Es2 represents settling of the sediments suspended in the water column during the impact event. This section does not contain indigenous biota, although reworked forms are present. The sub-horizontal, thick-walled burrows in Es1 and lower Es2 at Bayside and Eyreville do not extend into upper Es2, suggesting a decrease in oxygenation through time. Sand-filled, subvertical burrows in the stratified member and lower part of the Chickahominy Formation at Watkins School represent activity by a postimpact Chickahominy infauna that transferred sandy sediments upward from Es1 and the lower part of Es2.

Poag and colleagues (Poag, 2002; Poag and Norris, 2005; Poag et al., 2004) discussed a possible microspherule layer (“fallback layer”) in the Exmore stratified member at Langley. Poag (2002; and subsequent papers) illustrated hemispherical cavities (~0.5–1.0 mm) in a pyrite lattice that were considered to be molds of glassy microspherules. Alternatively, Horton et al. (2005a) illustrated thin sections of this layer that showed secondary pyrite surrounding and within cracks in well-rounded glauconite grains. Removal of the glauconite from the pyritic matrix also would produce hemispherical cavities.

Regarding this possible occurrence of microspherules in subunit Es2, minerals of the clinoptilolite-heulandite series are present in the Exmore-Chickahominy contact interval and not elsewhere in the Langley and Bayside sections (Tables 2 and 3). They were not found at Watkins School but may have been missed during sampling. Clinoptilolite/heulandite also is present in the Exmore-Chickahominy contact interval in the Eyreville core (Ferrell and Dypvik, 2009; Larsen et al., 2009; Schulte et al., 2009), where its concentration falls to near zero higher in the Chickahominy Formation before re-occurring near the middle of that formation.

Zeolites are common low-temperature hydrothermal alteration products of volcanic and impact glass (Stähle and Ottemann, 1977; Naumov, 2005; Osinski, 2005; Marantos et al., 2012). Their presence at the top of the crater-fill section lends credence to a concentration of glassy fallback microspherules at that level, which would correspond to the hemispherical cavities (microspherule molds) noted by Poag (2002). The zeolites also could represent ejected glass shards unrelated to the hemispherical cavities. Partially melted dinocysts at 235.85 m in the Langley core also represent thermally altered fine-grained ejecta in subunit Es2 (Edwards and Powars, 2003).

Early Postimpact Sedimentation

The microfossiliferous, fine-grained sediments of the Upper Eocene Chickahominy Formation record the return to normal shelf sedimentation and the local recovery of planktic and benthic faunas and floras after the impact event (Figs. 17 and 18F; Browning et al., 2009; Edwards et al., 2005, 2010; Poag, 2009, 2012; Poag and Norris, 2005; Powars et al., 2005; Schulte et al., 2009). These sediments accumulated in outer neritic to uppermost bathyal water columns (~200–300 m) within the areally restricted midshelf basin above the subsiding impact structure.

Chickahominy deposition probably occurred at middle neritic water depths (~70 m) on the inner shelf northwest (updip) of the basin's margin, but these sections subsequently were eroded (Browning et al., 2009; Poag, 2012, p. 69; Poag and Norris, 2005; Powars and Bruce, 1999). Thin intervals of fine-grained, Upper Eocene sediments probably are present on the outer shelf east of the impact structure, but no core holes have been drilled in that area.

The cored sections of the Chickahominy Formation thicken toward the center of the shelf basin (Fig. 17). This increase primarily resulted from initially greater accommodation space produced by the partial synimpact filling of the collapsed transient cavity and by long-term compaction of the rapidly deposited crater fill. Slickensided fractures and small-displacement faults in the Chickahominy Formation also resulted from continued compaction of the crater fill and the Chickahominy sediments. Local variations in the thickness of the Chickahominy section related to relief on the upper surface of the crater fill are apparent on seismic reflection profiles (e.g., Catchings et al., 2005; Poag et al., 2004; Powars et al., 2009), but they are not discernible using the widely spaced cores studied for this report.

The Chickahominy sediments are coarser grained and less laminated in the Watkins School core as compared to the Langley and Bayside cores (Edwards et al., 2010), reflecting the location of the Watkins School site in shallower water near the shelf-basin margin and closer to the postimpact source of continent-derived sediments (Figs. 17 and 18). Fining-upward cycles of fine-grained shelf sediments in the Chickahominy Formation at Watkins School probably represent cyclic changes in sea level and related proximity to paleoshorelines.

The quartz/feldspar ratios of sediments in the lower part of the Chickahominy Formation are significantly higher than

those of underlying, texturally similar sediments in subunit Es2 of the Exmore stratified member at Watkins School, Langley, and Bayside (Tables 1–3). The plagioclase/total feldspar ratios remain unchanged across the same interval. These trends suggest a decreasing supply of typically feldspathic Potomac sediments from suspension in the water column, from feldspathic resurge sediments near the outer margin of the brim, and from outside the impact structure. The presence of clinoptilolite/heulandite in the basal part of the Chickahominy Formation may represent continuing fallback of glassy ejecta and (or) reworking of ejecta from Exmore subunit Es2 (Tables 2 and 3).

The areally restricted midshelf basin persisted as a subsea topographic feature above the impact structure due to autocompaction of the rapidly deposited crater fill (Fig. 18G). However, sediment facies and depositional rates in this basin also were controlled by global sea-level changes and by regionally active processes, including variations in sediment supply and continental margin tectonism.

DISCUSSION: COMPARISON TO SELECTED MARINE-TARGET IMPACT STRUCTURES

Overview

Dypvik and Jansa (2003) stated that 170 Earth impact structures were known in that year. Dypvik and Kalleson (2010) increased the number to 176, and the Earth Impact Database (online at <http://www.passc.net/EarthImpactDatabase/>) listed 190 impact structures as of January 2018. Of these, Dypvik and Jansa (2003) identified 17 proven marine-target impact structures, including the deep-water Eltanin structure, and seven possible or suggested marine-target impact structures. These structures were interpreted to represent impacts into continental shelf and slope environments where water depths varied from <50–800 m, except Eltanin. Ormö and Lindström (2000) listed 14 marine-target impact, including Eltanin. Therefore, given the existing data, marine-target impact structures apparently constitute a maximum of ~12% of the known Earth impact structures.

This is an unexpectedly low number, considering that oceans have covered much of the Earth's surface (~70% today) throughout most of its history (Dypvik and Kalleson, 2010). However, it is certain that the evidence for additional impact structures has been lost to tectonism and erosion. In addition, evidence for many deep ocean impacts is inherently missing because of the effect of a thick water layer on the transfer of energy and momentum from the projectile to the target. Specifically, variations in the ratio of water depth to impactor diameter (depth/diameter) affect the diameters and morphologies of the resulting impact structures (Wünnemann and Lange, 2002; King et al., 2006; Davison and Collins, 2007; Ormö et al., 2010). This effect ranges from nearly negligible in the case of a low ratio, for many impacts into continental shelves and epicontinental seas, to extreme in the case of a high ratio in deep-ocean impacts, where a water cavity will be formed but the seafloor may or may not be affected.

Ormö and Lindström (2000) listed seven impact structures found on continental shelves or upper slopes that contained seawater-resurge sediments. Poag et al. (2004) considered five of these structures to contain or probably contain surge-back (resurge) deposits. Of these, the Montagnais and Mjølnir impact structures are the closest analogues to the Chesapeake Bay impact structure with regard to their physiographic settings, their pre-impact target material, and the resulting structure. They display the “inverted sombrero” shape, including the brim, and the erosional and depositional effects of seawater resurge, including reworking of the proximal ejecta field and mass transport of target sediments and ejecta into the center of the structure. They are discussed in the following sections.

Montagnais

Overview

The early Eocene (ca. 51 Ma, Ypresian) Montagnais impact structure is located on the outer Scotian Shelf (offshore Nova Scotia, Canada) and was the first impact structure identified in a marine setting (Jansa and Pe-Piper, 1987; Jansa et al., 1989). Early drilling programs and seismic surveys provided the initial data sets (Jansa et al., 1989; Aubry et al., 1990; Poag et al., 2002, 2004; Dypvik and Jansa, 2003), which were supplemented by later regional drilling and seismic surveys (Deptuck and Campbell, 2012; Weston et al., 2012).

The Montagnais and Chesapeake Bay impact structures are similar with regard to their locations on the North America Atlantic continental shelf and their Eocene ages (Fig. 19). Also, the three-layer target at Montagnais resembles the Chesapeake Bay impact structure target with regard to layer thickness and general composition (Jansa et al., 1989; Deptuck and Campbell, 2012; Weston et al., 2012). However, certain distinct differences between the two resulting structures also are apparent, as discussed below.

Impact Target

The rock layer of the Montagnais target consisted of the Paleozoic Meguma terrane, which included Cambrian–Ordovician metasedimentary rocks of the Meguma Group and middle Paleozoic granitic plutons (White, 2010; White and Barr, 2010). A petroleum test hole, Montagnais I-94 (Fig. 19), penetrated a basement section in the central peak of the impact structure, which consisted of highly fractured and shocked, low-grade metasedimentary rocks of the Meguma Group (Jansa et al., 1989; Dypvik and Jansa, 2003).

The sediment layer of the target consisted of postrift Jurassic to Eocene sediments (Wade et al., 1995; Weston et al., 2012). Triassic and Jurassic synrift continental sediments and Lower Jurassic volcanic rocks overlie the basement rocks locally (Pe-Piper et al., 1992; Weston et al., 2012), but they do not appear to have been present within the Montagnais target (Jansa et al., 1989).

The Middle Jurassic through lower Upper Cretaceous section primarily consists of delta and shelf siliciclastic sequences and some carbonate units. Carbonate sediments of the Coniacian–Campanian

Wyandot Formation are overlain by siliciclastic sediments of the lower part (Campanian–lower Eocene) of the Banquereau Formation (Weston et al., 2012). The presence of thick carbonate units in the Montagnais target contrasts with the paucity of carbonate sediments in the Chesapeake Bay impact structure target.

The thickness of the pre-impact Montagnais target-sediment layer is difficult to ascertain exactly, as most of the available off-structure drill-hole data represent the upper slope rather than the outer shelf. Thicknesses of the target sediments in these slope sections are substantially greater than those found regionally on the shelf.

The Mohawk P-93 drill hole, located ~40 km southwest of the Montagnais structure on the outer shelf (Fig. 19), penetrated ~1500 m of upper Middle Jurassic through Upper Cretaceous (Campanian) pre-impact sediment (Ascoli, 1990). In contrast, the Bonnet P-23 drill hole, located ~80 km southwest of the Montagnais structure at the shelf-slope transition, penetrated ~3000 m of upper Middle Jurassic through Lower Cretaceous sediments (Albian and below; Weston et al., 2012).

The thickness of the target sediments at the Mohawk drill hole probably is not the maximum shelf thickness, as Upper Campanian to Ypresian sediments (Upper Cretaceous–Lower Eocene) are present regionally (Weston et al., 2012). An inferred maximum thickness of 1500+ m for Montagnais’s sediment layer is similar to the maximum thickness of 1700 m cited herein for the Chesapeake Bay impact structure target-sediment layer. The modern water depth at the center of the Montagnais structure is ~100 m, but the estimated paleodepth at the time of impact is 200–600 m (Jansa et al., 1989; Poag et al., 2004).

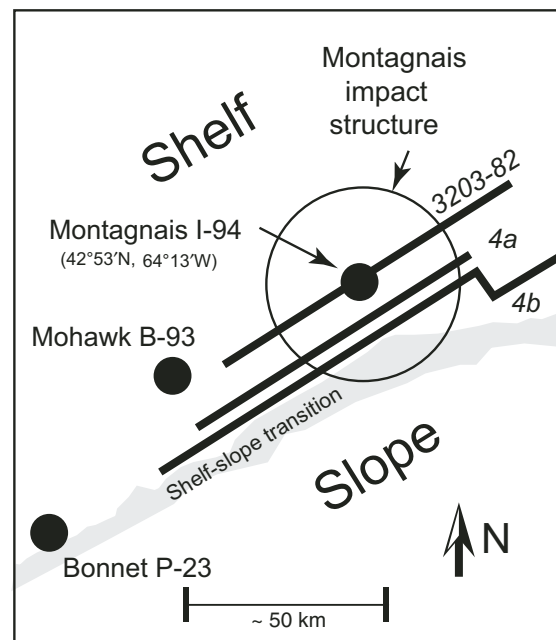


Figure 19. Sketch map showing the locations of the Montagnais impact structure, drill holes, and seismic survey lines on the outer Scotian shelf, offshore Canada.

Impact Structure

Jansa et al. (1989) published an interpreted seismic profile (3203–82) that crosses the Montagnais structure near its center (Fig. 19). They illustrated an ~45-km-wide complex impact structure with a broad, flat-topped “central high” that is overlain and surrounded by polymictic breccias. The Montagnais I-94 drill hole encountered a 512-m-thick section of the polymictic breccias above the shocked metasedimentary rocks of the “central high” (Jansa et al., 1989; Dypvik and Jansa, 2003).

In the polymictic section penetrated by the drill hole, a basal autochthonous, 391-m-thick interval consists of zones of melt rock alternating with zones of shocked and variably melted rock clasts. This interval appears to represent the melt-rich lining of the transient cavity. An overlying allochthonous, 120.5-m-thick interval consists of clasts of Jurassic, Cretaceous, and Paleocene–Eocene target sediments and clasts of granite and metamorphic rocks. This interval might be interpreted as resurge sediments, except that it is overlain by a 40.5-m-thick interval of suevite. Instead, the sediment-bearing breccia may represent collapsed materials from higher on the transient crater wall, and the suevite layer likely represents air-fall melt material.

Dypvik and Jansa (2003) and Poag et al. (2002, 2004) interpreted the impact structure imaged on profile 3203–82 as a central peak structure that also included a low peak ring that did not breach the overlying target-sediment layer (e.g., Poag et al., 2004, their figure 10-6). More recently, Deptuck and Campbell (2012) published line drawings of two seismic profiles that cross the Montagnais structure (Fig. 19). One profile intersects the central peak of the structure below the maximum height of the peak and extends outside the structure to the west and partway through the structure to the east (Fig. 20).

Figure 20A presents a generalized version of the line drawing in Deptuck and Campbell’s (2012) figure 4a, which is their interpretation of the seismic line across the central peak. The T50 horizon on the figure is the impact unconformity, which defines the structural morphology of the Montagnais structure. Figure 20B uses the T50 horizon as a guide to the interpretations and nomenclature of the structure as discussed by Jansa et al. (1989), Poag et al. (2002, 2004), and Dypvik and Jansa (2003), whereas figure 20C uses the nomenclature from the present report.

The central crater of the Montagnais structure consists of a central peak surrounded by an annular inner basin (moat). These features resemble the central crater of the Chesapeake Bay impact structure (Fig. 2). However, a structural high near the middle of the moat at Montagnais appears on both sides of the central peak in figure 20 of Deptuck and Campbell (2012), suggesting that it is a continuous or discontinuous annular feature (also see Deptuck and Campbell, 2012, their figure 2). This unnamed feature consists of nonlayered material (Deptuck and Campbell, 2012, their figure 4) and therefore appears to be part of the inner basin (moat). A structure map of the central part of the Montagnais structure (0.2 s, two-way traveltime) and a corresponding gravity map (Poag et al., 2002, 2004) indicate the presence of discontinuous closed depressions with intervening highs along the axis

of the inner basin (moat). Therefore, the relief in the inner basin (moat) on the T50 contact (Fig. 20) seems to be substantiated by the gravity data. Relief of this magnitude has not been observed on seismic profiles of the Chesapeake Bay impact structure moat.

The transition from the moat to the brim at Montagnais (Fig. 20) is distinctly different from the equivalent transition at the Chesapeake Bay impact structure. A broad “pinnacle” of normal-faulted, pre-impact Cretaceous sediments that dip at low angles is present at the inner edge of the brim (Poag et al., 2002, their figures 10 and 11). The presence of this feature at similar distances from the structure’s center on both sides of the central peak (Fig. 20) suggests that it also might be an annular structure. This feature is the peak ring of earlier interpretations (Fig. 20B). However, the prominent, surviving central peak conflicts with current ideas regarding the creation of peak rings (Morgan et al., 2016). We have not chosen from among the possible interpretations of this feature, but it remains a feature of interest because it bounds the inner margin of the brim at Montagnais.

The Montagnais brim is ~18 km in width at its top, excluding the “pinnacle.” This is ~25% smaller than the width of the Chesapeake Bay impact structure brim. The Montagnais brim also appears to contain a relatively thin section of resurge sediments. The syn- to postimpact Eocene section between seismic markers T50 and T35 in the brim likely consists of basal resurge sediments overlain by middle and upper Eocene, postimpact shelf sediments, as the resurge would have continued through only a small fraction of the ~15 m.y. period represented by this interval. In addition, the cross section in figure 20 of Deptuck and Campbell (2012) shows that the upper part of the western outer-rim escarpment apparently is covered by postimpact (post-T35) sediments and not resurge sediments.

Summary

The Montagnais impact structure resembles the Chesapeake Bay impact structure with regard to their major features. Both consist of a central, collapsed and filled transient crater with a central peak surrounded by a brim filled with syn- to postimpact sediments that also extend across the center of the structure. However, the ostensibly large relief on the surface of the moat in the Montagnais central crater is not seen on seismic profiles of the Chesapeake Bay impact structure. The “pinnacle” of pre-impact sediments at the inner edge of the Montagnais brim is an enigmatic feature of uncertain origin that also is not present in the Chesapeake Bay impact structure (Fig. 2).

The details of the Montagnais brim sediments remain largely unknown due to the absence of drill holes into those materials. This includes confirmation of the presence of resurge sediments. However, their presence can be inferred from the location of the structure on the outer continental paleoshelf, which mitigates against the possibility that the Montagnais structure became emergent immediately after impact. At present, the amount of detailed information about the major aspects of the Montagnais structure is distinctly less than the amount known about similar features of the Chesapeake Bay impact structure. This difference

results directly from the relative abundance of core holes and seismic profiles available for study of the impact structure when contrasted with those for Montagnais.

Mjølnir

Overview and Impact Target

The Early Cretaceous Mjølnir impact structure (ca. 142 Ma, Berriasian) is located in the Barents Sea offshore Norway (Tsika-

las et al., 1998; Dypvik et al., 1996). The structure is ~40 km in diameter and is buried by ~400 m of postimpact sediments and a modern water column of 350–400 m depth.

The Mjølnir impact target differs from the other targets discussed herein in that the rock layer was too deep to be affected significantly during the impact event. Permian and older sedimentary rocks are found today at and below ~4–4.5 km depth, but numerical models suggest that the transient cavity did not extend below ~5 km and that only a relatively

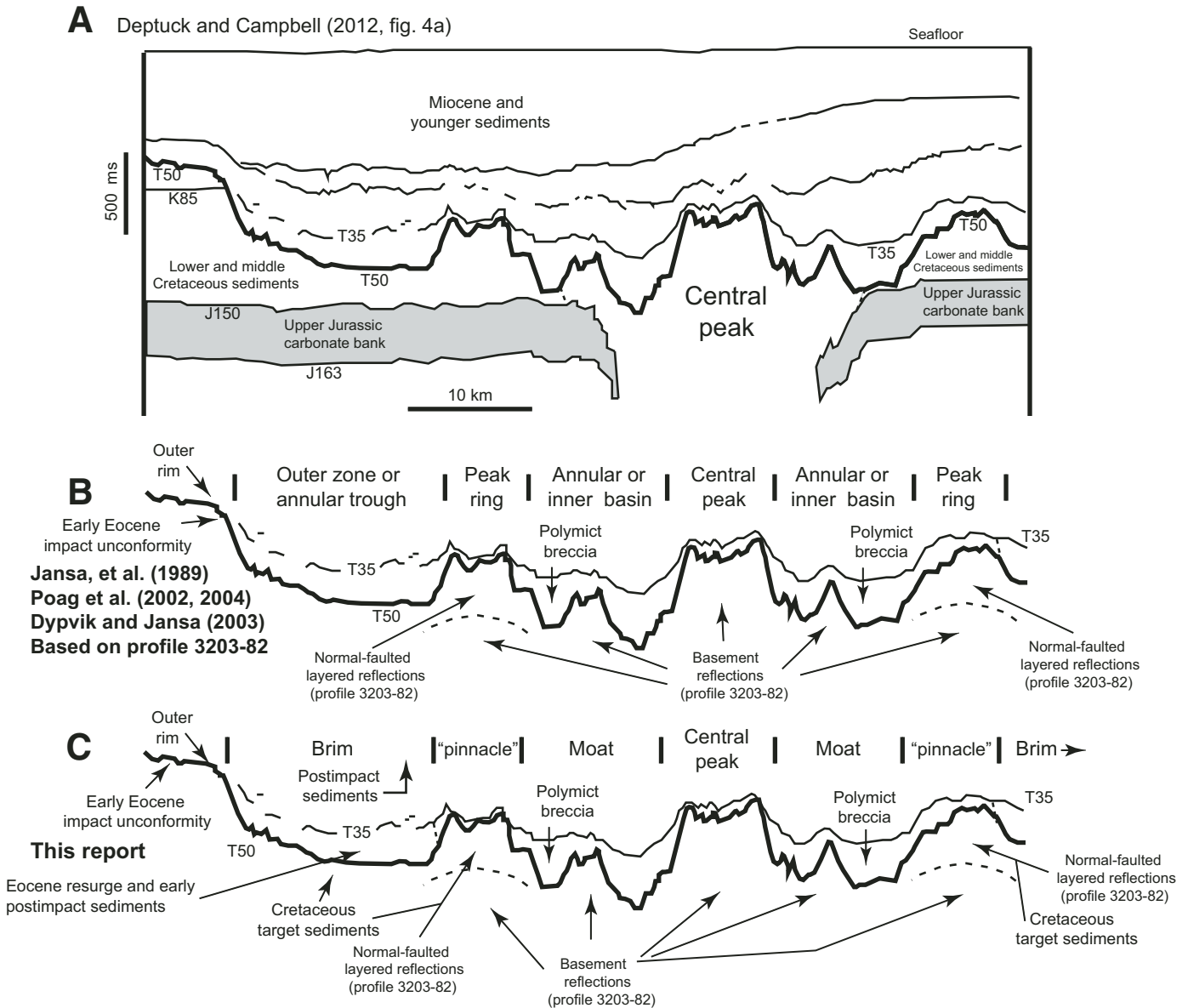


Figure 20. Interpretive cross sections of the Montagnais impact structure. (A) Generalized line drawing of a seismic profile based on a more detailed line drawing by Deptuck and Campbell (2012, their figure 4A). Labels shown in the figure are those used by the original authors. Labels for key seismic markers indicate their age (e.g., T50 = Tertiary, 50 Ma; K85 = Cretaceous, 85 Ma). (B) Line drawing showing seismic marker T50, the impact unconformity, from part A. The nomenclature for the principal parts of the impact structure is from interpretations of equivalent features on seismic line 3203-82 by Jansa et al. (1989), Poag et al. (2002, 2004), and Dypvik and Jansa (2003). (C) Line drawing showing seismic marker T50 from part A with nomenclature determined during the present study.

thin layer of Permian rocks would have been affected by the excavation flow (Shuvalov and Dypvik, 2004). Poag et al. (2004, p. 314) stated that no crystalline rocks are present in the Mjølner structure, which is likely correct in that basement igneous and metamorphic rocks were too deep to be greatly affected by the impact event. The possibility remains, however, that some upper Paleozoic rocks may have been excavated. Jurassic target sediments constituted essentially all of the target-sediment layer that was struck by the Cretaceous (early Berriasian) impactor.

Impact Structure

The Mjølner impact structure consists of a central crater (collapsed transient cavity) that is ~20 km in diameter and contains a distinct central peak surrounded by an inner annular trough (moat; Tsikalas et al., 1998, their figure 6). The central crater is bounded by a raised rim that has been referred to as a peak ring (Tsikalas et al., 1998; Dypvik and Jansa, 2003), but this feature appears to lack the characteristics of peak rings known in larger Earth impact structures such as Chicxulub (Morgan et al., 2016) or the prototypical Schrödinger peak-ring impact structure on the Moon (e.g., French, 1998, his figure 3.11).

Beginning with the earliest studies (Gudlaugsson, 1993; Dypvik et al., 1996; Tsikalas et al., 1998), the Mjølner impact structure was recognized as having an “outer zone” that we now refer to as the brim. Figure 21 illustrates the general configuration of this brim, in which a layer of “impact breccia” (Poag et al., 2004) occurs above disrupted pre-impact sediments and below postimpact sediments. This layer is interpreted here to consist of seawater-resurge sediments and possibly underlying parautochthonous to allochthonous target sediments.

Summary

The details of the Mjølner brim sediments remain largely unknown due to the absence of drill holes into those materials. This includes confirmation of the presence of resurge sediments. As at Montagnais, their presence can be inferred from the location of the structure on the outer continental paleoshelf, which mitigates against the possibility that the Mjølner structure became emergent immediately after impact.

SUMMARY AND CONCLUSIONS

Integration of new and previously generated data from three cores in the brim of the Chesapeake Bay impact structure produced an improved understanding of the impact processes, their relative timing, and their results in the outer part of a complex, central-peak crater developed in a multilayered marine target. A new perspective provided by the first detailed analysis of the Bayside core from the inner brim (Fig. 17) led to a significantly improved resolution of the stratigraphy across the entire brim. The results of this study provide a reference point for study of other known or suspected marine-target impacts, particularly those where only a minimal number of core holes and seismic surveys have been acquired.

Impact deformation outside the transient crater in the brim primarily occurred in the target-sediment layer where later impact-related processes tended to modify or completely alter the effects of earlier processes. Evidence is limited in the brim for effects produced during the contact and compression stage of the impact event. Shocked minerals and impact melt are absent in the Langley and Bayside granites and as clasts in the overlying units GS and PPF. Observed structural damage in the granites is limited to minor faults in the Bayside granite and vertical faults

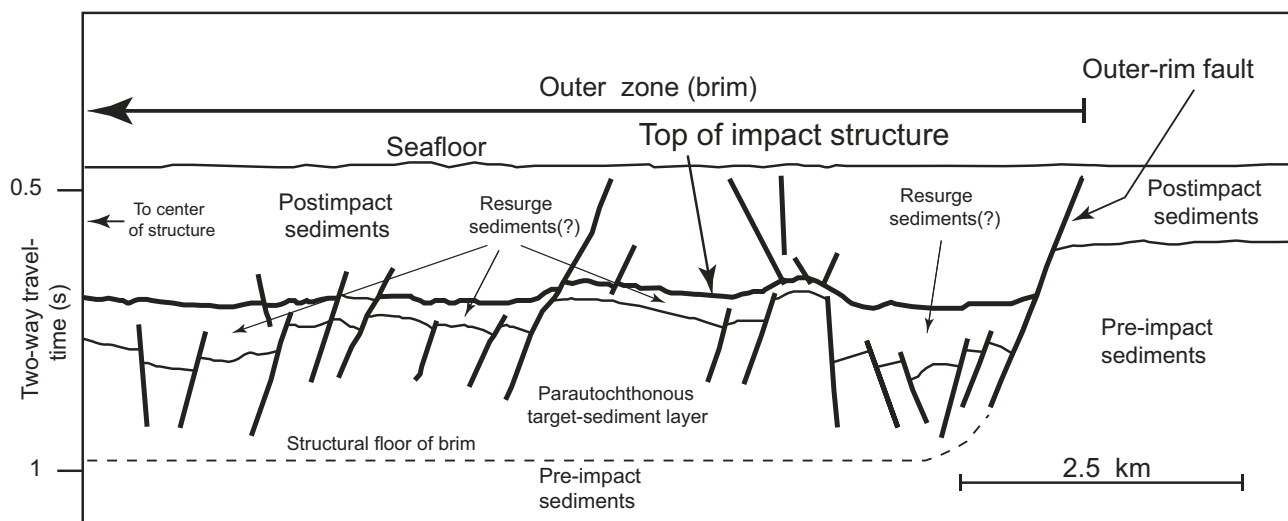


Figure 21. Generalized line drawing of a seismic profile (Tsikalas et al., 1998) across the outer part of the northeast quadrant of the Mjølner impact structure. The drawing shows the distribution of probable resurge sediments lying above faulted, parautochthonous target sediments at and near the outer margin of the brim. The interpretation of the units follows Poag et al. (2004, their figure 10.10).

with larger displacements seen on published seismic profiles. The records of early tensile fragmentation of the target and outgoing tsunamis in the brim were obliterated by succeeding events and could not be identified in the cores.

The powerful excavation processes that opened the transient crater did not occur in the brim. However, secondary effects of those processes did occur there. Collapse of the overturned flap onto the brim may or may not be represented by a granite megaclast at the bottom of the Bayside core. Shocked and (or) cataclastic rock clasts and single-mineral grains, melt clasts, and thermally altered microfossils accumulated in the seawater-resurge deposits of the Exmore Formation as fallback ejecta.

The preserved record of impact effects in the brim is dominated by modification-stage events. Outgoing tsunamis and collapse of the overturned flap deformed and eroded the target sediments to some unknown degree, but their effects were modified completely by later processes. Lateral extension of partially liquefied target sediments in the brim caused by seismic shaking resulted in their disruption and lateral transport. This lateral spreading quickly became concurrent with erosion and mass transport of target sediments outside and within the brim by seawater-resurge density flows.

The interaction of lateral spreading and resurge carried target sediments toward and into the collapsing transient crater. The lateral spreading extended the target sediments in the brim at inwardly increasing depths and transported them toward or into the transient crater. This lateral spreading facilitated incorporation of the brim sediments into the early resurge flow at inwardly increasing depths toward the transient crater, as observed in the studied cores. The raised rim and collapsed overturned flap at the margin of the transient crater were not significant obstacles to the resurge flow.

Early lateral spreading and resurge erosion of target sediments in the brim likely proceeded in a radially headward manner outward from the transient cavity. The resulting transported megaclasts consisted in large part of Potomac Formation sediments, as indicated by the near absence of younger marine-target sediments in the block-dominated member of the Exmore Formation. The glauconitic sediments of the lower diamicton member below the block-dominated member may represent movement of the Potomac megaclasts by resurge mass flow, earlier deep infiltration of Upper Cretaceous or Paleogene marine sediments during initial seismic shaking, or both. Additional coring in the innermost part of the brim might reveal glauconitic sediments between these Potomac megaclasts in the lower diamicton member.

Later resurge erosion primarily was limited to areas outside the brim, to the outer brim margin, and to the uppermost earlier resurge sediments. The resulting longer transport distances, and waning resurge energy, resulted in smaller maximum clast sizes in the later resurge diamictons. A relative increase in the amount of Upper Cretaceous and Paleogene target sediments derived from outside the brim (relative to Potomac sediments) occurred because the previously accessible sections of the Potomac For-

mation within the structure were now covered by the earlier resurge sediments.

Remnant parautochthonous sections of the Potomac Formation remain between the basement rocks and the erosional base of the resurge deposits in the outer (Watkins School) and middle (Langley) parts of the brim. Sections of alluvial-fluvial sediments in this interval in the inner part of the brim (Bayside) also may be parautochthonous remnants, or they may consist of target rocks and sediments that were variably disrupted and transported due to seismic shaking, and perhaps disrupted by megaclasts from the collapsing overturned flap, before arrival of the resurge flow.

Following the end of resurge flow and re-establishment of the pre-impact sea level, mass sediment transport became limited to density flows and turbidity(?) currents within the shelf basin above the partially filled and auto-compacting impact structure. The final stage of impact-related sedimentation was deposition across the entire structure of suspended fine-grained sediments that had been concentrated in the water column during the impact event.

ACKNOWLEDGMENTS

This work was partly supported by the Research Council of Norway through its Centres of Excellence funding program, project number 223272 (CEED). Other funding was supplied by the Research Council of Norway and the Fulbright Foundation. Drilling programs in the Chesapeake Bay impact structure were supported financially by the International Continental Scientific Drilling Program, the Virginia Department of Environmental Quality, the Hampton Roads Planning District Commission, the National Aeronautics and Space Administration (NASA) Science Mission Directorate, the U.S. Geological Survey (USGS) National Cooperative Geologic Mapping Program, and the USGS National Research Program (Water).

We thank the following groups that contributed to the successful completion of drilling and research in the Chesapeake Bay impact structure: the international managerial and scientific staff of the ICDP-USGS Eyreville drilling program; DOSECC Exploration Services; Major Drilling Group International, Inc.; the scientific staff of the Virginia Department of Environmental Quality; USGS drilling crews from Reston, Virginia, and Denver, Colorado; and the scientists of the USGS Virginia Water Science Center, the USGS National Research Program (Water), and the USGS Chesapeake Bay Impact Crater Project. Adrian Read provided valuable comments on an earlier draft of this report. We thank MaryAnn L. Malinconico (Lafayette College), Robert E. Weems (USGS), John E. Warne (Colorado School of Mines), David T. King (Auburn University), and Christian Koeberl (Vienna Natural History Museum, University of Vienna) for their useful reviews of the manuscript. Any use of trade, firm, or product names is for descriptive purposes only and does not imply endorsement by the U.S. Government.

APPENDIX A. DINOFLAGELLATE SPECIES IN THE BAYSIDE CORES

By Lucy E. Edwards

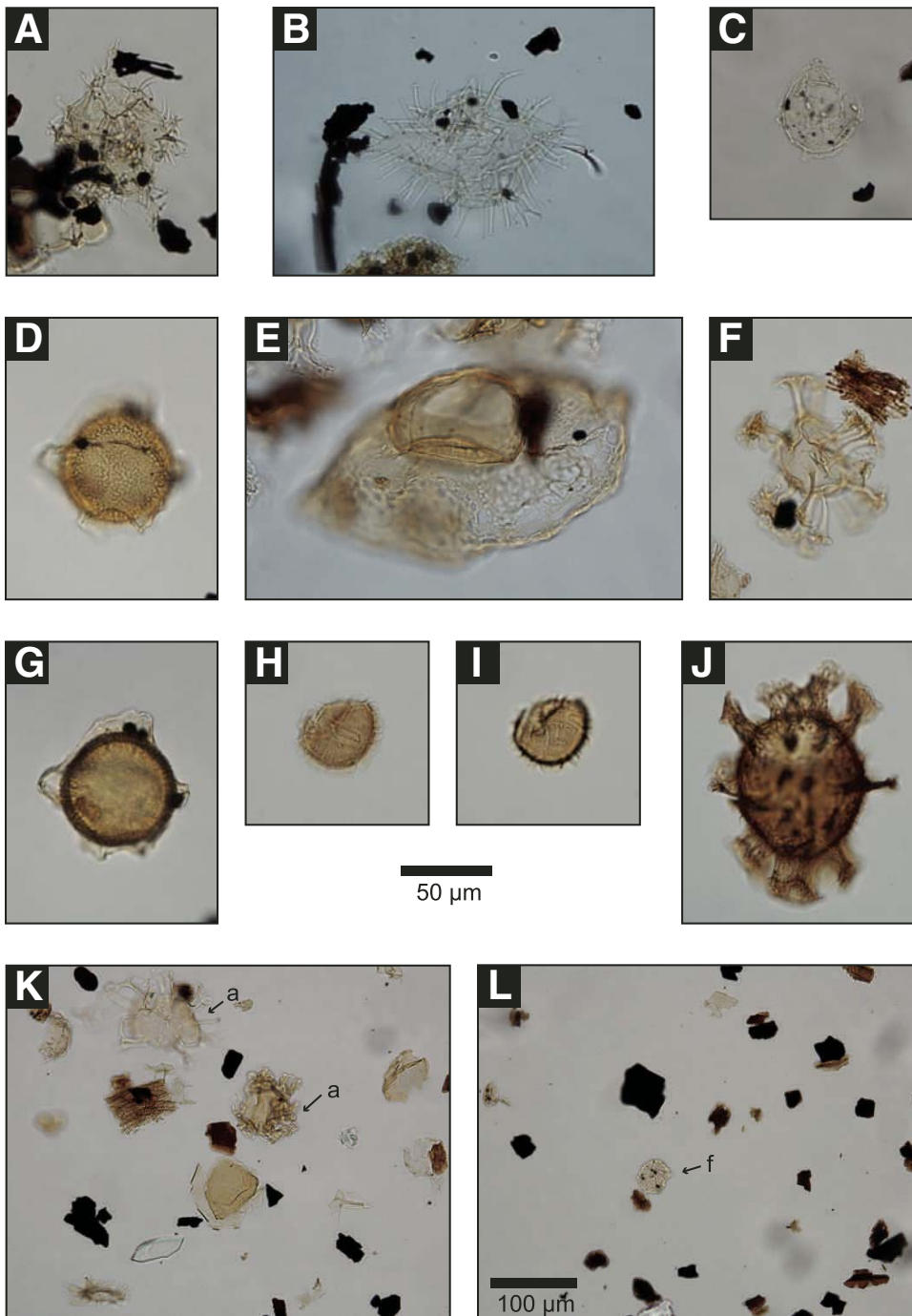


Plate A1. Dinocysts from clasts and matrix of the Exmore Formation in the Bayside core. The 50 µm scale bar applies to all images, except as noted. Laboratory "R" numbers are listed. (A–C) R6190BF; early Eocene; clay clast from the upper diamicton member (sample midpoint at 295.64 m, Bayside #1): (A) *Apectodinium parvum*; (B) *Apectodinium* cf. *A. augustum*; (C) *Phthanoperidium crenulatum*. (D–G) R6190IC; late in the middle Eocene or early in the late Eocene; limestone clast from the upper diamicton member (sample midpoint at 303.23 m, Bayside #1): (D) *Pentadinium membranaceum*, high and midfocus; (E) *Thalassiphora fenestrata*; (F) *Cordosphaeridium cantharellus*. (G) *Pentadinium membranaceum*, high and midfocus. (H–J) R6190IA; Paleocene; glauconitic sandstone clast from the upper diamicton member (sample midpoint at 326.17 m, Bayside #1): (H, I) *Systematophora?* sp. I of Edwards (1989), high and low focus. (J) *Turbiosphaera filosa*. (K) R6190E; mixed age; matrix sample from the upper diamicton member (sample midpoint at 296.97 m, Bayside #1). Note the variation in preservation of the two areoligeracean specimens (a) and the presence of both whole specimens and fragments. See 100 µm scale bar on L. (L) R6190CD; mixed age; matrix sample from the lower diamicton member (sample midpoint at 653.63 m, Bayside #2). Note that dinocysts are less abundant than is typically found in the Exmore matrix. The figured specimen (*Cordosphaeridium funiculatum*) is a fragment (f).

REFERENCE CITED (Appendix A)

- Edwards, L.E., 1989, Dinoflagellate cysts from the lower Tertiary formations, Haynesville cores, Richmond County, Virginia, in Mixon, R.B., ed., *Geology and Paleontology of the Haynesville Cores—Northeastern Virginia Coastal Plain*: U.S. Geological Survey Professional Paper 1489-C, p. C1–C12, plates 1–5.

APPENDIX B. BIOSTRATIGRAPHIC AND PALEOENVIRONMENTAL INTERPRETATION OF FOSSIL POLLEN SAMPLES FROM GRAVEL AND SAND UNIT (UNIT GS) AND PARAUTOCHTHONOUS POTOMAC FORMATION (UNIT PPF) IN THE U.S. GEOLOGICAL SURVEY (USGS) BAYSIDE #2 CORE

By Ronald J. Litwin

Two samples from the USGS Bayside #2 core were analyzed for biostratigraphic and paleoecologic evidence (Table B1). The core hole is located in Mathews County, Virginia, at 37°19'30.57"N, 76°9'33.25"W, and spudded at 1.2 m elevation. The samples came from two separate depth intervals: 2248.8–2249.0 ft and 2261.4–2261.5 ft (sample midpoints were 685.4 m and 689.3 m depth, respectively). The upper sample yielded only a sparse terrestrial palynomorph assemblage, but palynomorphs were moderately abundant in the lower sample. These samples are here designated R6190BA (upper sample) and R6190HE (lower sample), respectively.

The upper sample R6190BA yielded a well-preserved, moderately diverse, but sparse palynomorph assemblage of Mesozoic age. It dominantly consisted of the trilete fern spore taxa *Apiculatisporis* sp., *Matonisporites* sp., *Cyathidites* sp., *Phlebopterites* sp., *Concavissimisporites variverrucatus*, and *Trilobosporites marylandicus*. The coniferalean taxon *Corollina* sp. and the inaperturate lower vascular plant taxa *Inaperturopollenites* sp. and *Schizosporis reticulatus* also were observed (but rarely) in this sample. Bisaccate gymnosperm pollen and schizaeaceous striate fern spores (e.g., *Cicatricosisporites*) were notably absent in this sample, yet both commonly occur in U.S. Atlantic and Gulf Coastal Plain Mesozoic palynomorph assemblages. R6190BA consisted mostly of wide-ranging taxa (e.g., *Concavissimisporites*, *Matonisporites*, *Schizosporis*), with the exception of *Trilobosporites marylandicus*. Brenner (1963) reported *T. marylandicus* to be “more common in zone I assemblages” (i.e., Aptian to lower Albian per Hochuli et al., 2006) along the Mid-Atlantic Coastal Plain, but Bebout (1981) reported a broader *T. marylandicus* range (Valanginian/Hauterivian–Albian) from cores taken along the western Atlantic outer continental shelf. The proposed range base of *T. marylandicus* and its presence in this sample suggest this sample assemblage is geologically younger than palynomorph assemblages recovered from the Waste Gate Formation of eastern Maryland (i.e., Berriasian; Doyle, 1982; Hansen and Doyle, 1982). Clasts of Berriasian age previously have been recovered by one of us (R.J.L.) from the Eyreville core <20 mi (32 km) east of the Bayside #2 core, from inside the central crater (see Self-Trail et al., 2009). Ages attributed to the “zone I” biostratigraphic interval in Self-Trail et al. (2009, their figure 12) likely should be considered “Aptian–lower Albian?” and the zone II C interval should be considered as “early Cenomanian” (per Hochuli et al., 2006). Doyle (1982) noted *T. marylandicus* in palynomorph assemblages in core samples from Crisfield, Maryland, but only in samples from younger strata stratigraphically above the top of the Waste Gate Formation (Doyle, 1982, table 2). Due to the lack of other age-diagnostic taxa in R6190BA, we suggest its age range most likely was Valanginian–Hauterivian to Albian. Its age possibly can be restricted further to no younger than early Albian, as the sample lacks any occurrences of zone II–zone IV indicator taxa (e.g., *Apiculatisporis babsae*, *Rugubivesiculites reductus*, *Striatopollis* spp., *Taurocusporites spackmani*, *Complexiopollis* spp., *Tricolporopollenites* spp., *Atlantopollis* spp.; Brenner, 1963; Christopher, 1979; Doyle et al., 2008). We correlated this sample to “pre–zone I/zone I” (per Brenner, 1963; Bebout, 1981; Doyle, 1982) but note that this fossil assemblage is not as old as those recovered directly from the Waste Gate Formation (Berriasian).

The lower sample R6190HE yielded a palynomorph assemblage of Mesozoic age that was diverse, well preserved, and moderately abundant. It was dominated by bisaccate gymnosperm pollen (*Abietinaepollenites* spp., *Alisporites* spp., *Parvisaccites* spp., and *Podocarpidites* spp.) and

the coniferalean taxa *Araucariacites australis*, *Callialasporites trilobatus*, *Corollina meyeriana*, *Corollina torosa*, *Eucommiidites troedssonii* (less common), and *Exesipollenites tumulus*. The sample also contained common schizaeaceous spores, including *Cicatricosisporites* cf. *C. hallei*, *C. australiensis*, and *C. dorogensis*. Rare *Appendicisporites potomacensis* and *Appendicisporites* sp. were observed in this sample. Several distinctive nonstriate trilete spore taxa also were present, including *Cingulatisporites* sp., *Concavispores jurienensis*, *Coronatispora valdensis*, *Densoisporites perinatus*, *Granulatisporites dailyi*, *Kuylisporites lunaris*, *Psilatrilletes circumundulatus*, *Taurocusporites segmentatus*, *Trilobosporites marylandicus*, and *Tuberositrilletes* sp., along with wide-ranging sporomorphs such as *Apiculatisporis asymmetricus*, *Converrucosisporites* sp., *Cyathidites* sp., *Inaperturopollenites* sp., and *Matonisporites* sp. The ?Gnetalean taxa present in this sample included moderately common *Ephedripites multicostatus* and less common *E. virginianus*. Angiospermous taxa observed (low to rare abundance) in this sample included *Pennipollis (Retimonocolpites) peroreticulatus* (per Friis et al., 2000), *Clavatipollenites hughesii*, and *Clavatipollenites minutus*. Many of the common taxa in R6190HE, e.g., *Abietinaepollenites* sp., *Alisporites* sp., *Parvisaccites* sp., *Podocarpidites* sp., *Araucariacites australis*, *Callialasporites trilobatus*, *Corollina meyeriana*, *Corollina torosa*, *Eucommiidites troedssonii*, and *Exesipollenites tumulus*, range from Jurassic or older strata (e.g., Litwin et al., 1998) to Cretaceous strata (Brenner, 1963; Bebout, 1981; Self-Trail et al., 2009). However, the occurrences of *Cicatricosisporites australiensis*, *Cicatricosisporites dorogensis*, *Cicatricosisporites* cf. *C. hallei*, *Ephedripites virginianaensis*, *Kuylisporites lunaris*, *Pennipollis (Retimonocolpites) peroreticulatus*, *Clavatipollenites minutus*, and *Trilobosporites marylandicus* in this sample restrict its age assignment to the Early Cretaceous. We correlated this sample to zone I palynological assemblages (per Brenner, 1963; Doyle and Robbins, 1977; Bebout, 1981). Evidence for that correlation includes the taxa *C. dorogensis*, *E. virginianaensis*, and *K. lunaris*, which were reported by Brenner (1963) to occur exclusively in the Early Cretaceous zone I; by comparison, the taxa *Cicatricosisporites australiensis* and *Trilobosporites marylandicus* were reported by Brenner to be “relatively more common in zone I” assemblages. Commonly occurring zone II to zone IV taxa (e.g., *Retitricolpites* spp., *Taurocusporites spackmani*, *Rugubivesiculites reductus*, *Striatopollis* spp., *Complexiopollis* spp., *Tricolporopollenites* spp., etc.) are notably absent in this sample, thereby precluding a mid-Albian or younger Cretaceous age assignment (Brenner, 1963, 1967; Doyle and Robbins, 1977; Hochuli et al., 2006).

The age range of zone I assemblages has been revised since its first description. Brenner (1963) originally proposed zone I assemblages to range from Barremian to Aptian, whereas Doyle and Robbins (1977) proposed zone I assemblages to range from Barremian to (?)early Albian. Hochuli et al. (2006) and Doyle et al. (2008) more recently suggested an Aptian–early Albian age range for zone I. On this basis, we suggest its age range most likely is Aptian to early Albian. The youngest age of sample R6190HE may be further restricted by the occurrence of *C. trilobatus*; Bebout (1981) suggested that this taxon terminated in the Aptian, based on its occurrence in cores from the Atlantic outer continental shelf.

The age of the first occurrence of the angiosperm taxon *Pennipollis (Retimonocolpites) peroreticulatus* in this lower sample similarly has been revised over time. Brenner (1963) noted its occurrence as a rare element (as *Peromonolites peroreticulatus*) throughout the Potomac Group, the base of which he considered to have a Barremian age. Bebout (1981) noted this taxon (as *Retimonocolpites peroreticulatus*) in samples ranging from Barremian to Cenomanian from cores taken on the Atlantic outer continental shelf. Doyle (1992) recovered this taxon (as *Brenneripollis peroreticulatus*) from the Cocobeach sequence of Gabon and considered this taxon to indicate an Aptian (post-Barremian) basal age. Friis et al. (2000) recovered this taxon from strata in the northern Lusitanian Basin of Portugal, to which they

assigned a basal age of Barremian. Those authors recombined its taxonomy as *Pennipollis (Retimonocolpites) peroreticulatus*. Heimhofer et al (2007) later revised the age of those same Portuguese strata to “post-Aptian” (i.e., Albian). Present evidence suggests the base of this taxon’s geologic range likely is “post-Barremian.”

Paleoclimatological evidence from these two samples is limited. No dinoflagellate cysts or foraminifera tests were observed in either sample (after a survey of >3000 palynomorph specimens), which indicated that the two samples were not deposited in fully marine or even marginal marine (estuarine) environments. Both samples exhibited only low-grade thermal alteration; other fossilized biological evidence within these assemblages indicated a fully terrestrial original depositional environment for both (e.g., fragmented woody tissue and leaf cuticle were commonly observed). Charcoal occurred commonly throughout the less-altered and stratigraphically lower pollen assemblage (R6190HE), indicating that a fire event occurred locally near the sample’s original depositional environment. Previous paleogeography reconstructions based on global paleomagnetic studies variously suggested that the core site existed either in a subtropical (Smith et al., 1981; Heimhofer et al., 2007) or in a fully tropical (Scotese and Golonka, 1993) setting between ca. 145 Ma and ca. 110 Ma.

Based on those observations, we interpreted each of the two assemblages to have been deposited originally in a fully terrestrial, low-energy environment within a subtropical or tropical setting (~15°N–30°N). We note that the abundance and diversity of ferns and other lower vascular plants (using fossil spore evidence) in both samples likely are not consistent with original deposition in a dominantly arid climate. The presence of charcoal, without a correlative and proportional increase in thermal alteration of palynomorphs in the lower sample, indicates fire and least occasional-to-seasonal aridity at the original depositional environment. From present microscopic evidence, we cannot determine conclusively if either or both of these samples are allochthonous (redeposited clasts) or parautochthonous (nearly in original position). Clasts containing zone I biostratigraphic markers previously have been identified throughout the ~1020–570 m depth interval within the Eyreville core.

REFERENCES CITED (Appendix B)

- Bebout, J.W., 1981, An informal palynologic zonation for the Cretaceous System of the United States Mid-Atlantic (Baltimore Canyon area) outer continental shelf: *Palynology*, v. 5, p. 159–194, <https://doi.org/10.1080/01916122.1981.9989224>.
- Brenner, G.J., 1963, The Spores and Pollen of the Potomac Group of Maryland: Maryland Department of Geology, Mines, and Water Resources Bulletin 27, 215 p.
- Brenner, G.J., 1967, Early angiosperm pollen differentiation in the Albian to Cenomanian deposits of Delaware (U.S.A.): Review of Palaeobotany and Palynology, v. 1, no. 1–4, p. 219–227, [https://doi.org/10.1016/0034-6667\(67\)90124-8](https://doi.org/10.1016/0034-6667(67)90124-8).
- Christopher, R.A., 1979, Normapollis and triporate pollen assemblages from the Raritan and Magothy Formations (Upper Cretaceous) of New Jersey: *Palynology*, v. 3, no. 1, p. 73–121, <https://doi.org/10.1080/01916122.1979.9989185>.
- Doyle, J.A., 1982, Waste Gate Formation, Part 2: Palynology of Continental Cretaceous Sediments, Crisfield Geothermal Test Well, Eastern Maryland: Maryland Geological Survey Open-File Report/ OFR, _82-02-01, p. 51–87.
- Doyle, J.A., 1992, Revised palynological correlations of the lower Potomac Group (USA) and the Cocobeach sequence of Gabon (Barremian–Aptian): *Cretaceous Research*, v. 13, p. 337–349, [https://doi.org/10.1016/0195-6671\(92\)90039-S](https://doi.org/10.1016/0195-6671(92)90039-S).
- Doyle, J.A., and Robbins, E.L., 1977, Angiosperm pollen zonation of the continental Cretaceous of the Atlantic Coastal Plain and its application in the deep wells of the Salisbury embayment: *Palynology*, v. 1, p. 41–78, <https://doi.org/10.1080/01916122.1977.9989150>.
- Doyle, J.A., Endress, P.K., and Upchurch, G.R., Jr., 2008, Early Cretaceous monocots: A phylogenetic evaluation: *Acta Musei Nationalis Pragae, ser. B, Historia Naturalis*, v. 64, no. 2–4, p. 59–87.
- Friis, E.M., Pederson, K.R., and Crane, P.M., 2000, Fossil floral structures of a basal angiosperm with monocolpate, reticulate-acolumellate pollen from the Early Cretaceous of Portugal: *Grana*, v. 39, p. 226–239, <https://doi.org/10.1080/00173130052017262>.
- Hansen, H.J., and Doyle, J.A., 1982, Waste Gate Formation, Part 1: Hydrogeologic Framework and Potential Utilization of the Brine Aquifers of the Waste Gate Formation, a New Unit of the Potomac Group Underlying the Delmarva Peninsula: Maryland Geological Survey Open-File Report/ OFR_82-02.01, p. 1–50.
- Heimhofer, U., Hochuli, P.A., Burla, S., and Weissert, H., 2007, New records of Early Cretaceous angiosperm pollen from Portuguese coastal deposits: Implications for the timing of early angiosperm radiation: Review of Palaeobotany and Palynology, v. 144, p. 39–76, <https://doi.org/10.1016/j.revpalbo.2005.09.006>.
- Hochuli, P.A., Heimhofer, U., and Weissert, H., 2006, Timing of early angiosperm radiation: Recalibrating the classical succession: *Journal of the Geological Society*, v. 163, p. 587–594, <https://doi.org/10.1144/0016-764905-135>.
- Litwin, R.L., Turner, C.E., and Peterson, F., 1998, Palynological evidence on the age of the Morrison Formation, Western Interior, U.S.: *Modern Geology*, v. 22, p. 297–319.
- Scotese, C.R., and Golonka, J., 1993, Paleomap Paleogeographic Atlas: Arlington, Texas, University of Texas, PALEOMAP Project, 33 p.
- Self-Trail, J.M., Edwards, L.E., and Litwin, R.J., 2009 Paleontological interpretations of crater processes and infilling of syn-impact sediments from the Chesapeake Bay impact structure, in Gohn, G.S., Koeberl, C., Miller, K.G., and Reimold, W.U., eds., *The ICDP-USGS Deep Drilling Project in the Chesapeake Bay Impact Structure: Results from the Eyreville Core Holes: Geological Society of America Special Paper 458*, p. 633–654, [https://doi.org/10.1130/2009.2458\(28\)](https://doi.org/10.1130/2009.2458(28)).
- Smith, A.G., Hurley, A.M., and Briden, J.C., 1981, *Phanerozoic Paleogeographic World Maps*: Cambridge, UK, Cambridge University Press, 102 p.

REFERENCES CITED

- Alemán González, W.B., Powars, D.S., Seefelt, E.L., Edwards, L.E., Self-Trail, J.M., Durand, C.T., Schultz, A.P., and McLaughlin, P.P., 2012, Preliminary Physical Stratigraphy, Biostratigraphy, and Geophysical Data of the USGS South Dover Bridge Core, Talbot County, Maryland: U.S. Geological Survey Open-File Report 2012-1218, 16 p.
- Allen, J.R.L., 1984, *Sedimentary Structures—Their Character and Physical Basis* (unabridged one-volume edition): Amsterdam, Elsevier Press, 1256 p.
- American Geosciences Institute, 2015, Glossary of Geology: <http://glossary.agiweb.org/dbtw-wpd/glossary/search.aspx> (accessed by subscription, 21 June 2018).
- Anderson, J., Gardner, J.A., Stephenson, L.W., Vokes, H.E., Lohman, K.E., Swain, F.M., Cushman, J.A., Dorsey, A., and Overbeck, R.M., 1948, Cretaceous and Tertiary Subsurface Geology: The Stratigraphy, Paleontology, and Sedimentology of Three Deep Test Wells on the Eastern Shore of Maryland: Maryland Geological Survey Bulletin 2, 456 p.
- Ascoli, P., 1990, Foraminiferal, ostracode and calpionellid zonation and correlation of 42 selected wells from the North Atlantic margin of North America: Bulletin of Canadian Petroleum Geology, v. 38, no. 4, p. 485–492.
- Aubry, M.-P., Gradstein, F.M., and Jansa, L.F., 1990, The late early Eocene Montagnais bolide: No impact on biotic diversity: Micropaleontology, v. 36, no. 2, p. 164–172, <https://doi.org/10.2307/1485500>.
- Azad, A.S., Dypvik, H., and Kalleeson, E., 2015, Sedimentation in marine impact craters—Insight from the Ritland impact structure: Sedimentary Geology, v. 318, p. 97–112, <https://doi.org/10.1016/j.sedgeo.2015.01.001>.
- Bartosova, K., Ferrière, L., Koeberl, C., Reimold, W.U., and Gier, S., 2009, Petrographic and shock metamorphic studies of the impact breccia section (1397–1551 m depth) of the Eyreville drill core, Chesapeake Bay impact structure, USA, *in* Gohn, G.S., Koeberl, C., Miller, K.G., and Reimold, W.U., eds., The ICDP-USGS Deep Drilling Project in the Chesapeake Bay Impact Structure: Results from the Eyreville Core Holes: Geological Society of America Special Paper 458, p. 317–348, [https://doi.org/10.1130/2009.2458\(15\)](https://doi.org/10.1130/2009.2458(15)).
- Bebout, J.W., 1981, An informal palynologic zonation for the Cretaceous System of the United States Mid-Atlantic (Baltimore Canyon area) outer continental shelf: Palynology, v. 5, p. 159–194, <https://doi.org/10.1080/01916122.1981.9989224>.
- Benson, R.N., 2006, Internal Stratigraphic Correlation of the Subsurface Potomac Formation, New Castle County, Delaware, and Adjacent Areas in Maryland and New Jersey: Delaware Geological Survey Report of Investigations 71, 15 p.
- Blair, T.C., 1999, Cause of dominance by sheetflood vs. debris-flow processes on two adjoining alluvial fans, Death Valley, California: Sedimentology, v. 46, p. 1015–1028, <https://doi.org/10.1046/j.1365-3091.1999.00261.x>.
- Blair, T.C., and McPherson, J.G., 1994, Alluvial fans and their natural distinction from rivers based on morphology, hydraulic processes, sedimentary processes, and facies assemblages: Journal of Sedimentary Research, v. A64, no. 3, p. 450–489.
- Blair, T.C., and McPherson, J.G., 1999, Grain-size and textural classification of coarse sedimentary particles: Journal of Sedimentary Research, v. 69, no. 1, p. 6–19, <https://doi.org/10.2110/jsr.69.6>.
- Blair, T.C., and McPherson, J.G., 2009, Processes and forms of alluvial fans, *in* Parsons, A.J., and Abrahams, A.D., eds., *Geomorphology of Desert Environments* (2nd ed.): Springer Science+Business Media B.V., Dordrecht, Netherlands, p. 413–467, https://doi.org/10.1007/978-1-4020-5719-9_14.
- Bobyarchick, A.R., and Glover, L., III, 1979, Deformation and metamorphism in the Hylas zone and adjacent parts of the eastern Piedmont in Virginia: Geological Society of America Bulletin, v. 90, no. 8, part 1, p. 739–752, [https://doi.org/10.1130/0016-7606\(1979\)90<739:DAMITH>2.0.CO;2](https://doi.org/10.1130/0016-7606(1979)90<739:DAMITH>2.0.CO;2).
- Brenner, G.J., 1963, The Spores and Pollen of the Potomac Group of Maryland: Maryland Department of Geology Mines and Water Resources Bulletin 27, 215 p.
- Brierley, G.J., Liu, K., and Crook, K.A.W., 1993, Sedimentology of coarse-grained alluvial fans in the Markham Valley, Papua New Guinea: Sedimentary Geology, v. 86, no. 3–4, p. 297–324, [https://doi.org/10.1016/0037-0738\(93\)90027-3](https://doi.org/10.1016/0037-0738(93)90027-3).
- Browning, J.V., Miller, K.G., McLaughlin, P.P., Edwards, L.E., Kulpez, A.A., Powars, D.S., Wade, B.S., Feigenson, M.D., and Wright, J.D., 2009, Integrated sequence stratigraphy of the postimpact sediments from Eyreville core holes, Chesapeake Bay impact structure inner basin, *in* Gohn, G.S., Koeberl, C., Miller, K.G., and Reimold, W.U., eds., The ICDP-USGS Deep Drilling Project in the Chesapeake Bay Impact Structure: Results from the Eyreville Core Holes: Geological Society of America Special Paper 458, p. 775–810, [https://doi.org/10.1130/2009.2458\(33\)](https://doi.org/10.1130/2009.2458(33)).
- Catchings, R.D., Powars, D.S., Gohn, G.S., and Goldman, M.R., 2005, High-resolution seismic-reflection image of the Chesapeake Bay impact structure, NASA Langley Research Center, Hampton, Virginia, *in* Horton, J.W., Jr., Powars, D.S., and Gohn, G.S., eds., *Studies of the Chesapeake Bay Impact Structure—The USGS-NASA Langley Corehole, Hampton, Virginia, and Related Coreholes and Geophysical Surveys*: U.S. Geological Survey Professional Paper 1688, Chapter I, p. II–12.
- Catchings, R.D., Powars, D.S., Gohn, G.S., Horton, J.W., Jr., Goldman, M.R., and Hole, J.A., 2008, Anatomy of the Chesapeake Bay impact structure revealed by seismic imaging, Delmarva Peninsula, Virginia, USA: Journal of Geophysical Research, v. 113, B08413, p. 1–23, <https://doi.org/10.1029/2007JB005421>.
- Cederstrom, D.J., 1943, Deep Wells in the Virginia Coastal Plain: Charlottesville, Virginia Geological Survey Report, Ser. 6, 14 p.
- Cederstrom, D.J., 1945, Structural geology of southeastern Virginia: American Association of Petroleum Geologists Bulletin, v. 29, no. 1, p. 71–95.
- Cederstrom, D.J., 1957, Geology and Ground-Water Resources of the York-James Peninsula: U.S. Geological Survey Water-Supply Paper 1361, 237 p.
- Cohen, K.M., Finney, S.C., Gibbard, P.L., and Fan, J.-X., 2013, The ICS International Chronostratigraphic Chart: Episodes, v. 36, p. 199–204.
- Collins, G.S., and Wünnemann, K., 2005, How big was the Chesapeake Bay impact? Insight from numerical modeling: Geology, v. 33, no. 12, p. 925–928, <https://doi.org/10.1130/G21854.1>.
- Collins, G.S., Kenkmann, T., Osinski, G.R., and Wünnemann, K., 2008a, Mid-sized complex crater formation in mixed crystalline-sedimentary targets: Insight from modeling and observation: Meteoritics & Planetary Science, v. 43, no. 12, p. 1955–1977, <https://doi.org/10.1111/j.1945-5100.2008.tb00655.x>.
- Collins, G.S., Kenkmann, T., Wünnemann, K., Wittmann, A., Reimold, W.U., and Melosh, H.J., 2008b, A model for the formation of the Chesapeake Bay impact crater as revealed by drilling and numerical simulation, *in* 39th Lunar and Planetary Science Conference: Lunar and Planetary Institute Contribution 1423, paper 3059.
- Crawford, D.A., and Barnouin-Jha, O.S., 2004, Computational investigations of the Chesapeake Bay impact structure, *in* 35th Lunar and Planetary Science Conference: Lunar and Planetary Institute Contribution 1197, paper 1757.
- Davison, T., and Collins, G.S., 2007, The effect of the oceans on the terrestrial crater size-frequency distribution: Insight from numerical modeling: Meteoritics & Planetary Science, v. 42, p. 1915–1927.
- Deptuck, M.E., and Campbell, D.C., 2012, Widespread erosion and mass failure from the ~51 Ma Montagnais marine bolide impact off southwestern Nova Scotia, Canada. Canadian Journal of Earth Sciences, v. 49, no. 12, p. 1567–1594, <https://doi.org/10.1139/e2012-075>.
- Deynoux, M., Çiner, A., Monod, O., Karabiyikoglu, M., Manatschal, G., and Tuzcu, S., 2005, Facies architecture and depositional evolution of alluvial fan to fan-delta complexes in the tectonically active Miocene Köprüçay Basin, Isparta angle, Turkey: Sedimentary Geology, v. 173, no. 1–4, p. 315–343, <https://doi.org/10.1016/j.sedgeo.2003.12.013>.
- Doyle, J.A., and Robbins, E.I., 1977, Angiosperm pollen zonation of the continental Cretaceous of the Atlantic Coastal Plain and its application to deep wells in the Salisbury embayment: Palynology, v. 1, p. 41–78, <https://doi.org/10.1080/01916122.1977.9989150>.
- Doyle, J.A., Endress, P.K., and Upchurch, G.R., Jr., 2008, Early Cretaceous monocots: A phylogenetic evaluation: Acta Musei Nationalis Pragae, Ser. B, Historia Naturalis, v. 64, no. 2–4, p. 59–87.
- Dypvik, H., and Jansa, L.F., 2003, Sedimentary signatures and processes during marine bolide impacts: A review: Sedimentary Geology, v. 161, p. 309–337, [https://doi.org/10.1016/S0037-0738\(03\)00135-0](https://doi.org/10.1016/S0037-0738(03)00135-0).
- Dypvik, H., and Kalleeson, E., 2010, Mechanisms of late synimpact to early postimpact crater sedimentation in marine-target impact structures, *in* Gibson, R.L., and Reimold, W.U., eds., *Large Meteorite Impacts and Planetary Evolution IV*: Geological Society of America Special Paper 465, p. 301–318, [https://doi.org/10.1130/2010.2465\(18\)](https://doi.org/10.1130/2010.2465(18)).
- Dypvik, H., Gudlaugsson, S.T., Tsikalas, F., Attrep, M., Jr., Ferrell, R.E., Jr., Krinsley, D.H., Mørk, A., Faleide, J.I., and Nagy, J., 1996, Mjølnir

- structure: An impact crater in the Barents Sea: *Geology*, v. 24, no. 9, p. 779–782, [https://doi.org/10.1130/0091-7613\(1996\)024<0779:MLSAIC>2.3.CO;2](https://doi.org/10.1130/0091-7613(1996)024<0779:MLSAIC>2.3.CO;2).
- Dypvik, H., Burchell, M.J., and Claeys, P., 2004, Impacts into marine and icy environments—A short review, *in* Dypvik, H., Burchell, M., and Claeys, P., eds., *Cratering in Marine Environments and on Ice*: New York, Springer, p. 1–20, https://doi.org/10.1007/978-3-662-06423-8_1.
- Earth Impact Database, 2018, <http://www.passc.net/EarthImpactDatabase/index.html>.
- Edwards, L.E., 1996, Palynology helps detect major impact crater, *in* Jansonius, J., and McGregor, D.C., eds., *Palynology: Principles and Applications: Volume 3. New Directions, Other Applications, and Floral History*: Dallas, Texas, American Association of Stratigraphic Palynologists Foundation, p. 1281.
- Edwards, L.E., and Powars, D.S., 2003, Impact damage to dinocysts from the late Eocene Chesapeake Bay event: *Palaaios*, v. 18, p. 275–285, [https://doi.org/10.1669/0883-1351\(2003\)018<0275:IDTDF>2.0.CO;2](https://doi.org/10.1669/0883-1351(2003)018<0275:IDTDF>2.0.CO;2).
- Edwards, L.E., Barron, J.A., Bukry, D., Bybell, L.M., Cronin, T.M., Poag, C.W., Weems, R.E., and Wingard, G.L., 2005, Paleontology of the Upper Eocene to Quaternary postimpact section in the USGS-NASA Langley core, Hampton, Virginia, *in* Horton, J.W., Jr., Powars, D.S., and Gohn, G.S., eds., *Studies of the Chesapeake Bay Impact Structure—The USGS-NASA Langley Corehole, Hampton, Virginia, and Related Coreholes and Geophysical Surveys*: U.S. Geological Survey Professional Paper 1688, Chapter H, p. H1–H47, 9 plates.
- Edwards, L.E., Powars, D.S., Gohn, G.S., and Dypvik, H., 2009, Geologic columns for the ICDP-USGS Eyreville A and B cores, Chesapeake Bay impact structure: Sediment breccias, 1096 to 444 m depth, *in* Gohn, G.S., Koeberl, C., Miller, K.G., and Reimold, W.U., eds., *The ICDP-USGS Deep Drilling Project in the Chesapeake Bay Impact Structure: Results from the Eyreville Core Holes*: Geological Society of America Special Paper 458, p. 51–89, [https://doi.org/10.1130/2009.2458\(03\)](https://doi.org/10.1130/2009.2458(03)).
- Edwards, L.E., Powars, D.S., Horton, J.W., Jr., Gohn, G.S., Self-Trail, J.M., and Litwin, R.J., 2010, Inside the crater, outside the crater: Stratigraphic details of the margin of the Chesapeake Bay impact structure, Virginia, USA, *in* Gibson, R.L., and Reimold, W.U., eds., *Large Meteorite Impacts and Planetary Evolution IV*: Geological Society of America Special Paper 465, p. 319–393, [https://doi.org/10.1130/2010.2465\(19\)](https://doi.org/10.1130/2010.2465(19)).
- Ferrell, R.E., Jr., and Dypvik, H., 2009, The mineralogy of the Exmore beds–Chickahominy Formation boundary section of the Chesapeake Bay impact structure revealed in the Eyreville core, *in* Gohn, G.S., Koeberl, C., Miller, K.G., and Reimold, W.U., eds., *The ICDP-USGS Deep Drilling Project in the Chesapeake Bay Impact Structure: Results from the Eyreville Core Holes*: Geological Society of America Special Paper 458, p. 723–246, [https://doi.org/10.1130/2009.2458\(31\)](https://doi.org/10.1130/2009.2458(31)).
- Flint, R.F., Sanders, J.E., and Rodgers, J., 1960a, Symmictite: A name for non-sorted terrigenous sedimentary rocks that contain a wide range of particle sizes: *Geological Society of America Bulletin*, v. 71, p. 507–510, [https://doi.org/10.1130/0016-7606\(1960\)71\[507:SANFNT\]2.0.CO;2](https://doi.org/10.1130/0016-7606(1960)71[507:SANFNT]2.0.CO;2).
- Flint, R.F., Sanders, J.E., and Rodgers, J., 1960b, Diamictite: A substitute term for symmictite: *Geological Society of America Bulletin*, v. 71, p. 1809–1810, [https://doi.org/10.1130/0016-7606\(1960\)71\[1809:DASTFS\]2.0.CO;2](https://doi.org/10.1130/0016-7606(1960)71[1809:DASTFS]2.0.CO;2).
- Frederiksen, N.O., Edwards, L.E., Self-Trail, J.M., Bybell, L.M., and Cronin, T.M., 2005, Paleontology of the impact-modified and impact-generated sediments in the USGS-NASA Langley core, Hampton, Virginia, *in* Horton, J.W., Jr., Powars, D.S., and Gohn, G.S., eds., *Studies of the Chesapeake Bay Impact Structure—The USGS-NASA Langley Corehole, Hampton, Virginia, and Related Coreholes and Geophysical Surveys*: U.S. Geological Survey Professional Paper 1688, Chapter D, p. D1–D37, 5 plates.
- French, B.M., 1998, *Traces of Catastrophe: A Handbook of Shock-Metamorphic Effects in Terrestrial Meteorite Impact Studies*: Houston, Texas, Lunar and Planetary Institute, LPI Contribution 954, 120 p.
- Glass, B.P., 1989, North American tektite debris and impact ejecta from DSDP Site 612: Meteoritics, v. 24, p. 209–218, <https://doi.org/10.1111/j.1945-5100.1989.tb00695.x>.
- Gohn, G.S., Powars, D.S., Bruce, T.S., and Self-Trail, J.M., 2005, Physical geology of the impact-modified and impact-generated sediments in the USGS-NASA Langley core, Hampton, Virginia, *in* Horton, J.W., Jr., Powars, D.S., and Gohn, G.S., eds., *Studies of the Chesapeake Bay Impact Structure—The USGS-NASA Langley Corehole, Hampton, Virginia, and Related Coreholes and Geophysical Surveys*: U.S. Geological Survey Professional Paper 1688, p. C1–C38.
- Gohn, G.S., Sanford, W.E., Powars, D.S., Horton, J.W., Jr., Edwards, L.E., Morin, R.H., and Self-Trail, J.M., 2007, Site Report for USGS Test Holes Drilled at Cape Charles, Northampton County, Virginia, in 2004: U.S. Geological Survey Open-File Report 2007–1094, 22 p.
- Gohn, G.S., Koeberl, C., Miller, K.G., and Reimold, W.U., eds., 2009a, *The ICDP-USGS Deep Drilling Project in the Chesapeake Bay Impact Structure: Results from the Eyreville Core Holes*: Geological Society of America Special Paper 458, 975 p., <https://doi.org/10.1130/SPE458>.
- Gohn, G.S., Powars, D.S., Dypvik, H., and Edwards, L.E., 2009b, Rock-avalanche and ocean-resurge deposits in the late Eocene Chesapeake Bay impact structure: Evidence from the ICDP-USGS Eyreville cores, Virginia, USA, *in* Gohn, G.S., Koeberl, C., Miller, K.G., and Reimold, W.U., eds., *The ICDP-USGS Deep Drilling Project in the Chesapeake Bay Impact Structure: Results from the Eyreville Core Holes*: Geological Society of America Special Paper 458, p. 587–615, [https://doi.org/10.1130/2009.2458\(26\)](https://doi.org/10.1130/2009.2458(26)).
- Gudlaugsson, S.T., 1993, Large impact crater in the Barents Sea: *Geology*, v. 21, no. 4, p. 291–294, [https://doi.org/10.1130/0091-7613\(1993\)021<0291:LICITB>2.3.CO;2](https://doi.org/10.1130/0091-7613(1993)021<0291:LICITB>2.3.CO;2).
- Hansen, H.J., 1982, Waste Gate Formation, Part 1: Hydrogeologic Framework and Potential Utilization of the Brine Aquifers of the Waste Gate Formation, a New Unit of the Potomac Group Underlying the Delmarva Peninsula: Baltimore, Maryland Geological Survey Open-File Report, 50 p.
- Hansen, H.J., and Doyle, J.A., 1982, Waste Gate Formation: Maryland: U.S. Geological Survey Open-File Report 82-02-1, 50 p.
- Hochuli, P.A., Heimhofer, U., and Weissert, H., 2006, Timing of early angiosperm radiation: Recalibrating the classical succession: *Journal of the Geological Society*, v. 163, p. 587–594, <https://doi.org/10.1144/0016-764905-135>.
- Horton, J.W., Jr., and Izett, G.A., 2005, Crystalline-rock ejecta and shocked minerals of the Chesapeake Bay impact structure, USGS-NASA Langley core, Hampton, Virginia, with supplemental constraints on the age of impact, *in* Horton, J.W., Jr., Powars, D.S., and Gohn, G.S., eds., *Studies of the Chesapeake Bay Impact Structure—The USGS-NASA Langley Corehole, Hampton, Virginia, and Related Coreholes and Geophysical Surveys*: U.S. Geological Survey Professional Paper 1688, p. E1–E30.
- Horton, J.W., Jr., Aleinikoff, J.N., Izett, G.A., Naeser, N.D., Naeser, C.W., and Kunk, M.J., 2002a, Crystalline basement and impact-derived clasts from three coreholes in the Chesapeake Bay impact structure, southeastern Virginia [abs.]: *Eos (Transactions, American Geophysical Union)*, v. 83, no. 19, Spring Meeting supplement, abstract T21A-03, p. S351.
- Horton, J.W., Jr., Kunk, M.J., Naeser, C.W., Naeser, N.D., Aleinikoff, J.N., and Izett, G.A., 2002b, Petrography, geochronology, and significance of crystalline basement rocks and impact-derived clasts in the Chesapeake Bay impact structure, southeastern Virginia [abs.]: *Geological Society of America Abstracts with Programs*, v. 34, no. 6, p. 466.
- Horton, J.W., Jr., Gohn, G.S., Powars, D.S., Jackson, J.C., Self-Trail, J.M., Edwards, L.E., and Sanford, W.E., 2004, Impact breccias of the central uplift, Chesapeake Bay impact structure: Initial results of a test hole at Cape Charles, Virginia [abs.]: *Geological Society of America Abstracts with Programs*, v. 36, no. 5, abstract 110-119, p. 266.
- Horton, J.W., Jr., Aleinikoff, J.N., Kunk, M.J., Gohn, G.S., Edwards, L.E., Self-Trail, J.M., Powars, D.S., and Izett, G.A., 2005a, Recent research on the Chesapeake Bay impact structure, USA—Impact debris and reworked ejecta, *in* Kenkmann, T., Hörz, F., and Deutsch, A., eds., *Large Meteorite Impacts III*: Geological Society of America Special Paper 384, p. 147–170.
- Horton, J.W., Jr., Aleinikoff, J.N., Kunk, M.J., Naeser, C.W., and Naeser, N.D., 2005b, Petrography, structure, age, and thermal history of granitic coastal plain basement in the Chesapeake Bay impact structure, USGS-NASA Langley core, Hampton, Virginia, *in* Horton, J.W., Jr., Powars, D.S., and Gohn, G.S., eds., *Studies of the Chesapeake Bay Impact Structure—The USGS-NASA Langley Corehole, Hampton, Virginia, and Related Coreholes and Geophysical Surveys*: U.S. Geological Survey Professional Paper 1688, p. B1–B29.
- Horton, J.W., Jr., Gohn, G.S., Jackson, J.C., Aleinikoff, J.N., Sanford, W.E., Edwards, L.E., and Powars, D.S., 2005c, Results from a scientific test hole in the central uplift, Chesapeake Bay impact structure, Virginia, USA [abs.], *in* Lunar and Planetary Science Conference XXXVI: Lunar and Planetary Institute Contribution 1156, abstract 2003, 2 p., <http://www.lpi.usra.edu/meetings/lpsc2005/pdf/2003.pdf>.

- Horton, J.W., Jr., Powars, D.S., and Gohn, G.S., 2005d, Studies of the Chesapeake Bay impact structure—Introduction and discussion, *in* Horton, J.W., Jr., Powars, D.S., and Gohn, G.S., eds., *Studies of the Chesapeake Bay Impact Structure—The USGS-NASA Langley Corehole, Hampton, Virginia, and Related Coreholes and Geophysical Surveys: U.S. Geological Survey Professional Paper 1688*, p. A1–A24.
- Horton, J.W., Jr., Powars, D.S., and Gohn, G.S., eds., 2005e, *Studies of the Chesapeake Bay Impact Structure—The USGS-NASA Langley Corehole, Hampton, Virginia, and Related Coreholes and Geophysical Surveys: U.S. Geological Survey Professional Paper 1688*, chapter pagination.
- Horton, J.W., Jr., Ormö, J., Powars, D.S., and Gohn, G.S., 2006, Chesapeake Bay impact structure: Morphology, crater fill, and relevance for impact structures on Mars: *Meteoritics & Planetary Science*, v. 41, p. 1613–1624, <https://doi.org/10.1111/j.1945-5100.2006.tb00439.x>.
- Horton, J.W., Jr., Gohn, G.S., Powars, D.S., and Edwards, L.E., 2008, Origin and emplacement of impactites in the Chesapeake Bay impact structure, Virginia, USA, *in* Evans, K.R., Horton, J.W., Jr., King, D.T., Jr., and Morrow, J.R., eds, *The Sedimentary Record of Meteorite Impacts: Geological Society of America Special Paper 437*, p. 73–97, [https://doi.org/10.1130/2008.2437\(06\)](https://doi.org/10.1130/2008.2437(06)).
- Horton, J.W., Jr., Gibson, R.L., Reimold, W.U., Wittmann, A., Gohn, G.S., and Edwards, L.E., 2009a, Geologic columns for the ICDP-USGS Eyreville B core, Chesapeake Bay impact structure: Impactites and crystalline rocks, 1766 to 1096 m depth, *in* Gohn, G.S., Koeberl, C., Miller, K.G., and Reimold, W.U., eds., *The ICDP-USGS Deep Drilling Project in the Chesapeake Bay Impact Structure: Results from the Eyreville Core Holes: Geological Society of America Special Paper 458*, p. 21–49, [https://doi.org/10.1130/2009.2458\(02\)](https://doi.org/10.1130/2009.2458(02)).
- Horton, J.W., Jr., Kunk, M.J., Belkin, H.E., Aleinikoff, J.N., Jackson, J.C., and Chou, I.-M., 2009b, Evolution of crystalline target rocks and impactites in the Chesapeake Bay impact structure, ICDP-USGS Eyreville B core, *in* Gohn, G.S., Koeberl, C., Miller, K.G., and Reimold, W.U., eds., *The ICDP-USGS Deep Drilling Project in the Chesapeake Bay Impact Structure: Results from the Eyreville Core Holes: Geological Society of America Special Paper 458*, p. 277–316, [https://doi.org/10.1130/2009.2458\(14\)](https://doi.org/10.1130/2009.2458(14)).
- Horton, J.W., Jr., Daniels, D.L., and Powars, D.S., 2011, Geologic and geophysical mapping of pre-Cretaceous basement rocks beneath the Atlantic Coastal Plain, Virginia to southern New Jersey [abs.]: *Geological Society of America Abstracts with Programs*, v. 43, no. 2, p. 65.
- Horton, J.W., Jr., Daniels, D.L., and Powars, D.S., 2014, Pre-Cretaceous terranes, basins, and faults beneath the Atlantic Coastal Plain: Analysis of subsurface samples and borehole data in relation to magnetic and gravity anomalies [abs.]: *Geological Society of America Abstracts with Programs*, v. 46, no. 6, p. 59.
- Horton, J.W., Jr., Owens, B.E., Hackley, P.C., Burton, W.C., Sacks, P.E., and Hibbard, J.P., 2016, Geology of the Eastern Piedmont in Virginia, *in* Bailey, C.M., Sherwood, W.C., Eaton, L.S., and Powars, D.S., eds., *The Geology of Virginia: Virginia Museum of Natural History Special Publication 18*, p. 125–158.
- Jansa, L.F., 1993, Cometary impacts into ocean: Their recognition and the threshold constraints for biological extinction: *Palaeogeography, Palaeoclimatology, Palaeoecology*, v. 104, p. 271–286, [https://doi.org/10.1016/0031-0182\(93\)90137-8](https://doi.org/10.1016/0031-0182(93)90137-8).
- Jansa, L.F., and Pe-Piper, G., 1987, Identification of an underwater extraterrestrial impact crater: *Nature*, v. 327, p. 612–614, <https://doi.org/10.1038/327612a0>.
- Jansa, L.F., Pe-Piper, G., Robertson, P.B., and Friedenreich, O., 1989, Montagnais: A submarine impact structure on the Scotian shelf, eastern Canada: *Geological Society of America Bulletin*, v. 101, no. 4, p. 450–463, [https://doi.org/10.1130/0016-7606\(1989\)101<0450:MASISO>2.3.CO;2](https://doi.org/10.1130/0016-7606(1989)101<0450:MASISO>2.3.CO;2).
- Kar, R., Chakraborty, T., Chakraborty, C., Ghosh, P., Tyagi, A.K., and Singhvi, A.K., 2014, Morpho-sedimentary characteristics of the Quaternary Matiali fan and associated river terraces, Jalpaiguri, India: Implications of climatic controls: *Geomorphology*, v. 227, p. 137–152, <https://doi.org/10.1016/j.geomorph.2014.05.014>.
- Kenkmann, T., Collins, G.S., Wittmann, A., Wünnemann, K., Reimold, W.U., and Melosh, H.J., 2009, A model for the formation of the Chesapeake Bay impact crater as revealed by drilling and numerical simulation, *in* Gohn, G.S., Koeberl, C., Miller, K.G., and Reimold, W.U., eds., *The ICDP-USGS Deep Drilling Project in the Chesapeake Bay Impact Structure: Results from the Eyreville Core Holes: Geological Society of America Special Paper 458*, p. 571–585, [https://doi.org/10.1130/2009.2458\(25\)](https://doi.org/10.1130/2009.2458(25)).
- Kenkmann, T., Collins, G.S., and Wünnemann, K., 2013, The modification stage of crater formation, *in* Osinski, G.R., and Pierazzo, E., eds., *Impact Cratering, Processes and Products: Chichester, UK, Wiley-Blackwell*, p. 60–75.
- King, D.T., Jr., Ormö, J., Petruny, L.W., and Neathery, T.L., 2006, Role of water in the formation of the Late Cretaceous Wetumpka impact structure, inner Gulf Coastal Plain of Alabama, USA: *Meteoritics & Planetary Science*, v. 41, no. 10, p. 1625–1631, <https://doi.org/10.1111/j.1945-5100.2006.tb00440.x>.
- Koeberl, C., Poag, C.W., Reimold, W.U., and Brandt, D., 1996, Impact origin of the Chesapeake Bay structure and the source of the North American tektites: *Science*, v. 271, no. 5253, p. 1263–1266, <https://doi.org/10.1126/science.271.5253.1263>.
- Kramer, S.L., 2013, Chapter L, lateral spreading, *in* Bobrowsky, P.T., ed., *Encyclopedia of Natural Hazards*, p. 623, https://link.springer.com/content/pdf/10.1007%2f978-1-4010-4399-4_215.pdf.
- Kulpecz, A.A., Miller, K.G., Browning, J.V., Edwards, L.E., Powars, D.S., McLaughlin, P.P., Jr., Harris, A.D., and Feigenson, M.D., 2009, Postimpact deposition in the Chesapeake Bay impact structure: Variations in eustasy, compaction, sediment supply, and passive-aggressive tectonism, *in* Gohn, G.S., Koeberl, C., Miller, K.G., and Reimold, W.U., eds., *The ICDP-USGS Deep Drilling Project in the Chesapeake Bay Impact Structure: Results from the Eyreville Core Holes: Geological Society of America Special Paper 458*, p. 811–837, [https://doi.org/10.1130/2009.2458\(34\)](https://doi.org/10.1130/2009.2458(34)).
- Larsen, D., Stephens, E.C., and Zivkovic, V.B., 2009, Postimpact alteration of sedimentary breccias in the ICDP-USGS Eyreville A and B cores with comparison to the Cape Charles core, Chesapeake Bay impact structure, Virginia, USA, *in* Gohn, G.S., Koeberl, C., Miller, K.G., and Reimold, W.U., eds., *The ICDP-USGS Deep Drilling Project in the Chesapeake Bay Impact Structure: Results from the Eyreville Core Holes: Geological Society of America Special Paper 458*, p. 699–722.
- Leier, A.L., DeCelles, P.G., and Pelletier, J.D., 2005, Mountains, monsoons, and megafans: *Geology*, v. 33, no. 4, p. 289–292, <https://doi.org/10.1130/G21228.1>.
- Lowe, D.R., 1975, Water escape structures in coarse grained sediments: *Sedimentology*, v. 22, p. 157–204, <https://doi.org/10.1111/j.1365-3091.1975.tb00290.x>.
- Malinconico, M.L., Sanford, W.E., and Horton, J.W., Jr., 2009, Postimpact heat conduction and compaction-driven fluid flow in the Chesapeake Bay impact structure based on downhole vitrinite reflectance data, ICDP-USGS Eyreville deep core holes and Cape Charles test holes, *in* Gohn, G.S., Koeberl, C., Miller, K.G., and Reimold, W.U., eds., *The ICDP-USGS Deep Drilling Project in the Chesapeake Bay Impact Structure: Results from the Eyreville Core Holes: Geological Society of America Special Paper 458*, p. 905–930, [https://doi.org/10.1130/2009.2458\(38\)](https://doi.org/10.1130/2009.2458(38)).
- Marantos, I., Christidis, G.E., and Ulmanu, M., 2012, Zeolite formation and deposits, *in* Inglezakis, V.J., and Zorpas, A.A., eds., *Handbook of Natural Zeolites: Sharjah, United Arab Emirates, Bentham Sciences Publishers Ltd*, p. 28–51.
- McFarland, E.R., and Bruce, T.S., 2005, Distribution, origin, and resource-management implications of ground-water salinity along the western margin of the Chesapeake Bay impact structure in eastern Virginia, *in* Horton, J.W., Jr., Powars, D.S., and Gohn, G.S., eds., *Studies of the Chesapeake Bay Impact Structure—The USGS-NASA Langley Corehole, Hampton, Virginia, and Related Coreholes and Geophysical Surveys: U.S. Geological Survey Professional Paper 1688*, p. K1–K32.
- Melosh, H.J., 1984, Impact ejection, spallation, and the origin of meteorites: *Icarus*, v. 59, p. 234–260, [https://doi.org/10.1016/0019-1035\(84\)90026-5](https://doi.org/10.1016/0019-1035(84)90026-5).
- Melosh, H.J., 1989, *Impact Cratering, a Geologic Process: New York, Oxford University Press*, 245 p.
- Melosh, H.J., 2013, The contact and compression stage of impact cratering, *in* Osinski, G.R., and Pierazzo, E., eds., *Impact Cratering, Processes and Products: Chichester, UK, Wiley-Blackwell*, p. 32–42.
- Melosh, H.J., and Ivanov, B.A., 1999, Impact crater collapse: *Annual Review of Earth and Planetary Science*, v. 27, p. 385–415.
- Miall, A., 2010, Alluvial deposits, *in* James, N.P., and Dalrymple, R.W., eds., *Facies Models 4: Geological Association of Canada IV Series, Geotext 6*, p. 105–138.
- Morgan, J.V., Gulick, S.P.S., Bralower, T., Chenot, E., Christenson, G., Claeys, P., Cockell, C., Collins, G.S., Coolen, M.J.L., Ferrière, L., Gebhardt, C., Goto, K., Jones H., Kring, D.A., Le Ber, E., Lofi, J., Long, X., Lowery, C., Mellett, C., Ocampo-Torres, R., Osinski, G.R., Perez-Cruz, L., Pickersgill, A.,

- Poelchau, M., Rae, A., Rasmussen, C., Rebolledo-Vieyra, M., Riller, U., Sato, H., Schmitt, D.R., Smit, J., Tikoo, S., Tomioka, N., Urrutia-Fucugauchi, J., Whalen, M., Wittmann A., Yamaguchi K.E., and Zylberman, W., 2016, The formation of peak rings in large impact craters: *Science*, v. 354, no. 6314, p. 878–882, <https://doi.org/10.1126/science.aah6561>.
- Mulder, T., and Alexander, J., 2001, The physical character of subaqueous sedimentary density flows and their deposits: *Sedimentology*, v. 48, p. 269–299, <https://doi.org/10.1046/j.1365-3091.2001.00360.x>.
- Naumov, M.V., 2005, Principal features of impact-generated hydrothermal circulation systems: Mineralogical and geochemical evidence: *Geofluids*, v. 5, p. 165–184, <https://doi.org/10.1111/j.1468-8123.2005.00092.x>.
- North, C.P., and Davidson, S.K., 2012, Unconfined alluvial flow processes: Recognition and interpretation of their deposits, and the significance for palaeogeographic reconstruction: *Earth-Science Reviews*, v. 111, no. 1–2, p. 199–223, <https://doi.org/10.1016/j.earscirev.2011.11.008>.
- Oberbeck, V.R., and Quaide, W.L., 1968, Genetic implications of lunar regolith thickness variations: *Icarus*, v. 9, p. 446–465, [https://doi.org/10.1016/0019-1035\(68\)90039-0](https://doi.org/10.1016/0019-1035(68)90039-0).
- Obermeier, S.F., 1996, Use of liquefaction-induced features for paleoseismic analysis—An overview of how seismic liquefaction features can be distinguished from other features and how their regional distribution and properties can be used to infer the location and strength of Holocene paleo-earthquakes: *Engineering Geology*, v. 44, p. 1–76, [https://doi.org/10.1016/S0013-7952\(96\)00040-3](https://doi.org/10.1016/S0013-7952(96)00040-3).
- Obermeier, S.F., Pond, E.C., and Olson, S.M., 2001, Paleoliquefaction Studies in Continental Settings: Geologic and Geotechnical Factors in Interpretations and Back-Analysis: U.S. Geological Survey Open-File Report 01-029, 75 p., <https://pubs.usgs.gov/of/2001/of01-029/> (accessed 18 December 2017).
- Ormö, J., and Lindström, M., 2000, When a cosmic impact strikes the sea bed: *Geological Magazine*, v. 137, no. 1, p. 67–80, <https://doi.org/10.1017/S0016756800003538>.
- Ormö J., Shuvalov, V.V., and Lindström, M., 2002, Numerical modeling for target water depth estimation of marine target impact craters: *Journal of Geophysical Research*, v. 107, no. E12, 5120, <https://doi.org/10.1029/2002JE001865>.
- Ormö, J., Sturkell, E., Horton, J.W., Jr., Powars, D.S., and Edwards, L.E., 2009, Comparison of clast frequency and size in the resurge deposits at the Chesapeake Bay impact structure (Eyreville A and Langley cores): Clues to the resurge process, in Gohn, G.S., Koeberl, C., Miller, K.G., and Reimold, W.U., eds., *The ICDP-USGS Deep Drilling Project in the Chesapeake Bay Impact Structure: Results from the Eyreville Core Holes: Geological Society of America Special Paper 458*, p. 617–632, [https://doi.org/10.1130/2009.2458\(27\)](https://doi.org/10.1130/2009.2458(27)).
- Ormö, J., Lepinette, A., Sturkell, E., Lindström, M., Housen, K.R., and Holsapple, K.A., 2010, Water resurge at marine-target impact craters analyzed with a combination of low-velocity impact experiments and numerical simulations, in Gibson, R.L., and Reimold, W.U., eds., *Large Meteorite Impacts and Planetary Evolution IV: Geological Society of America Special Paper 465*, p. 81–101, [https://doi.org/10.1130/2010.2465\(06\)](https://doi.org/10.1130/2010.2465(06)).
- Osinski, G.R., 2005, Hydrothermal activity associated with the Ries impact event, Germany: *Geofluids*, v. 5, no. 3, p. 202–220, <https://doi.org/10.1111/j.1468-8123.2005.00119.x>.
- Osinski, G.R., and Pierazzo, E., 2013, Impact cratering: Processes and products, in Osinski, G.R., and Pierazzo, E., eds., *Impact Cratering, Processes and Products*: Chichester, UK, Wiley-Blackwell, p. 1–20.
- Osinski, G.R., Grieve, R.A.F., and Tornabene, L.L., 2013, Excavation and impact ejecta emplacement, in Osinski, G.R., and Pierazzo, E., eds., *Impact Cratering, Processes and Products*: Chichester, UK, Wiley-Blackwell, p. 43–59.
- Owens, J.P., and Gohn, G.S., 1985, Depositional history of the Cretaceous Series in the U.S. Atlantic Coastal Plain: Stratigraphy, paleoenvironments, and tectonic controls of sedimentation, in Poag, C.W., ed., *Geologic Evolution of the United States Atlantic Margin*: New York, Van Nostrand Reinhold Co., p. 25–86.
- Pe-Piper, G., Jansa, L.F., and Lambert, R.St.J., 1992, Early Mesozoic magmatism on the eastern Canadian margin: Petrogenetic and tectonic significance, in Puffer, J.H., and Ragland, P.C., eds., *Eastern North American Mesozoic Magmatism: Geological Society of America Special Paper 268*, p. 13–36, <https://doi.org/10.1130/SPE268-p13>.
- Pickering, K.T., and Hiscott, R.N., with contribution from T. Heard, 2016, *Deep Marine Systems: Processes, Deposits, Environments, Tectonics and Sedimentation*: Chichester, UK, American Geophysical Union and John Wiley & Sons, Ltd., 657 p.
- Poag, C.W., 1996, Structural outer rim of Chesapeake Bay impact crater: Seismic and bore hole evidence: *Meteoritics & Planetary Science*, v. 31, p. 218–226, <https://doi.org/10.1111/j.1945-5100.1996.tb02015.x>.
- Poag, C.W., 1997, The Chesapeake Bay bolide impact: A convulsive event in Atlantic Coastal Plain evolution: *Sedimentary Geology*, v. 108, p. 45–90, [https://doi.org/10.1016/S0037-0738\(96\)00048-6](https://doi.org/10.1016/S0037-0738(96)00048-6).
- Poag, C.W., 2002, Synimpact-postimpact transition inside Chesapeake Bay crater: *Geology*, v. 30, p. 995–998, [https://doi.org/10.1130/0091-7613\(2002\)030<0995:SPTICB>2.0.CO;2](https://doi.org/10.1130/0091-7613(2002)030<0995:SPTICB>2.0.CO;2).
- Poag, C.W., 2007, Postimpact biotic recovery inside the late Eocene Chesapeake Bay submarine impact crater, in 70th Annual Meeting of the Meteoritical Society Abstracts: *Meteoritics & Planetary Science*, v. 42, no. 8, Supplement, p. A126, abstract 5043.
- Poag, C.W., 2009, Paleoenvironmental recovery from the Chesapeake Bay bolide impact: The benthic foraminiferal record, in Gohn, G.S., Koeberl, C., Miller, K.G., and Reimold, W.U., eds., *The ICDP-USGS Deep Drilling Project in the Chesapeake Bay Impact Structure: Results from the Eyreville Core Holes: Geological Society of America Special Paper 458*, p. 747–773, [https://doi.org/10.1130/2009.2458\(32\)](https://doi.org/10.1130/2009.2458(32)).
- Poag, C.W., 2012, Foraminiferal repopulation of the late Eocene Chesapeake Bay impact crater: *Micropaleontology*, v. 58, no. 1–2, p. 1–206.
- Poag, C.W., and Aubry, M.-P., 1995, Upper Eocene impactites of the U.S. East Coast: Depositional origins, biostratigraphic framework, and correlation: *Palaio*, v. 10, no. 1, p. 16–33, <https://doi.org/10.2307/3515005>.
- Poag, C.W., and Commeau, J.A., 1995, Paleocene to Middle Miocene planktic foraminifera of the southwestern Salisbury Embayment, Virginia and Maryland: Biostratigraphy, allostratigraphy, and sequence stratigraphy: *Journal of Foraminiferal Research*, v. 25, p. 134–155, <https://doi.org/10.2113/gsjfr.25.2.134>.
- Poag, C.W., and Norris, R.D., 2005, Stratigraphy and paleoenvironments of early postimpact deposits at the USGS-NASA Langley corehole, Chesapeake Bay impact crater, chapter F, in Horton, J.W., Jr., Powars, D.S., and Gohn, G.S., eds., *Studies of the Chesapeake Bay Impact Structure—The USGS-NASA Langley Corehole, Hampton, Virginia, and Related Coreholes and Geophysical Surveys: U.S. Geological Survey Professional Paper 1688*, p. F1–F52.
- Poag, C.W., and Poppe, L.J., 1998, The Toms Canyon structure, New Jersey outer continental shelf: A possible late Eocene impact crater: *Marine Geology*, v. 145, p. 23–60, [https://doi.org/10.1016/S0025-3227\(97\)00113-8](https://doi.org/10.1016/S0025-3227(97)00113-8).
- Poag, C.W., Powars, D.S., Poppe, L.J., Mixon, R.B., Edwards, L.E., Folger, D.W., and Bruce, S., 1992, Deep Sea Drilling Project Site 612 bolide event: New evidence of a late Eocene impact-wave deposit and a possible impact site, U.S. east coast: *Geology*, v. 20, p. 771–774, [https://doi.org/10.1130/0091-7613\(1992\)020<0771:DSDPSB>2.3.CO;2](https://doi.org/10.1130/0091-7613(1992)020<0771:DSDPSB>2.3.CO;2).
- Poag, C.W., Powars, D.S., Poppe, L.J., and Mixon, R.B., 1994, Meteoroid mayhem in ole Virginny—Source of the North American tektite strewn field: *Geology*, v. 22, p. 691–694, [https://doi.org/10.1130/0091-7613\(1994\)022<0691:MMIOVS>2.3.CO;2](https://doi.org/10.1130/0091-7613(1994)022<0691:MMIOVS>2.3.CO;2).
- Poag, C.W., Hutchinson, D.R., Colman, S.M., and Lee, M.W., 1999, Seismic expression of the Chesapeake Bay impact crater: Structural and morphologic refinements based on new seismic data, in Dressler, B.O., and Sharpton, V.L., eds., *Large Meteorite Impacts and Planetary Evolution II: Geological Society of America Special Paper 339*, p. 149–164, <https://doi.org/10.1130/0-8137-2339-6.149>.
- Poag, C.W., Plescia, J.B., and Molzer, P.C., 2002, Ancient impact structures on modern continental shelves: The Chesapeake Bay, Montagnais, and Toms Canyon craters, Atlantic margin of North America. *Deep Sea Research Part II: Topical Studies in Oceanography*, v. 49, no. 6, p. 1081–1102, [https://doi.org/10.1016/S0967-0645\(01\)00144-8](https://doi.org/10.1016/S0967-0645(01)00144-8).
- Poag, C.W., Koeberl, C., and Reimold, W.U., 2004, *The Chesapeake Bay Crater: Geology and Geophysics of a Late Eocene Submarine Impact Structure*: Berlin, Springer-Verlag, 522 p. with CD-ROM.
- Postma, G., 1983, Water escape structures in the context of a depositional model of a mass flow dominated conglomeratic fan-delta (Abrija Formation, Pliocene, Almeria Basin, SE Spain): *Sedimentology*, v. 30, p. 91–103, <https://doi.org/10.1111/j.1365-3091.1983.tb00652.x>.
- Powars, D.S., 2000, The Effects of the Chesapeake Bay Impact Crater on the Geologic Framework and the Correlation of Hydrogeologic Units of Southeastern Virginia, South of the James River: U.S. Geological Survey Professional Paper 1622, 53 p., 1 plate.

- Powars, D.S., and Bruce, T.S., 1999, The Effects of the Chesapeake Bay Impact on the Geological Framework and Correlation of Hydrogeologic Units of the Lower York-James Peninsula, Virginia: U.S. Geological Survey Professional Paper 1612, 82 p., 7 plates.
- Powars, D.S., Mixon, R.B., and Bruce, S.T., 1992, Uppermost Mesozoic and Cenozoic geologic cross section, outer coastal plain of Virginia, *in* Gohn, G.S., ed., Proceedings of the 1988 U.S. Geological Survey Workshop on the Geology and Geohydrology of the Atlantic Coastal Plain: U.S. Geological Survey Circular 1059, p. 85–101.
- Powars, D.S., Poag, C.W., and Mixon, R.B., 1993, The Chesapeake Bay "impact crater"; Stratigraphic and seismic evidence: Geological Society of America Abstracts with Programs, v. 25, no. 6, p. 378.
- Powars, D.S., Johnson, G.H., Edwards, L.E., Horton, J.W., Jr., Gohn, G.S., Catchings, R.D., McFarland, E.R., Izett, G.A., Bruce, T.S., Levine, J.S., and Pierce, H.A., 2002, An expanded Chesapeake Bay impact structure, eastern Virginia: New corehole and geophysical data, *in* 33rd Lunar and Planetary Science Conference: Lunar and Planetary Science Institute Contribution 1109, abstract 1034, <http://www.lpi.usra.edu/meetings/lpsc2002/pdf/1034.pdf>.
- Powars, D.S., Bruce, T.S., Edwards, L.E., Gohn, G.S., Self-Trail, J.M., Weems, R.E., Johnson, G.H., Smith, M.J., and McCartan, C.T., 2005, Physical stratigraphy of the Upper Eocene to Quaternary postimpact section in the USGS-NASA Langley core, Hampton, Virginia, chapter G, *in* Horton, J.W., Jr., Powars, D.S., and Gohn, G.S., eds., Studies of the Chesapeake Bay Impact Structure—The USGS-NASA Langley Corehole, Hampton, Virginia, and Related Coreholes and Geophysical Surveys: U.S. Geological Survey Professional Paper 1688, p. G1–G44.
- Powars, D.S., Edwards, L.E., Catchings, R.D., Gohn, G.S., and Horton, J.W., Jr., 2008, Asymmetric (dipping) layered target constrained infilling of the Chesapeake Bay impact structure: Geological Society of America Abstracts with Programs, v. 40, no. 6, p. 407, https://gsa.confex.com/gsa/2008AM/finalprogram/abstract_150780.htm.
- Powars, D.S., Catchings, R.D., Goldman, M.R., Gohn, G.S., Horton, J.W., Jr., Edwards, L.E., Rymer, M.J., and Gandhok, G., 2009, High-resolution seismic-reflection images across the ICDP-USGS Eyreville deep drilling site, Chesapeake Bay impact structure, *in* Gohn, G.S., Koeberl, C., Miller, K.G., and Reimold, W.U., eds., The ICDP-USGS Deep Drilling Project in the Chesapeake Bay Impact Structure: Results from the Eyreville Core Holes: Geological Society of America Special Paper 458, p. 209–233, [https://doi.org/10.1130/2009.2458\(11\)](https://doi.org/10.1130/2009.2458(11)).
- Powars, D.S., Edwards, L.E., Johnson, G.H., and Berquist, C.R., 2016, Geology of the Virginia Coastal Plain: New insights from continuous cores and geophysical surveys, *in* Bailey, C.M., Sherwood, W.C., Eaton, L.S., and Powars, D.S., eds., The Geology of Virginia: Virginia Museum of Natural History Special Publication 18, p. 193–240.
- Reimold, W.U., Bartosova, K., Schmitt, R.T., Hansen, B., Crasselt, C., Koeberl, C., Wittmann, A., and Powars, D.S., 2009, Petrographic observations on the Exmore breccia, *in* Gohn, G.S., Koeberl, C., Miller, K.G., and Reimold, W.U., eds., The ICDP-USGS Deep Drilling Project in the Chesapeake Bay Impact Structure: Results from the Eyreville Core Holes: Geological Society of America Special Paper 458, p. 655–699, [https://doi.org/10.1130/2009.2458\(29\)](https://doi.org/10.1130/2009.2458(29)).
- Sanford, S., 1913, The Underground Water Resources of the Coastal Plain Province of Virginia: Virginia Geological Survey Bulletin 5, 361 p.
- Sanford, W.E., 2002, Possible hydrothermal activity following the Chesapeake Bay bolide impact: Geological Society of America Abstracts with Programs, v. 34, no. 6, p. 466.
- Sanford, W.E., 2003, Heat flow and brine evolution following the Chesapeake Bay bolide impact: Journal of Geochemical Exploration, v. 78–79, p. 243–247, [https://doi.org/10.1016/S0375-6742\(03\)00108-0](https://doi.org/10.1016/S0375-6742(03)00108-0).
- Sanford, W.E., Gohn, G.S., Powars, D.S., Horton, J.W., Jr., Edwards, L.E., Self-Trail, J.M., and Morin, R.H., 2004, Drilling the central crater of the Chesapeake Bay impact structure: A first look: Eos (Transactions, American Geophysical Union), v. 85, no. 39, p. 369, 377.
- Sanford, W.E., Voytek, M.A., Powars, D.S., Jones, B.F., Cozzarelli, I.M., Cockell, C.S., and Eganhouse, R.P., 2009, Pore-water chemistry from the ICDP-USGS core hole in the Chesapeake Bay impact structure—Implications for paleohydrology, microbial habitat, and water resources, *in* Gohn, G.S., Koeberl, C., Miller, K.G., and Reimold, W.U., eds., The ICDP-USGS Deep Drilling Project in the Chesapeake Bay Impact Structure: Results from the Eyreville Core Holes: Geological Society of America Special Paper 458, p. 867–890, [https://doi.org/10.1130/2009.2458\(36\)](https://doi.org/10.1130/2009.2458(36)).
- Sanford, W.E., Doughten, M.W., Coplen, T.B., Hunt, A.G., and Bullen, T.D., 2013, Evidence for high salinity of Early Cretaceous sea water from the Chesapeake Bay crater: Nature, v. 503, no. 7475, p. 252–256, <https://doi.org/10.1038/nature12714>.
- Schenk, P.M., 2002, Thickness constraints on the icy shells of the Galilean satellites from a comparison of crater shapes: Nature, v. 417, p. 419–421, <https://doi.org/10.1038/417419a>.
- Schulte, P., Wade, B.S., Kontny, A., and Self-Trail, J.M., 2009, The Eocene–Oligocene sedimentary record in the Chesapeake Bay impact structure: Implications for climate and sea-level changes on the western Atlantic margin, *in* Gohn, G.S., Koeberl, C., Miller, K.G., and Reimold, W.U., eds., The ICDP-USGS Deep Drilling Project in the Chesapeake Bay Impact Structure: Results from the Eyreville Core Holes: Geological Society of America Special Paper 458, p. 839–865, [https://doi.org/10.1130/2009.2458\(35\)](https://doi.org/10.1130/2009.2458(35)).
- Self-Trail, J.M., 2003, Shock-wave–induced fracturing of calcareous nannofossils from the Chesapeake Bay impact crater: Geology, v. 31, p. 697–700, <https://doi.org/10.1130/G19678.1>.
- Self-Trail, J.M., Edwards, L.E., and Litwin, R.J., 2009, Paleontological interpretations of crater processes and infilling of synimpact sediments from the Chesapeake Bay impact structure, *in* Gohn, G.S., Koeberl, C., Miller, K.G., and Reimold, W.U., eds., The ICDP-USGS Deep Drilling Project in the Chesapeake Bay Impact Structure: Results from the Eyreville Core Holes: Geological Society of America Special Paper 458, p. 633–654, [https://doi.org/10.1130/2009.2458\(28\)](https://doi.org/10.1130/2009.2458(28)).
- Senft, L.E., and Stewart, S.T., 2007, Modeling impact cratering in layered surfaces: Journal of Geophysical Research, v. 112, E11002, <https://doi.org/10.1029/2007JE002894>.
- Senft, L.E., and Stewart, S.T., 2008, Impact crater formation in icy layered terrains on Mars: Meteoritics & Planetary Science, v. 43, no. 12, p. 1993–2013, <https://doi.org/10.1111/j.1945-5100.2008.tb00657.x>.
- Shelton, J., Lockwood, R., and Bybell, L.M., 2006, The effects of the Chesapeake Bay impact on calcareous nannofossil assemblages: Patterns from the Watkins School core, Newport News, Virginia (USA): Journal of Nanoplankton Research, v. 28, no. 2, p. 71–80.
- Shuvalov, V., and Dypvik, H., 2004, Ejecta formation and crater development of the Mjølner impact: Meteoritics & Planetary Science, v. 39, no. 3, p. 467–479, <https://doi.org/10.1111/j.1945-5100.2004.tb00105.x>.
- Shuvalov, V.V., and Trubestkaya, I.A., 2002, Numerical modeling of marine target impacts: Solar System Research, v. 36, no. 5, p. 417–430, <https://doi.org/10.1023/A:1020467522340>.
- Stähle, V.V., and Ottemann, J., 1977, Ries-Forschungsbohrung 1973: Zeolithisierung der Gläser im Suevit und Petrographie der Beckensuevite und Gangbreccien: Geologica Bavarica, v. 75, p. 191–217.
- Townsend, G.N., Gibson, R.L., Horton, J.W., Jr., Reimold, W.U., Schmitt, R.T., and Bartosova, K., 2009, Petrographic and geochemical comparisons between the lower crystalline basement–derived section and the granite megablock and amphibolite megablock of the Eyreville B core, *in* Gohn, G.S., Koeberl, C., Miller, K.G., and Reimold, W.U., eds., The ICDP-USGS Deep Drilling Project in the Chesapeake Bay Impact Structure: Results from the Eyreville Core Holes: Geological Society of America Special Paper 458, p. 255–276, [https://doi.org/10.1130/2009.2458\(13\)](https://doi.org/10.1130/2009.2458(13)).
- Tsikalas, F., Gudlaugsson, S.T., and Faleide, J.I., 1998, Collapse, infilling, and post-impact deformation at the Mjølner impact structure, Barents Sea: Geological Society of America Bulletin, v. 110, no. 5, p. 537–552, [https://doi.org/10.1130/0016-7606\(1998\)110<0537:CIAPDA>2.3.CO;2](https://doi.org/10.1130/0016-7606(1998)110<0537:CIAPDA>2.3.CO;2).
- Turtle, E.P., Pierazzo, E., Collins, G.S., Osinski, G.R., Melosh, H.J., Morgan, J.V., and Reimold, W.U., 2005, Impact structures: What does crater diameter mean?, *in* Kenkmann, T., Hörz, F., and Deutsch, A., eds., Large Meteorite Impacts III: Geological Society of America Special Paper 384, p. 1–24, <https://doi.org/10.1130/0-8137-2384-1.1>.
- Vanderhurst, W.L., Hart, M.W., and Warren, C., 2011, The Otay Mesa lateral spread, a late Tertiary megalandslide in metropolitan San Diego County, CA: Environmental & Engineering Geoscience, v. 17, no. 3, p. 241–253, <https://doi.org/10.2113/gsegeosci.17.3.241>.
- Wade, J.A., Williams, G.L., and MacLean, B.C., 1995, Mesozoic and Cenozoic stratigraphy, eastern Scotian shelf: New interpretations: Canadian Journal of Earth Sciences, v. 32, no. 9, p. 1462–1473, <https://doi.org/10.1139/e95-118>.
- Ward, L.W., 1984, Stratigraphy of outcropping Tertiary beds along the Pamunkey River, central Virginia Coastal Plain, *in* Ward, L.W., and Krafft, K., eds., Stratigraphy and Paleontology of the Outcropping Tertiary Beds in

- the Pamunkey River Region, Central Virginia Coastal Plain—Guidebook for Atlantic Coastal Plain Geological Association Field Trip, October 6–7, 1984: Norfolk, Virginia, Atlantic Coastal Plain Geological Association, p. 11–77, 12 plates.
- Weems, R.E., Seefelt, E.L., Wrege, B.M., Self-Trail, J.M., Prowell, D.C., Durand, C., Cobbs, E.F., III, and McKinney, K.C., 2007, Preliminary Physical Stratigraphy and Geophysical Data of the USGS Hope Plantation Core (BE-110), Bertie County, North Carolina: U.S. Geological Survey Open-File Report 2007-1251, 63 p.
- Weston, J.F., MacRae, R.A., Ascoli, P., Cooper, M.K.E., Fensome, R.A., Shaw, D., and Williams, G.L., 2012, A revised biostratigraphic and well-log sequence-stratigraphic framework for the Scotian margin, offshore eastern Canada, *in* Mesozoic-Cenozoic Geology of the Scotian Basin Special Issue: Canadian Journal of Earth Sciences, v. 49, no. 12, p. 1417–1462, <https://doi.org/10.1139/e2012-070>.
- White, C.E., 2010, Stratigraphy of the Lower Paleozoic Goldenville and Halifax groups in southwestern Nova Scotia: Atlantic Geology, v. 46, p. 136–154, <https://doi.org/10.4138/atlgeol.2010.008>.
- White, C.E., and Barr, S.M., 2010, Lithochemistry of the Lower Paleozoic Goldenville and Halifax Groups, southwestern Nova Scotia, Canada: Implications for stratigraphy, provenance, and tectonic setting of Meguma, *in* Tollo, R.P., Bartholomew, M.J., Hibbard, J.P., and Karabinos, P.M., eds., From Rodinia to Pangea: The Lithotectonic Record of the Appalachian Region: Geological Society of America Memoir 206, p. 347–366, [https://doi.org/10.1130/2010.1206\(15\)](https://doi.org/10.1130/2010.1206(15)).
- Wittmann, A., Reimold, W.U., Schmitt, R.T., Hecht, L., and Kenkmann, T., 2009, The record of ground zero in the Chesapeake Bay impact crater—Suevites and related rocks, *in* Gohn, G.S., Koeberl, C., Miller, K.G., and Reimold, W.U., eds., The ICDP-USGS Deep Drilling Project in the Chesapeake Bay Impact Structure: Results from the Eyreville Core Holes: Geological Society of America Special Paper 458, p. 349–376, [https://doi.org/10.1130/2009.2458\(16\)](https://doi.org/10.1130/2009.2458(16)).
- Wünnemann, K., and Lange, M.A., 2002, Numerical modeling of impact-induced modifications of the deep-sea floor: Deep-Sea Research II, Topical Studies in Oceanography, v. 49, p. 969–981, [https://doi.org/10.1016/S0967-0645\(01\)00148-5](https://doi.org/10.1016/S0967-0645(01)00148-5).
- Wünnemann, K., Collins, G.S., and Weiss, R., 2010, Impact of a cosmic body into Earth's ocean and the generation of large tsunami waves: Insight from numerical modeling: Reviews of Geophysics, v. 48, no. 4, RG4006, <https://doi.org/10.1029/2009RG000308>.

MANUSCRIPT ACCEPTED BY THE SOCIETY 5 APRIL 2018

MANUSCRIPT PUBLISHED ONLINE 11 SEPTEMBER 2018